GeoAI in Regionalization: Community Detection in Spatial Networks and Its Application to Health Service Area Delineation

by

Yunlei Liang

A dissertation submitted in partial fulfillment of
the requirements for the degree of

Doctor of Philosophy

(Geography)

at the

UNIVERSITY OF WISCONSIN-MADISON

2024

Date of final oral examination: 04/24/2024

The dissertation is approved by the following members of the Final Oral Committee:
Song Gao (Chair), Associate Professor, Geography
Qunying Huang, Associate Professor, Geography
Jordan S. Ellenberg, Professor, Mathematics
Qin Li, Associate Professor, Mathematics

This dissertation is dedicated to my parents

ACKNOWLEDGMENTS

First, I would like to thank my advisor, Professor Song Gao, who has provided me with continuous support and guidance since I started my master's here back in 2018. I have learned so much in the past six years from him and I always feel very lucky to have him as my advisor. Not only did his professional knowledge and support help me overcome many difficult research problems, but also his optimism, kindness and patience encouraged me to ask any questions and learn how to become a better researcher in my academic life. I really appreciate the opportunity to study here and work with him.

I would like to thank my committee members, Professor Qunying Huang, Professor Jordan S. Ellenberg and Professor Qin Li for their valuable guidance and feedback on my dissertation. I appreciate the opportunity to work with them and learn from their expertise. I would like to thank Professor Huang for her constant support and encouragement, and I always enjoyed talking with her to learn how to be a successful and independent researcher. I would like to thank Professor Jordan S. Ellenberg and Professor Qin Li; their advice from the Mathematics perspective has brought important inspiration to my dissertation, and I appreciate their time in supporting my research.

I would like to thank the SafeGraph for providing the data support and the Wisconsin Department of Health Services Primary Care Program officers Aleksandr Kladnitsky and Regina Vidaver for providing the health resource data and guidance on this dissertation.

In addition, I would like to thank my cohorts in the GeoDS lab and the Geography Department for their support and feedback on my dissertation work. I especially want to thank Jiawei Zhu for her help and collaboration on the graph embedding study.

I would like to thank my friends for their support throughout my PhD time. They have encouraged me so many times along the way and are the persons with whom I share my happiness and tears.

Last but not least, I want to thank my parents for their support, understanding, and encouragement. I can never accomplish this without their love and efforts in raising me.

CONTENTS

LIST OF TABLES

LIST OF FIGURES

ABSTRACT

Regionalization refers to the process of partitioning geographic space into regions that are internally similar yet distinct from each other. This process is fundamental for understanding complex spatial relationships and how areas interact with each other. Spatial networks provide a rich source of data (e.g., flows of people, goods or information) that can be used to generate regions. How to extract useful information from the spatial networks for better regionalization has been a longstanding topic of interest, and methods such as community detection and node clustering have been well studied. However, nowadays, many regionalization tasks remain confined to domain-specific datasets and traditional methods, while the rapid growth of the big data era and Artificial Intelligence (AI) methods has created more opportunities for improved regionalization. This dissertation focuses on how to utilize mobility-based spatial networks and Geospatial Artificial Intelligence (GeoAI) methods for better regionalization.

This dissertation will start by demonstrating how spatial networks can be applied to delineate Rational Service Areas (RSAs) in the public health domain. Existing RSAs are usually developed based on the local knowledge of public health needs and are created through time-intensive manual work by health service officials. In this dissertation, a data-driven and spatially constrained community detection method based on aggregated human mobility flow data is proposed to automate the process of establishing the statewide RSAs in GIS software. The proposed method outperforms other baselines in the multiple metrics and shows the promising potential of mobility-based regionalization in the public health domain. Then, the dissertation improves the existing community detection method by proposing GeoAI-enhanced models based on Graph Convolutional Networks and Graph Attention Networks. The methods identify regions by considering attribute similarity, geographic adjacency and spatial interactions. The methods are compared with multiple baselines and perform best when one wants to maximize node attribute similarity and spatial interaction intensity simultaneously within the communities. It is applied to the

shortage area delineation problem in public health and demonstrates its promise in solving regionalization problems. Lastly, the dissertation improves the interpretability of the proposed GeoAI methods. Most of the AI methods are considered black boxes, meaning that humans cannot understand the internal process, leading to low transparency and trustworthiness of the AI-generated results. However, geographic research often requires an explanation and discussion of why certain predictions are generated to understand the processes underlying the observed data. To promote the application of GeoAI methods to regionalization, the dissertation applies an explainable AI model to the proposed GeoAI-based community detection method. The explanations provide important node features and subgraph structures that contribute the most to each prediction. By examining individual and aggregated explanations, community activity spaces are compared, and potential regional patterns are discovered to support the reasoning of regionalization results.

In summary, this dissertation aims to provide valuable insights into how human mobility data and GeoAI methods can be applied to regionalization tasks in spatial networks. It proposes a framework for automatic area delineation using mobility data that can be expanded to other use cases. Then, it improves the existing regionalization methods by introducing GeoAI models to combine node attributes and edge connections. Thirdly, it provides insights into how GeoAI models can be interpreted and explained to better understand the underlying geographic phenomena.

1 INTRODUCTION

Chapter 1 provides a general introduction to the dissertation. First, it introduces the concept of regionalization and its importance in geography. Then, it presents a literature review that starts with a health domain regionalization application, and then it discusses more details on applying regionalization methods to spatial networks. This chapter then summarizes the existing challenges, proposes three Research Questions (RQs) inspired by the challenges, and describes the corresponding research aims conducted to answer the questions.

1.1 Regionalization

Regionalization refers to the process of dividing the Earth's surface into distinct areas, known as regions, based on common characteristics (Flinn and Engdahl, 1965). In the domain of geography, regionalization has always been of central importance. "Understanding the idea of region and the process of regionalization is fundamental to being geographically informed" (Geography Education Standards Project, 1994, p.70). The process of regionalization helps geographers understand the complexity of many ongoing phenomena and gain insights into the nature of the world's landscapes and societies.

Depending on the specific goals, the criteria used to divide regions can be multifaceted, including geographical, cultural, economic, political, etc. In the real world, many domains, such as health care, economics, or urban planning, require regions to be the basic unit for conducting further analyses, organizing and summarizing patterns. For example, comparing hospital visit statistics at the regional level can help policy-makers discover potential resource disparity, make reasonable decisions, and propose strategies for future directions.

Central to regionalization is the concept of spatial networks, which are structures that represent the complex relationships and interactions among different regions. Spatial

networks can be physical (roads) or abstract (social connections or movement flows). They are always represented using a graph consisting of nodes and edges. The nodes can be geographic entities such as locations, roads, road intersections or administrative areas, and edges can represent the spatial interactions among nodes. Spatial networks provide valuable insights into how different areas are interconnected and influence one another. The study of these networks involves examining the patterns of connections and flows – people, resources, information – that traverse the geographical space. A widely used data to model spatial networks is human mobility data, which depicts how humans move across geographic space. For instance, travel-to-work, travel-to-school flows, and migration data have been analyzed by various methods to define functional regions (Klapka et al., 2020).

In recent decades, the emergence of advanced computational techniques and the availability of big data have greatly transformed traditional regionalization studies and opened the door for more opportunities. Solving the regionalization tasks with approaches such as Machine Learning (ML) and Deep Learning (DL) enables a more accurate and comprehensive understanding of the patterns and relationships that were previously undiscovered. DL offers the following advantages compared with traditional methods: 1) it can convert the high-dimensional input into low-dimensional representations while maintaining the important structure information (Hinton and Salakhutdinov, 2006); 2) it can integrate multiple types of information in various formats, which is ideal for modeling spatial networks and solving regionalization tasks.

1.1.1 Health Regionalization

Regionalization in health geography has been used to refer to "programs that alter the functions and relationships among health providers within an area to achieve better access to health care, a higher quality of services, greater equity and more responsiveness to patient needs" (Ginzberg, 1977, p.1). Regionalization helps identify areas with specific healthcare needs or disparities in health services and supports allocating resources efficiently. The

regions in health care domains are usually defined as Health Service Areas (HSAs) or Rational Service Areas (RSAs), and they are usually delineated to represent local health markets.

Traditional Health Service Area Delineation One of the most widely used methods in health regionalization is the Dartmouth method proposed by the Dartmouth Institute for Health Policy and Clinical Practice in the United States (Wennberg and Cooper, 1998). Based on the Medicare hospitalization records that indicate how patients travel from their ZIP Code to seek health services, this method defines HSAs to represent community-based local healthcare markets and Hospital Referral regions (HRRs) to represent regional healthcare markets for tertiary medical care (Wennberg and Cooper, 1998). Following the traditional Dartmouth method, a primary care service area method was also developed using only the Medicare data for primary care physicians (Goodman et al., 2003).

The Dartmouth method can be summarized in three steps.

1. The hospitals are collected and assigned to the city/town where they are located at.

2. Based on the Medicare hospitalization data between the hospital and the patient's zip code area, each zip code is assigned to the town containing the hospital that mostly used by the residents in the zip code area.

3. Visual examinations are conducted to ensure the shapes are contiguous and the final HSAs are determined.

Many states have used the Dartmouth method for delineating HSAs in the United States (Jia et al., 2015). However, researchers have also realized that there are some issues with the original Dartmouth method. First, it was developed using the Medicare data, which only includes certain types of patients (e.g., people over the age of 65). Therefore, the results may not be representative of other types of population (Hu et al., 2018; Wennberg and Cooper, 1998). Second, the last step of the Dartmouth method involves visual examination and introduces uncertainties into the result as the designation may be arbitrary (Hu et al.,

2018; Wang et al., 2021a). Third, the health service markets are dynamic and have changed over time, but the results of the Dartmouth method have been static since its proposal (Wennberg and Cooper, 1998).

Multiple researchers have worked on improving the Dartmouth method in different ways to solve those problems. Klauss et al. (2005) developed a Swiss method similar to the Dartmouth method using the hospital discharge records for all patients. This method was also population-based by using a small area analysis at the census level and can accurately describe the differences across regions with homogeneous population groups (Klauss et al., 2005). Following that, a Dartmouth-Swiss hybrid method was used to compare the temporal variations of Medicare-derived HSAs over the two decades (Jia et al., 2015). The study found that the boundaries of the HSAs have been significantly changed and are not representative of the whole population (Jia et al., 2015). To provide a more solid result, the authors applied the Huff model to re-demarcate the HSAs by assuming that the probability of visiting a hospital is positively related to the number of beds and negatively related to the travel distance (Jia et al., 2015). The Huff model method was further improved by designing the distance decay function based on the actual hospitalization travel patterns (Jia et al., 2017; Bai et al., 2023). However, the Huff model may oversimplify the visit patterns of seeking health services as there are many other factors affecting whether people would visit a hospital, for example, the specialties of physicians or people's work location. A refined Dartmouth method was also developed, where the authors resolved some uncertainties in the original method and developed a standardized delineation approach that can be automated in a GIS tool (Wang and Wang, 2022a).

1.1.2 Community Detection Algorithms on Spatial Networks

A major innovation in Health Service Area delineation was inspired by the network theory, which models the visit flows from patients to health providers in a spatial network (Hu et al., 2018; Wang et al., 2021a). Specifically, the approach named community detection

aims to identify strongly connected communities based on the movement flows in the network, and those communities can then be used as RSAs (Newman, 2006). With the goal of maximizing the hospital visit flows within each community and minimizing the flows between communities, this approach divides regions based on their interactions and reveals the hidden relationship among areas (Hu et al., 2018; Newman, 2006).

Most of the traditional community detection algorithms divide the networks primarily based on topological structures. For example, the minimum-cut method partitions the graph by minimizing the number of edges between communities, the hierarchical clustering method uses the topological type of similarity between node pairs to group nodes, and the modularity maximization considers the concentration of edges within communities (Flake et al., 2004; Johnson, 1967; Newman, 2006). The modularity-based maximization methods have particularly performed well on spatial networks (Gao et al., 2013; Expert et al., 2011). The modularity proposed by Newman (2006) is a measure of how good a graph partition is. It compares the number of edges that fall within the communities to a null network with edges placed randomly (Newman, 2006). A large modularity value indicates a robust community structure and dense connections among nodes within communities (Newman, 2006; Hu et al., 2018).

One of the most popular modularity maximization methods is Louvain (Blondel et al., 2008). The Louvain method achieves the maximum modularity through two stages: 1) in a local network, move individual nodes to the community that maximizes the modularity gain, 2) aggregate the updated local networks and treat them as nodes recursively (Blondel et al., 2008). The two stages are repeated until no improvement can be made. However, it has been found that the Louvain method tends to generate poorly connected communities in some cases (Wang et al., 2021b). The Leiden method was recently proposed to improve the Louvain method and guaranteed to generate well-connected communities (Traag et al., 2019).

The Louvain and Leiden methods have been applied to the public health domain to

identify health service areas and spatially connected communities (Hu et al., 2018; Wang et al., 2021b; Pinheiro et al., 2020; Wang and Wang, 2022b). The Louvain method was first applied to identify the hospital service areas based on the patient-to-hospital flows in Florida (Hu et al., 2018). Later on, Wang et al. (2021b) proposed spatially constrained Louvain and Leiden algorithms to identify health service areas. The algorithms have shown great performance in delineating health service areas with a goal of maximizing flows within communities and minimizing flows between communities (Hu et al., 2018; Wang et al., 2021b). They are effective and efficient for capturing the natural structure of the health visit patterns. In addition, traditional community detection methods have also been widely used in identifying spatial interaction communities using human mobility data, social media check-ins, cellphone call data, and community travel surveys (Ratti et al., 2010; Liu et al., 2014; Nelson and Rae, 2016; Hou et al., 2021).

1.1.3 Graph Embedding Learning with Node Attributes and Edge Connections

Graph embedding is a powerful technique that reduces the dimensionality of data by incorporating both node attribute information and topological graph structures into vectors (Goyal and Ferrara, 2018). With the information captured in vectors, node clustering is naturally extended from it. When nodes represent geographic units, graph embedding can be considered as another approach for regionalization where nodes with similar embeddings can be grouped into regions. It has been shown in various scenarios that leveraging attribute information in addition to the graph structure yields better results for regionalization tasks (Cui et al., 2020). DL algorithms, including random walk-based algorithms and Graph Neural Network (GNN)-based algorithms, have both shown promising performance in graph embedding tasks (Goyal and Ferrara, 2018).

Large-scale Information Network Embedding (LINE) was among the first graph embedding methods that scaled well with large networks (Grover and Leskovec, 2016; Tang et al., 2015). LINE proposed to sample edges with probabilities based on weights and treat them

as unweighted edges to solve the gradient explosion problem in stochastic gradient descent (Tang et al., 2015). Random walk-based algorithms such as DeepWalk and Node2vec, both inspired by the skip-gram models in natural language processing, aim to preserve high-order proximity between nodes in a graph by sampling fixed-length random walks and maximizing the probability of its neighbors in the walk (Perozzi et al., 2014; Grover and Leskovec, 2016). Node2vec improves on DeepWalk by having a more flexible sampling strategy that balances between breadth-first-search and depth-first-search traversal, which allows it to learn a mixture of homophily and structural equivalence in a graph (Grover and Leskovec, 2016). Another method called SDNE (Structural Deep Network Embedding) is also one of the earliest methods for graph embedding tasks (Wang et al., 2016). It jointly optimizes for first-order and second-order proximities to preserve both the local and global structure of the graph (Wang et al., 2016). This semi-supervised method is also robust to sparse networks (Wang et al., 2016). The GraphSAGE framework later leveraged node features and aggregated attribute information in neighborhoods of the graph to improve node embeddings (Hamilton et al., 2017).

In recent years, Graph Convolutional Networks (GCNs) have gained tremendous attention for their strong capability in graph embedding and node representation learning, which are highly beneficial for further downstream prediction and clustering tasks (Zeng et al., 2019; Molokwu et al., 2020). Some of the latest GCN methods like GALA (Graph convolutional Autoencoder using LAplacian smoothing and sharpening), MAGNN (Metapath Aggregated Graph Neural Network), and AGE (Adaptive Graph Encoder) have all shown superior performances in popular node clustering datasets like Cora, IMDB, Wiki etc.(Fu et al., 2020; Cui et al., 2020; Park et al., 2019). Both GALA and AGE utilize graph encoder while MAGNN utilizes node attributes transformation and metapath aggregation (Fu et al., 2020; Cui et al., 2020; Park et al., 2019). Metapath is defined as "an ordered sequence of node types and edge types defined on the network schema, which describes a composite relation between the node types involved" (Fu et al., 2020, p.2). MAGNN captures both semantic

attributes and topological structures from neighboring nodes and metapath context in between (Fu et al., 2020). CommDGI (Community Deep Graph Infomax) developed a more specific GCN for community detection given the inherent unsupervised nature of community detection tasks compared to the other general-purpose graph representation learning problems by adding a clustering layer with community-oriented objectives like modularity (Zhang et al., 2020).

Graph Attention Networks (GATs) were further proposed to improve the neighborhood aggregation in GCNs. In GCNs, the weights between the neighbor nodes and the central node are usually explicitly defined, either through the structural properties of the graph or a learnable weight, and this can affect the generalization power of GCNs (Velickovic et al., 2017). GATs define the one-hop neighborhood weights implicitly through a self-attention mechanism (Velickovic et al., 2017). The key idea is that different nodes in a neighborhood can have different importance to the central node (Velickovic et al., 2017). GATs have been proven to achieve or match state-of-the-art results and allow more interpretability through the learned attentional weights.

1.1.4 Explainable Artificial Intelligence on Graphs

The following part introduces the development of graph explanation methods and then summarizes how the methods have been used to understand problems in spatial networks.

Explainable Artificial Intelligence Methods for Graph Neural Networks Explainable Artificial Intelligence (XAI) refers to the category of methods that enable human-readable explanation and interpretation of the decisions provided by the AI (Samek et al., 2019). There are two major types of XAI methods for explaining GNNs. The first type focuses on designing a model that can provide explanations of GNN predictions in a model-agnostic way, meaning that it can work for any input model (Huang et al., 2022). The second type of model focuses on the relevant aspects of computation in the neural model being explained

(Huang et al., 2022). This dissertation will mostly focus on the first family of methods.

The first model-agnostic XAI method to explain and interpret GNNs is called GNNExplainer(Ying et al., 2019). It takes a trained GNN and its predictions as inputs and tries to maximize the mutual information between the predictions and the distribution of possible subgraph structures. The explanation includes a subgraph and a subset of node features that contribute the most to the node prediction. The GNNExplainer focuses primarily on providing instance-level interpretability and has been widely used in many studies (Xie et al., 2022; Pfeifer et al., 2022). However, it might be time-consuming and impractical in some real-world scenarios where the dataset can be very huge.

Following GNNExplainer, a variety of methods have been proposed to provide explanations of GNN models in different aspects. Luo et al. (2020) designed a method called PGExplainer, which applies to any GNN-based models in both transductive and inductive settings. It uses a deep neural network to parameterize the explanation generation process and allows multiple instances to be explained collectively. Huang et al. (2022) proposed GraphLIME, which is based on the existing novel model-agnostic technique LIME (Ribeiro et al., 2016) that can explain the predictions of any classifier. GraphLIME is specifically designed for GNN models, and it provides locally faithful explanations by sampling network neighbors of the node and locally captures the nonlinear dependency between features and predictions. But GraphLIME only focuses on extracting important features, and it cannot consider important subgraph structures.

There are also some methods that mainly focus on the subgraphs. Lucic et al. (2022) proposed a counterfactual GNNExplainer that identifies important edges that are crucial for the predictions if they are removed. Similarly, Schlichtkrull et al. (2022) introduces a post hoc method for interpreting the predictions of GNNs by identifying unnecessary edges. Given a trained GNN model, they learn a simple classifier that, for every edge in every layer, predicts if that edge can be dropped.

Another popular model-agnostic method for interpreting Machine Learning results is

SHAP (SHapley Additive exPlanations) (Lundberg and Lee, 2017). It is a game-theoretic approach that aims to fairly distribute the contributions of players when they collectively achieve a certain outcome (Li, 2022). The interpretation of the Shapley value of a feature is its marginal contribution to model prediction averaged over all possible models with different combinations of features. SHAP has been used broadly to understand the feature importance of different types of models.

Applications of XAI methods on spatial networks Most applications of XAI methods focus on traditional machine learning tasks with Euclidean-distance data such as images, video, and text (Shi et al., 2022). There is only a handful of research on XAI on geospatial tasks since the structure of geospatial data is often very different from the classical machine-learning tasks.

One of the early works applying the XAI method to the geospatial domain focuses on remote sensing images (Dikshit and Pradhan, 2021). The authors use a CNN model for spatial drought prediction and analyze the individual predictions using Shapley outputs to understand the model-predictor relationship for different drought conditions.

Li (2022) compares the results from SHAP-explained XGBoost to the Spatial Lag Model (SLM) and Multi-scale Geographically Weighted Regression (MGWR) at the parameter level. The study found that XGBoost estimates similar spatial effects as those in SLM and MGMR models, and suggested that locally interpreted machine learning models can be good alternatives to the traditional spatial statistical models when there are mixed spatial and non-spatial effects.

Tang et al. (2023) proposed an Explainable Spatio-Temporal Graph Neural Networks (STExplainer) framework that enhances STGNNs with inherent explainability. Here, explainability is defined as the ability to identify influential spatial and temporal subgraphs that have a significant impact on predictive results. The approach can provide accurate predictions and faithful explanations simultaneously on tasks such as traffic and crime

prediction.

One of the most recent applications of XAI methods in urban analytics uses GNNExplainer to understand the relationship among road networks. The author proposed a framework that combines a GCN model and a GNNExplainer. The GNNExplainer can offer insights into how certain predictions are made by relating to node features such as types of Points of Interest (POIs) and particular edge connections.

1.2 Existing Challenges and Research Questions

While all the previously introduced literature has contributed to the development and understanding of regionalization in different ways, there remain some research gaps. To fill the gaps in the current literature, three Research Questions (RQs) are proposed to support better regionalization on spatial networks.

All of the existing studies on Rational Service Area Delineation introduced the use of patient-hospital discharge data to extract the health/rational service areas. However, access to hospitalization data is very limited due to privacy concerns, and such data may not be available for many low-income and middle-income areas, which affects the scalability of the existing methods (Jia et al., 2015). In addition, the existing hospital visits may not reflect the needs for new hospitals/clinics. There are other data sources with great potential to reflect movement patterns and reveal local health markets, such as the anonymous human mobility data collected from mobile phones. Based on where the trip ends (e.g., clinics, hospitals, pharmacies), the human mobility data contains important information on how people travel to receive health services and can possibly be used to support regionalization tasks on healthcare use cases. In addition, given the limited access to hospitalization data, many public health officials are still relying on their local knowledge to select Rational Service Areas (RSAs) manually. They are experts in the health domain, but they are usually unfamiliar with the technical details of area delineation and have limited ability to make full use of the available data sources. Therefore, it is necessary to develop a systematic

service area delineation approach that can be automated, repeated, and adapted to different scenarios using human mobility data.

Given the current research gap, the following question is asked:

RQ1: *Can a framework that automatically identifies Rational Service Areas based on mobility data be developed, and how well is the performance of the mobility-based regionalization compared with traditional methods?*

To answer RQ1, I aim to develop a framework for automatically delineating RSAs based on human mobility data. Specifically, I will design the methodology based on the needs and requirements collected from experts in the health domain. The approach is based on existing community detection methods, and they will be modified based on domain-specific knowledge and additional spatial constraints for data-driven regionalization. I also aim to automate the whole process with Python toolboxes embedded in a GIS environment so that a broader range of users can access the approach and conduct analyses on their own. This chapter intends to provide insights into how the use of human mobility data and GIS automation workflow can help state health departments develop candidate regionalization plans.

After applying the community detection methods on spatial networks for a health domain regionalization problem, I am interested in further understanding the limitations of the existing methods and exploring the possibility of methodology improvement. Most of the existing community detection methods are based on topological structures (edge connections). The node attributes can also represent crucial characteristics such as people's demographic information or the region's economic status and should be incorporated into the process. How to better integrate both node attributes and network topology remains a challenge for traditional methods. The nodes and edges are represented in completely different formats, and there is a lack of research to combine them at the same time to obtain more comprehensive regionalization results.

Therefore, the following research question is asked:

RQ2: *How can node attributes and edge connections in spatial networks be combined to identify regions simultaneously?*

To answer this question, I will propose a family of Geospatial Artificial Intelligence (GeoAI)-enhanced unsupervised community detection methods based on Graph Neural Networks (GNNs). GNNs and their extensions have been very successful in modeling and predicting graph-structured data and, therefore, have great potential to be used for understanding spatial networks. I plan to design the models with convolutional layers, which support the aggregation of neighborhood attributes via edge connections. To solve the issue of no ground truth labels, a community-oriented loss function will be designed to guide the learning process so that nodes with similar attributes and strong edge connections will have similar latent representations. The spatial networks and the geographic adjacency graphs are used as the input of the methods to support the integration of muilt-sources information and provide a more comprehensive regionalization result. The result of RQ2 may allow us to understand how the node attributes and edge interactions on spatial networks can be better integrated to support regionalization.

After exploring how GeoAI models can be applied to regionalization tasks, I am interested in understanding why certain results are generated to improve the interpretability of AI models. Despite their powerful performance, the abovementioned AI methods are considered black-box models. It means that there are no satisfactory explanations for the internal logic, and the behavior cannot be fully understood (Benítez et al., 1997). The low transparency of the AI methods brings difficulties in interpreting their results, leading to a reduction of trustworthiness that hinders the applications of AI techniques. There are some recent approaches focusing on providing explanations of Graph-based models, but their applications on spatial networks are very limited.

With these challenges, I ask the following research question:

RQ3: *How can one improve the explainability of graph-based GeoAI models to understand regionalization results better?*

To answer this question, I aim to apply graph-based explanation methods to the previously proposed GeoAI-enhanced community detection models in RQ2. The explanation methods are expected to interpret what are the key features and graph structures that contribute most to the prediction at the instance level. I plan to incorporate local knowledge and the provided explanation to examine any potential regional characteristics and spatial patterns. The result of RQ3 aims to provide new insights into how GeoAI methods can be interpreted to support a better understanding of geographic phenomena and network characteristics.

1.3 Dissertation Structure

The remainder of this dissertation is structured according to the three research questions. Chapter 2, Chapter 3, and Chapter 4 aim to answer one research question.

In Chapter 2, a data-driven and spatially constrained community detection method based on aggregated human mobility flow data is proposed to automate the process of establishing the statewide RSAs and identifying Health Professional Shortage Areas in GIS software. The study applies the community detection method to spatial networks with additional constraints and evaluates its performance with other traditional regionalization methods.

In Chapter 3, based on the findings from Chapter 2, I develop a family of novel community detection methods based on Graph Convolutional Neural Networks and Graph Attention Networks. Using a community-oriented loss function, the method can consider node attributes, geography adjacency, and spatial interactions when grouping nodes into communities. The performance of the proposed method is then compared with multiple baselines. The results show that the proposed method can contribute to geographic regionalization when one wants to maximize both node similarity and spatial interactions.

Chapter 4 presents a study that focuses on providing interpretability of the GNN-based models to support understanding of regionalization results. The study applies an

Explainable AI method to identify the important subset of features and subgraphs in each instance. The explanations are then analyzed at the individual-level and the community level to identify insightful patterns related to activity spaces and potential social segregation. It helps researchers examine the reasons for certain spatial patterns and understand the driving factors for regionalization results.

Finally, in Chapter 5, I conclude this dissertation and summarize its contributions. I also list several potential directions to explore for future studies.

2 AUTOMATIC DELINEATION OF RATIONAL SERVICE AREAS AND HEALTH PROFESSIONAL SHORTAGE AREAS BASED ON HUMAN MOVEMENTS

2.1 Introduction

Health Professional Shortage Area (HPSA) designation identifies geographic areas or population groups with a shortage of health care services, including primary, dental, and mental health cares (HRSA, 2021; Wang and Luo, 2005). The designation of HPSAs can help understand the spatial distributions and variations of health services, better allocate health resources and support policy making. It is important to make sure that the designated HPSAs can identify the greatest amount of the shortage areas so that limited health resources can be directed to people with the greatest needs.

The first step of the HPSA designation is to identify rational service areas (RSAs), which are then used as the input area units of HPSAs. The RSAs are relatively self-contained geographic units that represent people's travel patterns of seeking health services (Lopes, 2000). The RSAs are usually groups of census tracts, county subdivisions, an entire county, or multiple counties (HRSA, 2020). Each state is required to develop its own statewide RSA plan that outlines the RSAs in a state/territory (Health Resources and Services Administration, 2020). To justify why a specific area is selected as an RSA, evidence of travel patterns, physical barriers or social-economic similarities should be provided (Lopes, 2000; Wang and Luo, 2005). However, there is no uniform approach to establishing the RSAs. Many of the RSAs are developed based on the local knowledge of public health needs and are created through time-intensive manual work by health service officials.

There has been much research working on the development of RSAs. Based on hospitalization records, the Dartmouth method was proposed in the 1990s to "assign zip code area into the town that contains the hospitals mostly used by the local residents (Wennberg

and Cooper, 1998). Jia et al. (2017) use a revised Huff model to delineate Hospital Service Areas based on the relationship between the hospital supply and patients' travel costs. In recent years, methods that apply the network theory have been proposed to model the patient discharge data in a spatial network where nodes are zip-code regions and edges are hospitalization flows between these regions (Hu et al., 2018; Wang et al., 2021a). Then the community detection approach is used to identify the strongly connected areas based on the hospitalization flows and those areas can then be used as RSAs (Newman, 2006). Some additional considerations such as the spatial constraints have also been incorporated into this process (Wang et al., 2021a).

Although the above-mentioned methods have demonstrated their effectiveness in health service area delineation, there are still some issues that need further consideration. For example, the HPSA designation aims to address the resource shortage problem, which is mostly caused by the unequal spatial distribution of population and health providers (Liu, 2007). Studies have examined the recent trends in physician density and found a steady decrease of primary care physicians in more than half of rural counties from 2010 to 2017 (Machado et al., 2021). The trend indicates that providers tend to move from rural areas to urban areas, probably because there are more potential patients in the population-dense area. The uneven spatial distribution of healthcare providers creates barriers to access health services, especially for rural area residents and it leads to potential health disparities. Therefore, rural/urban residents may generate significantly different visit patterns to health providers, and such differences should be considered in the development of the health service areas.

To fill the gap in the current research, a spatially-constrained community detection method that considers different characteristics and constraints of rural and urban areas was proposed to automate the delineation of RSAs and HPSAs (i.e., Auto-RSA-HPSA) in a geographic information system (GIS) environment. The general workflow is shown in Figure 2.1. By incorporating the urban/rural population threshold into the network-based

community detection algorithm, our method is adjustable based on the rural population percentage to account for the health access inequality. In addition, it has been realized by public health officials that a method that can be conducted automatically, adapted to different areas and evaluated by quantitative measurements is needed in the designation process. This study develops a completely automated process for the establishment of RSAs and the delineation of HPSAs. I first propose a data-driven and spatially constrained community detection method based on human mobility flow data collected from anonymous mobile phones to establish the statewide RSAs. Then, the generated RSAs are evaluated through multiple criteria including both spatial and non-spatial aspects to identify the HPSAs. The results are measured using health-related metrics and the performance is compared with the traditional Dartmouth method.

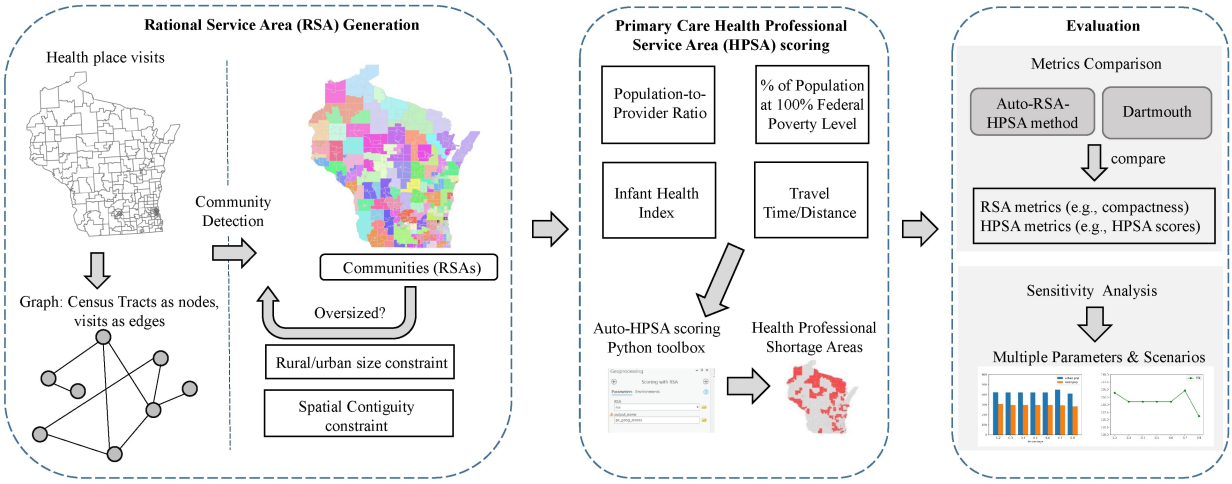

Figure 2.1: The workflow of the Auto-RSA-HPSA generation process for primary care.

The remaining sections of this chapter are organized as follows: the datasets used in this research and the proposed spatially constrained community detection method are introduced in section 2.2. Then, the result evaluation and sensitivity analyses are presented in section 2.3. Finally, the conclusion and some directions for future work are shared in section 2.4.

2.2 Method

2.2.1 Data and Study Area

The study area of this research is the State of Wisconsin in the United States. It is bordered by Lake Superior to the north, Michigan to the northeast, Lake Michigan to the east, Illinois to the south, Iowa to the southwest and Minnesota to the northwest (Martin, 1965).

This study uses the SafeGraph business venue database and place visit patterns (SafeGraph, 2023) as its main data source. SafeGraph collects over 8 million points of interest (POIs) with visit patterns in the United States. The POIs are classified based on the North American Industry Classification System (NAICS) 6-digit sector codes. Three categories of interest: 621 - *Ambulatory Health Care Services*, 622 - *Hospitals* and 446110 - *Pharmacies and Drug Stores* are selected. Only visits to health-related places are collected because the generated regions will be used to analyze healthcare problems. However, the framework can take any spatial network as the input, depending on the use cases. The fine-resolution visit patterns to those POIs were collected from anonymous smartphone users and were aggregated to the census block group level for privacy preservation. The aggregated visit data is from about 10% devices in the United States and the data sampling has been illustrated to be highly correlated with the U.S. Census populations (Kang et al., 2020). The visit data from census block groups to all health-related POIs are further aggregated to the census tract level. The origin census block group is aggregated to the census tract containing it, and the destination POIs are also aggregated to the census tract in which they are located. So the data becomes the origin-destination flows at the same spatial resolution. The time window used in this study was from August 2021 to October 2021.

The health providers' information, including locations, full-time equivalent (FTE), and specialty, are provided by the Wisconsin State Primary Care Office. The FTE means a provider's working hours divided by the hours for a full-time workweek, so if a provider works 40 hours a week, their FTE is 1. Other data sources include the U.S. Census American

Community Survey (ACS) 5-year estimates, and the Centers for Disease Control and Prevention (CDC) Period Linked Birth/Infant Death File 2014-2018.

2.2.2 Community Detection Methods

The RSA generation workflow with three phases in this study is shown in Figure 2.2. The method is built on spatial network-based community detection algorithms with multiple iterations and additional constraints designed for the targeted problem. More details are presented in the following sections.

Community Detection Algorithms The random walk, Louvain, and Leiden community detection algorithms are adopted in this study.

The random walk algorithm was proposed with the basic idea that short random walks tend to be 'trapped' in the same community in a network (Pons and Latapy, 2005). It uses a structural similarity to represent the distance between nodes and between communities. The distance is calculated based on the transition probability of moving from one node to another in a single step. This approach is a hierarchical clustering algorithm that groups nodes in the network iteratively into communities (Pons and Latapy, 2005). At the initial stage, every node (i.e., census tract in this study) is a single community, and the distances based on the structural similarity between all adjacent nodes are computed. Two communities will be chosen based on the distance measure and merged into a new one, and then the distances among new communities will be updated until there is only one community of all nodes. The algorithm captures much information on the community structure and is computationally efficient. However, the performance can vary based on the network's size and structure.

The Louvain algorithm was proposed by Blondel et al. (2008) as a popular method to extract communities based on modularity optimization. The modularity is used to measure the quality of the communities. It compares the fraction of edges that fall within

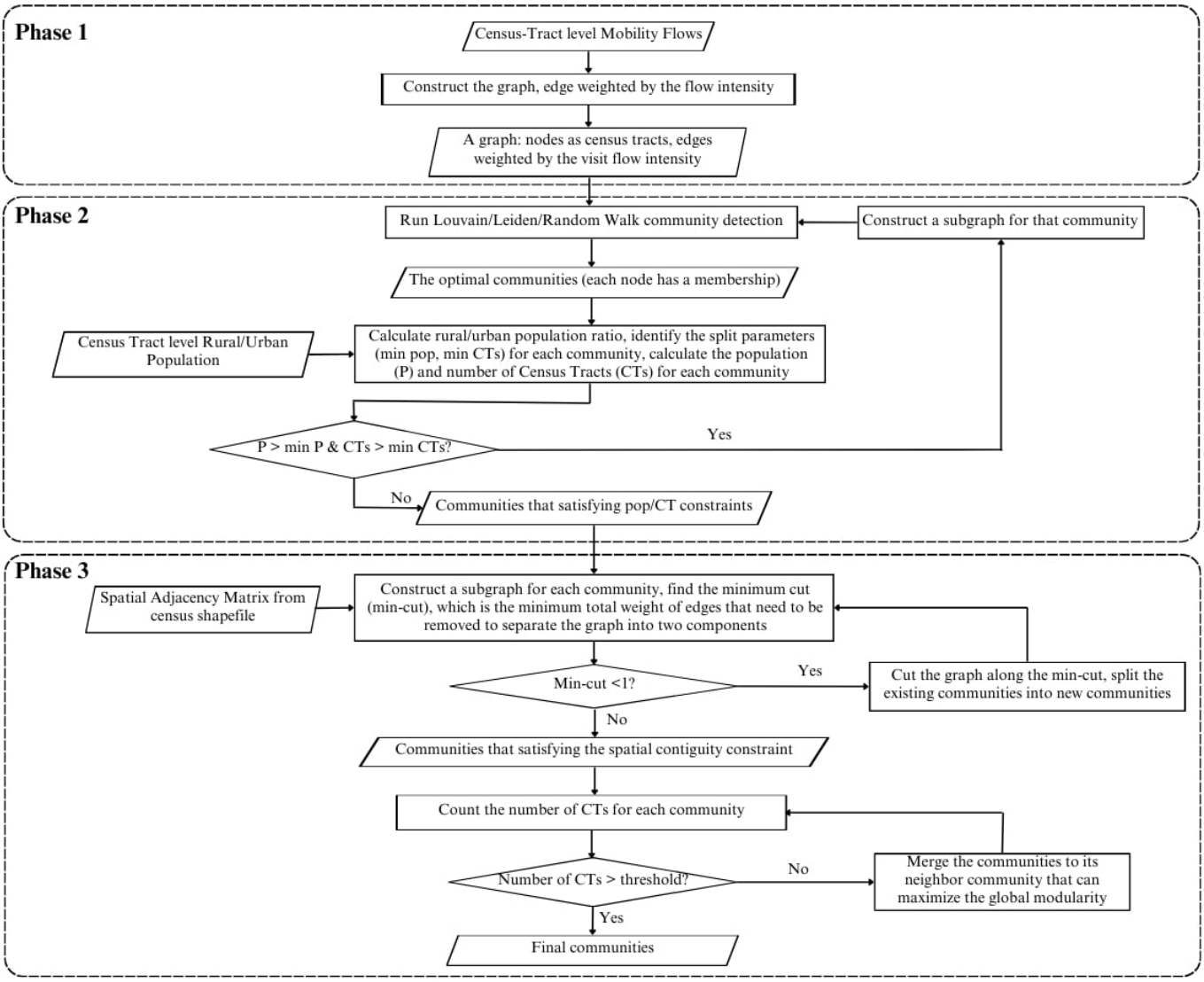

Figure 2.2: The Rational Service Area generation workflow.

the communities to a null network with edges placed randomly (Newman, 2006). The modularity ranges from -1 to 1 and is larger when the division result has more within-community edges. In other words, a larger modularity means the nodes with stronger connections are better grouped together. Exact modularity optimization is NP-hard, and the Louvain algorithm uses a heuristic method to identify high modularity partitions (Blondel et al., 2008). The algorithm has two phases: initially, each node is considered as a single community, and the method calculates the modularity gain by moving each

node to its neighbor's community, then the node will be placed in the community with the maximum gain (Blondel et al., 2008). This process is repeated until there is no modularity improvement. Then, in the second phase, the algorithm builds a new network where the nodes are the communities from the first phase and the first phase can be reapplied to this new network. The Louvain algorithm has been proven to be intuitive, and easy to implement. It runs very fast and can identify communities with good quality in large networks (Blondel et al., 2008). However, it suffers from a resolution limit that may prevent it from identifying small-size communities.

The Leiden algorithm is a recent improvement on the Louvain algorithm. It was found that the Louvain algorithm may generate disconnected communities, and the Leiden algorithm was proposed with better partitions so that all communities are internally connected (Traag et al., 2019). It has three phases: 1) moving nodes locally, 2) refining the partition and 3) aggregating the network. In the first phase, Leiden uses a fast local move procedure that only visits nodes whose neighborhood has changed. During the refinement phase, each community generated from the first phase is evaluated to make sure it is strongly connected and may be split into subcommunities. The Leiden algorithm has outperformed the Louvain algorithm in practical applications in terms of speed and the quality of the results (Traag et al., 2019).

One important characteristic of the above methods is that they are scale flexible (Pons and Latapy, 2005; Blondel et al., 2008; Traag et al., 2019; Hu et al., 2018). Each process generates a hierarchical structure and allows the examination of all hierarchical levels to select the most appropriate community structure for the use case. This property is very helpful for real-world planning as one may want to compare results at different scales to understand the scale effects. For example, to support the analysis of the Modifiable Area Unit Problem (MAUP) in geography (Openshaw, 1984).

The health-related place visit flows at the census-tract level will be used as inputs to the community detection algorithm. As shown in Figure 2.2 Phase 1, the census tract are

the nodes, the edges are health-related visits, and the edge weights are the intensity of flows. The generated hierarchical community structure will be evaluated at multiple levels to select the best community structure as the RSAs.

Population Constraints To evaluate the appropriate geographic scale of RSAs, one needs to understand how the size of an RSA is determined and measured. There are multiple aspects that affect the size of RSAs, for example, how populations are distributed across space, their demographic and socioeconomic status, and how people move around in their surrounding areas (Lopes, 2000). The most straightforward criterion that measures the scale of RSAs is population. One strict guidance of the shortage designation is that the population in the RSAs should not exceed 250,000 (HRSA, 2020). However, this upper population limit is not very powerful as the size of one RSA is always smaller than this threshold in practice. To better use the population limit to guide the RSA scale selection, different population thresholds will be examined to select the appropriate RSA sizes in the community structure hierarchy. More specifically, the population threshold is used as the upper population limit of the RSAs. In case the current result has RSAs over this population limit, one will go down a level in the hierarchical structure to select a finer scale of RSAs. An example is shown in Figure 2.3. The structure 1 has two communities, if community 1 is over the population threshold, it will be further split into its next hierarchy, generating structure 2 on the right side.

While population is an effective criterion for determining the RSA sizes, it is always a uniform threshold across the study area. However, people are not evenly distributed across the space and neither are health resources. In particular, rural and urban populations can have significantly different travel patterns to visit health providers (Luo, 2004). In rural areas, people need to travel further due to the sparsity of the health providers, while the urban population has relatively easier access to the providers. When the population limit is uniform, it will lead to significantly different areal sizes for RSAs in rural and urban areas.

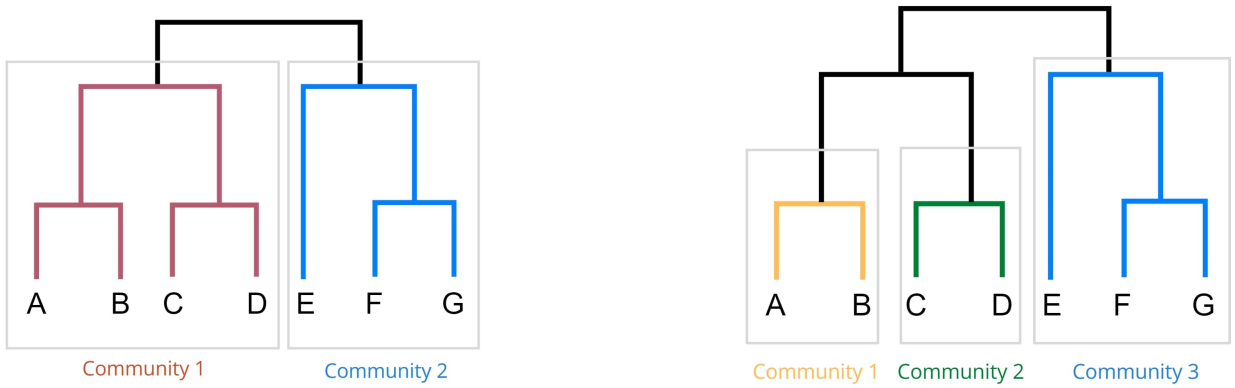

(a) Structure 1 (b) Structure 2

Figure 2.3: Hierarchical community structure examples.

Given the same population constraint, rural areas tend to form a larger community than urban areas due to the low population density. However, this can lead to disadvantages for rural areas as they have to travel further to receive health resources with larger areal sizes (Hart et al., 2002). In addition, there exist small areas with high needs for health resources, but once they are grouped with other areas into a larger-area RSA, their shortage cannot be identified. To address this problem, different population parameters are adopted in the RSA development to reduce the inequalities between rural and urban areas. The goal is to make sure that areas with large area sizes but low population density (such as some rural census tracts) can receive enough attention.

In summary, different population constraints in rural and urban areas are adopted in the RSA development. When multiple census tracts are grouped as an RSA, a rural population percentage is calculated. If the percentage exceeds a pre-defined value (e.g., 50%), the RSA is considered as a rural RSA and rural constraints are applied; otherwise, urban constraints are used. The rural and urban population definition is provided by the Health Resources and Services Administration (HRSA) (HRSA, 2021). It combined the rural area definitions from the United States Census Bureau and the Office of Management and Budget, and incorporated that with Rural-Urban Commuting Area codes to create their own definition. The final rural areas are defined at the census tract level. Figure 2.4

shows the spatial distribution of rural and urban census tracts in the State of Wisconsin.

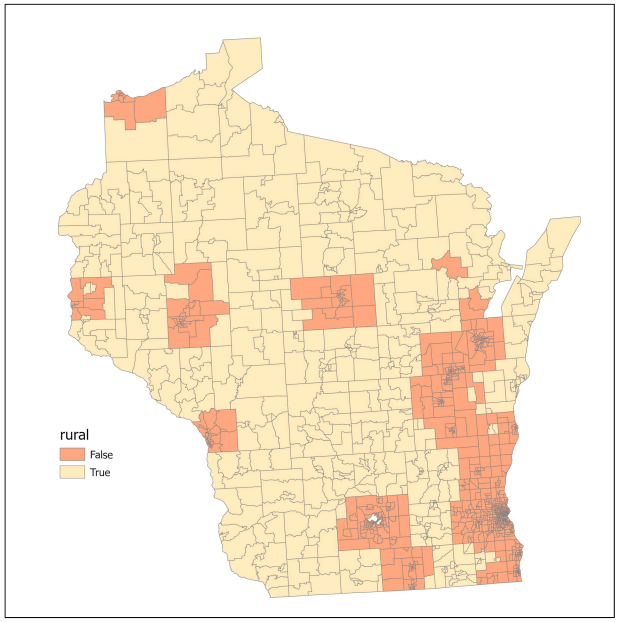

Figure 2.4: The rural and urban census tracts distribution in Wisconsin by HRSA definition (HRSA, 2021).

In addition to population, the number of census tracts in an RSA is jointly used as a constraint to ensure more stable results. Depending on the rural population percentage in each RSA, the population and census tract constraints are different. The RSAs with population and number of census tracts larger than the constraints will be selected and further split.

The process is implemented as Phase 2 in Figure 2.2. In each iteration, the community detection method is conducted first to generate the optimal communities. The rural population percentage is calculated to decide whether each community is considered as rural or urban, and be assigned with corresponding split parameters. Then the communities are evaluated based on the population and census tract number constraints to determine if they need to be further split. If they need to be split, the community is sent back to the community detection algorithm to be split into its lower hierarchy.

It should be emphasized that the creation of RSAs in no way implies that residents must seek and obtain services within their areas. The purpose of defining RSAs is to analyze

health-related travel patterns and to identify gaps in health resource allocation planning.

Spatial Constraints After the implementation of the community detection algorithm with the population constraint, the whole area is split into a set of communities (i.e., candidates of RSAs). However, the division cannot always be used immediately because the spatial relationship of geographic units is not directly considered in the community detection method and may lead to some disconnected or isolated communities. To solve this problem, geographic adjacency is used to enforce spatial contiguity by cutting disconnected communities and merging small communities with their neighboring communities.

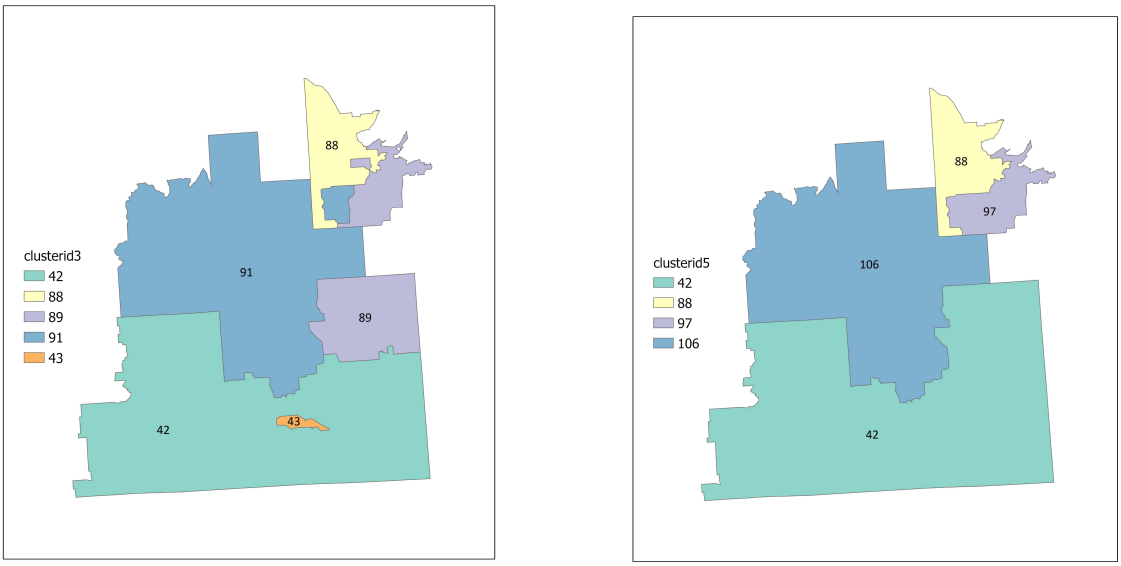

(a) Before (b) After

Figure 2.5: The communities before and after enforcing the spatial contiguity constraint.

First, all communities that are not spatially contiguous are identified, and this is implemented by building a subgraph for each generated RSA based on the spatial adjacency matrix and looking for the minimum cut in each subgraph. The minimum cut is the minimum total weight of edges that need to be removed to separate the graph into two components (Stoer and Wagner, 1997). If the graph is already not spatial contiguous, the minimum cut will be 0 and this indicator can help find all the disconnected RSAs. The

approach can support the automatic identification of non-contiguous RSAs and is very helpful especially when one has a large number of regions to analyze.

After cutting all the non-contiguous RSAs, the remaining problem is to merge the small and isolated RSAs with their neighboring RSAs. A threshold of census tract count is used to determine the size of small RSAs (e.g., if an RSA has only two census tracts, it is considered as a small RSA in this study). In the merging process, each small RSA or isolated RSA will go through an iteration, where it will be merged with each of its neighboring RSAs and the global modularity will be re-calculated after the merge. The RSA will finally be merged with the neighbor RSA that can generate the maximum modularity.

Figure 2.5 shows an example of enforcing the spatial constraint in our algorithm. Without considering spatial contiguity, the purple color community, number 89, is disconnected as shown in Figure 2.5a. So is the blue community, number 91. In addition, the orange community, number 43, is an isolated census tract surrounded by another community 42. The disconnected communities 89 and 91 are first cut into separate ones, with part of them being considered as small isolated communities that need to be merged. The small communities are then identified and merged into their neighboring communities. Figure 2.5b shows the result after the cut-merge steps; the remaining four communities are all spatially contiguous.

Phase 3 in Figure 2.2 describes the process of enforcing the spatial constraint. The min-cut of each community is calculated first to identify and cut the non-contiguous communities. The small communities are then merged into neighbor communities. The final communities are obtained after these two steps.

2.2.3 Evaluation Metrics

Two aspects are considered to measure the RSA performance using our proposed method. The first part focuses on the RSA shapes and its components, and the second part focuses on the health shortage areas identified based on RSAs.

RSA measures The evaluation of RSAs focuses on the division result of community detection, specifically on the geographic structures of generated communities. The following metrics are used.

The *geographic compactness* is used to measure the regularity of a region's shape based on the perimeter-area corrected (PAC) ratio. As shown in Equation 2.1, it calculates the ratio of the perimeter of a shape to the square root of its area (MacEachren, 1985; Hu et al., 2018). A low PAC value indicates a more compact region size around its central point (e.g., a circle) (Hu et al., 2018) while a high PAC value means a more irregular shape that spreads out.

$$\mathrm{PAC} = \frac{\mathrm{Perimeter}}{3.54 * \mathrm{sqrt}(\mathrm{Area})} \tag{2.1}$$

The *balance in region sizes* measures the evenness of several aspects across RSAs, such as the number of census tracts, population, and providers. A more balanced distribution of numbers across all RSAs means that they are more equally representative of the whole region and the variances of RSAs are small.

HPSA scoring Besides the RSA structure evaluation, one important application of RSAs is that they are used as the basic units for Health Professional Shortage Areas (HPSAs) designation. The providers in the HPSAs will receive incentives or financial assistance to support them in better serving the shortage areas (Luo, 2004). To understand the performance of developed RSAs, the Primary Care Geographic HPSAs are identified based on four criteria used in the Shortage Designation Management System (HRSA, 2020). The population-to-provider ratio, the percentage of the population at 100% Federal Poverty Level, the infant health rate, and the travel time or distance to the nearest non-designated provider are calculated and scored. Figure 2.6 shows how the HPSA score is calculated using the national guidebook (HRSA, 2020). The demographic information required to calculate the population-to-provider ratio and percent of individuals below 100% of

the federal poverty level is collected through the U.S. Census Bureau. The infant health index is calculated based on the infant mortality rate and low birthweight rate, and the data is collected from the Centers for Disease Control and Prevention (CDC). The travel time/distance is calculated based on the locations of providers using ArcGIS "Find nearby locations" tool. The final HPSA score is a weighted sum of the four criteria and is calculated for each RSA. A higher HPSA means that the area is under a greater shortage of providers. More details about how HPSAs are finalized can be found in the HPSA designation manual (HRSA, 2020).

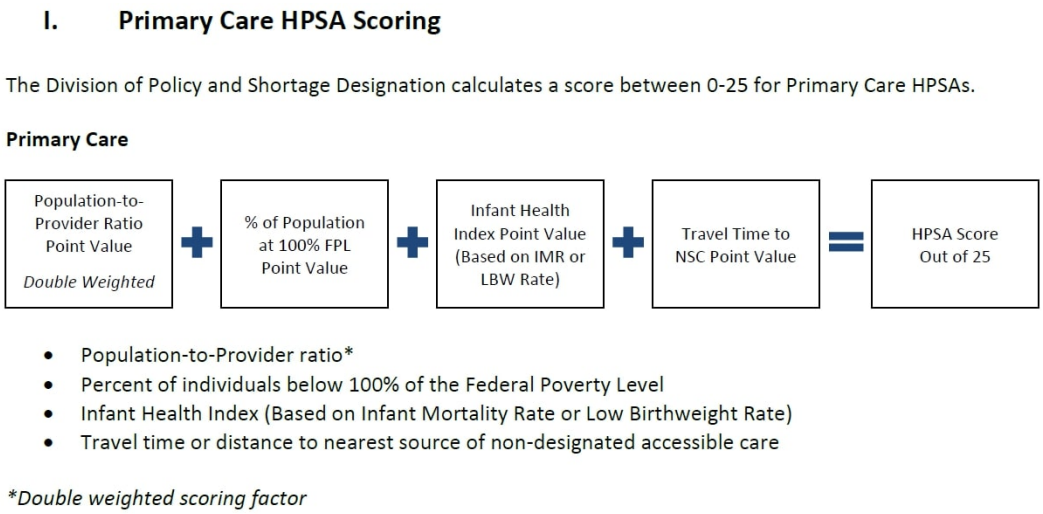

Figure 2.6: The Primary Care HPSA scoring criteria.

After establishing HPSAs in the study area, the number of HPSAs, the population covered by HPSAs, the population-to-provider ratio in HPSAs and the average HPSA scores are used as HPSA evaluation metrics. Given a certain RSA plan, the HPSA scores are generated, and the identified HPSAs are evaluated. A Python toolbox in ArcGIS is also developed to support the automation of the RSA generation and HPSA designation process.

2.3 Results

2.3.1 Community Detection

Five scenarios are implemented to compare the performance : (1) the proposed Auto-RSA-HPSA method with rural/urban constraints using the random walk algorithm, (2) the proposed Auto-RSA-HPSA method with rural/urban constraints using the Louvain algorithm, (3) the proposed Auto-RSA-HPSA method with rural/urban constraints using the Leiden algorithm, (4) the proposed method with only a population constraint of 250,000 using the random walk algorithm (abbreviated as random walk baseline), and (5) the Dartmouth method.

The number of derived RSAs for the five scenarios, the rural/urban constraint parameters, and their average running time over ten iterations are listed in Table 2.1. The random walk, Louvain and Leiden represent the proposed Auto-RSA-HPSA method implemented using the corresponding algorithm, respectively. The number of RSAs is closely related to the selection of rural/urban parameters. The optimal rural/urban parameters of Scenario 1 using the random walk algorithm are selected based on the sensitivity analysis that will be introduced later. Scenario 2 and 3 parameters are selected in order to generate a similar number of RSAs as Scenario 1 so that their scales are comparable. Scenario 4 - random walk baseline uses the proposed Auto-RSA-HPSA method with only a population constraint of 250,000. Therefore, the number of RSAs from the random walk baseline is fewer than that of the previous scenarios because of the population constraint. The Dartmouth method result is obtained from the official website of Dartmouth Atlas project (Wennberg and Cooper, 1998). The execution times of the scenarios are relatively similar, and the Auto-RSA-HPSA method using random walk requires a slightly longer execution time than the rest of the scenarios.

The result of the Auto-RSA-HPSA method with the random walk algorithm (Scenario 1) is used as an example to illustrate how the RSAs are derived step by step. The initial

derived RSA result from the random walk algorithm is a global optimal result when the maximum modularity is reached without any additional constraints. The result map is shown in Figure 2.7a, where in total there are 18 communities with each census tract colored according to its community membership. Based on the urban/rural constraints in Table 2.1, and the rural/urban population ratio threshold of 0.5, all 18 communities are selected to be further split. This process iterates until all communities fulfill the population constraints. The result after the splits is shown in Figure 2.7b. There are 205 communities in total and the communities (i.e., RSAs) become much smaller compared with Figure 2.7a. Then, the spatial contiguity constraint is enforced to cut and merge the communities. The final result of the community detection is shown in Figure 2.7c. The number of final communities is 164. Compared with the results before the spatial contiguity constraint step, many small communities are merged with nearby communities.

Table 2.1: The number of derived RSAs, the constraint parameters and the average execution time (seconds) over 10 iterations for all the scenarios

Scenario	**1**	**2**	**3**	**4**	**5**
Method	Random Walk	Louvain	Leiden	Random Walk baseline	Dartmouth
Number of RSAs	164	169	165	70	100
Rural population	20000	40000	40000	250000	N/A
Urban population	40000	70000	70000	250000	N/A
Rural Census Tracts	3	6	6	0	N/A
Urban Census Tracts	10	18	18	0	N/A
Execution time (s)	59.2	54.5	54.7	54.7	N/A

To ensure that the data in the selected time range (August-October 2021) are representative, an additional 1-year data in 2019 is also collected. The origin-destination flow matrices of these two periods have a high structure similarity of 0.94 (Jin et al., 2020). In addition, the same method in Scenario 1 is implemented using the 2019 data and the generated RSA results are compared with results using the Aug-Oct 2021 data. As shown in Figure 2.8a, using the data from 2019, the Auto-RSA-HPSA method using random walk generates 162 RSAs. The data from 2021 generates 164 RSAs and is on Figure 2.7c. By visual

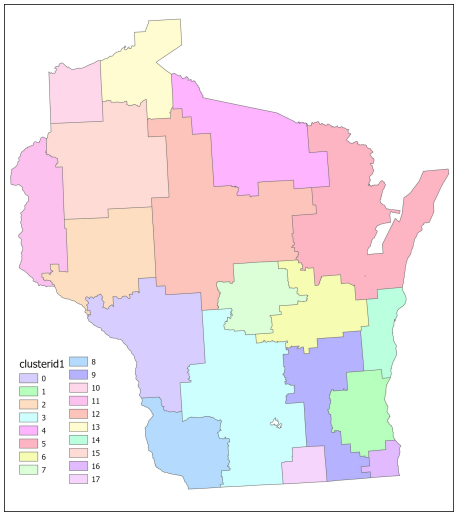

(a) With no constraints

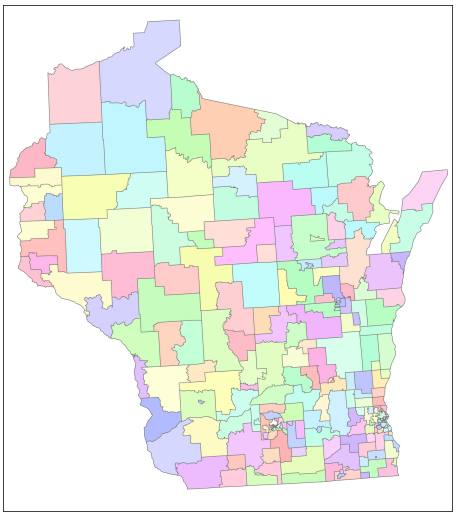

(b) With population constraints

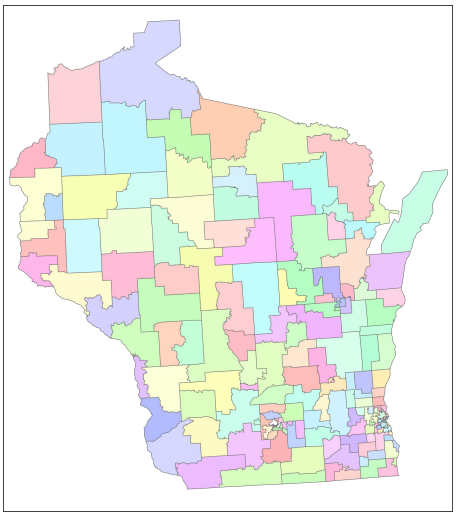

(c) With population and spatial constraints

Figure 2.7: The result maps of Scenario 1: Auto-RSA-HPSA method using random walk.

examination, many RSAs are identical in both results or have similar shapes. The two RSA results are overlaid together using different boundary colors (Figure 2.8b), and most of the boundaries are the same with a few differences. Therefore, the selected 3-month data result is representative enough to be used in our case study. It is suggested that when the method is implemented for practical applications in other regions, one may keep updating the mobility data regularly to obtain the most up-to-date RSA delineation results.

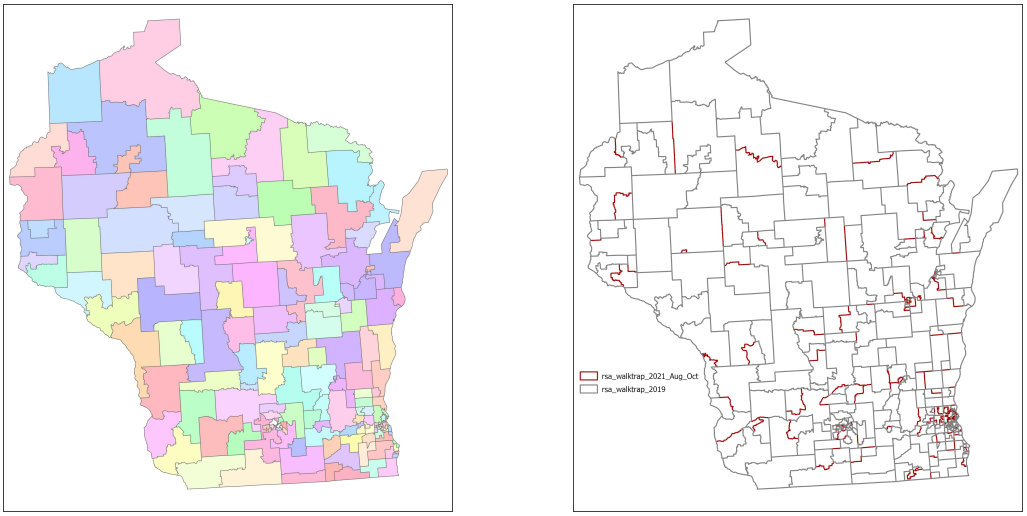

(a) RSAs generated from 2019 data (b) The overlaid boundaries

Figure 2.8: The RSAs generated using 1-year data in 2019 and the overlaid boundaries with the RSAs generated using 3-month data in 2021.

2.3.2 RSA Evaluation

Besides the visual comparison, multiple quantitative metrics are computed for the five scenarios to evaluate the quality of RSAs.

Geographic Compactness The PAC ratio measures the regularity and the compactness of the shapes. As shown in Figure 2.9a, the RSAs derived by the proposed Auto-RSA-HPSA method using random walk, Louvain and Leiden have very similar PAC values and their interquartile range (represented by the black rectangle) are lower than that of the random walk baseline and the Dartmouth method. The RSAs from Scenario 1 - random walk and Scenario 3 - Leiden have slightly lower median PAC values (represented by the orange line) than that of Scenario 2 - Louvain algorithm. The RSAs from Scenario 4 - random walk baseline have a larger median PAC value compared with the Auto-RSA-HPSA methods' results and the RSAs from the Dartmouth method have much larger PAC values. The small PAC values in Scenarios 1, 2 and 3 indicate that our proposed Auto-RSA-HPSA methods with rural/urban constraints generate more regular and consolidated shapes, which is more favorable in RSA development.

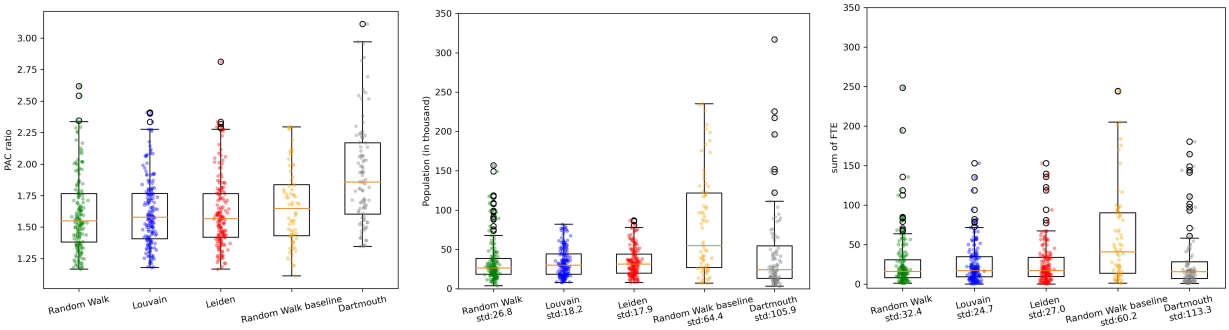

(a) Perimeter-Area Ratio (b) Population Range (c) FTE Range

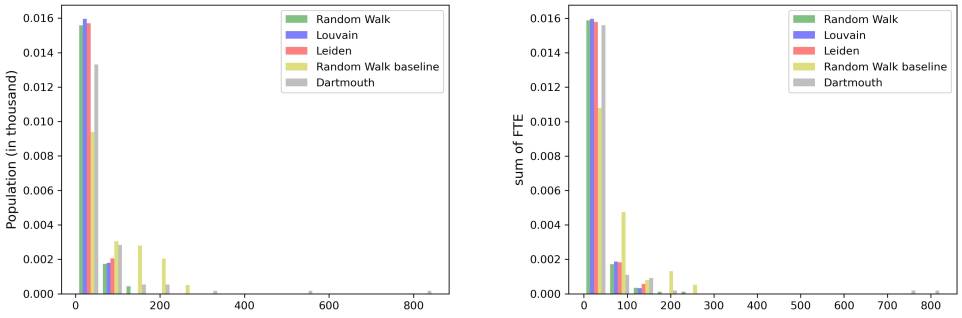

(d) Population Distribution (e) FTE Distribution

Figure 2.9: The multiple metrics used for evaluating RSAs (std: standard deviation).

Balance in region sizes The balance in region sizes is measured using the population in each RSA and the total providers in each RSA, represented by the full-time equivalent (FTE). The box plots of the population distribution in each scenario are shown in Figure 2.9b and the standard deviation is also calculated and shown in the x-axis labels. The data for the proposed methods using random walk, Louvain, and Leiden are generally more concentrated and have smaller values than the other two scenarios. Scenario 4 using the random walk baseline method has widely distributed data values. For Scenario 5 of the Dartmouth method, although there are data distributed at the bottom of the box plot, it also has a few outlier values that go beyond the whisker range, some of the outliers are over 350 thousand and removed from the figure. For the population standard deviation, the results from Scenarios 1, 2, and 3 have much smaller standard deviations than the results in Scenarios 4 and 5. Among the first three scenarios, the RSAs from the Leiden algorithm have the smallest population standard deviation. The random walk baseline using only

a population limit of 250,000 has the second-largest standard deviation. The Dartmouth method yields the greatest standard deviation. Figure 2.9d shows the histogram of the same population data, it is clear that the proposed methods using random walk, Louvain, and Leiden represented by the green, blue, and red bars are heavily right-skewed because of their small RSA sizes. Most of the data are distributed in the first bin. Figure 2.9c shows the box plot of the provider FTE. For the proposed methods using random walk, Louvain and Leiden, the data are mostly distributed near the bottom of the box plot. This is also reflected by the histogram of the FTE data in Figure 2.9e: data of Scenario 1, 2, 3 are heavily right-skewed. The FTE standard deviation shows similar trends as the population standard deviation, with the proposed Auto-RSA-HPSA methods yielding the smallest standard deviations and the Dartmouth method having the greatest standard deviation. The RSAs from the Auto-RSA-HPSA method using the Louvain algorithm have the smallest FTE standard deviation. The smallest standard deviations of population and FTE distribution indicate that the proposed methods generate more equally distributed regions, and the RSAs are more balanced in terms of population and provider distributions.

2.3.3 HPSA Delineation and Scoring

The five scenarios of RSAs are then used to further identify HPSAs, which include primary care, dental care, and mental health care providers but with different criteria. In this chapter, the effectiveness of our proposed Auto-RSA-HPSA method is only demonstrated using the primary care provider data while the analyses for all the care types are completed in collaboration with the Wisconsin Department of Health Services. Figure 2.10 shows the final HPSAs for the five scenarios, where the blue-shaded regions are Primary Care Geographic HPSAs. From the visual examination, the first three scenarios of the proposed methods with rural/urban constraints have greater HPSA coverages than the remaining two scenarios. The distribution of HPSAs for Scenarios 1, 2 and 3 are similar but with small differences. On the northern part of the study area, the area sizes of the HPSAs tend to

be large, and on the southern part the HPSA areas become smaller. Based on Figure 2.4, most of the northern part of the study area is defined as rural areas. The difference in area sizes reflects one goal of the proposed framework: people in rural and urban areas have different travel patterns to receive health services, and this difference should be reflected in the RSAs.

Table 2.2 shows the statistics of the HPSAs including the number of HPSAs, total population and providers Full-Time Equivalent (FTE) covered, the population-to-provider ratio and the average HPSA scores. Scenarios 1, 2, 3 are first compared, as they represent the proposed Auto-RSA-HPSA method with different community detection algorithms. Scenario 1 with the random walk algorithm generates the greatest number of HPSAs. For the total population covered by HPSAs, the HPSAs from Scenario 3 using the Leiden algorithm cover the maximum population of 804,277, which is significantly more than that of other scenarios. The population covered by the HPSAs from Scenario 1 using the random walk algorithm is a little more than that of Scenario 2 using the Louvain algorithm. For the number of providers covered by the HPSAs, it is measured using the full-time equivalent of providers. Among Scenarios 1-3, the HPSAs derived from Scenario 3 using the Leiden algorithm cover the least amount of providers. The following metric, the population-to-provider ratio measures the provider shortage. It reflects on average how many people visit the same provider. The HPSAs from Scenario 3 using the Leiden algorithm have the highest ratio of 7018.1, meaning that the HPSAs are under the greatest provider shortage compared with that in Scenario 1 and 2. Scenario 3 using the Leiden algorithm also has the highest average HPSA scores, and Scenario 1 and 2 have the same second highest score.

Then, Scenario 1-3 are compared with Scenario 4 and Scenario 5. Scenario 4 using the proposed framework with a population constraint of 250,000 identifies 12 HPSAs out of 70 RSAs, which is the fewest HPSAs of all scenarios. In addition, HPSAs from Scenario 4 have the lowest population-to-provider ratio as well as the lowest HPSA score. Scenario 5 using the Dartmouth method has 13 HPSAs out of 100 RSAs. The HPSAs identified from Scenario

5 cover the fewest amount of population with the second lowest population-to-provider ratio. The HPSA score is also lower than that of the first three scenarios.

In summary, the proposed Auto-RSA-HPSA methods with rural/urban constraints can outperform other baselines in the number of HPSAs, the level of HPSA shortage and the average HPSA score. The proposed Auto-RSA-HPSA method using the Leiden algorithm has the best performance in HPSA metrics among the three community detection algorithms.

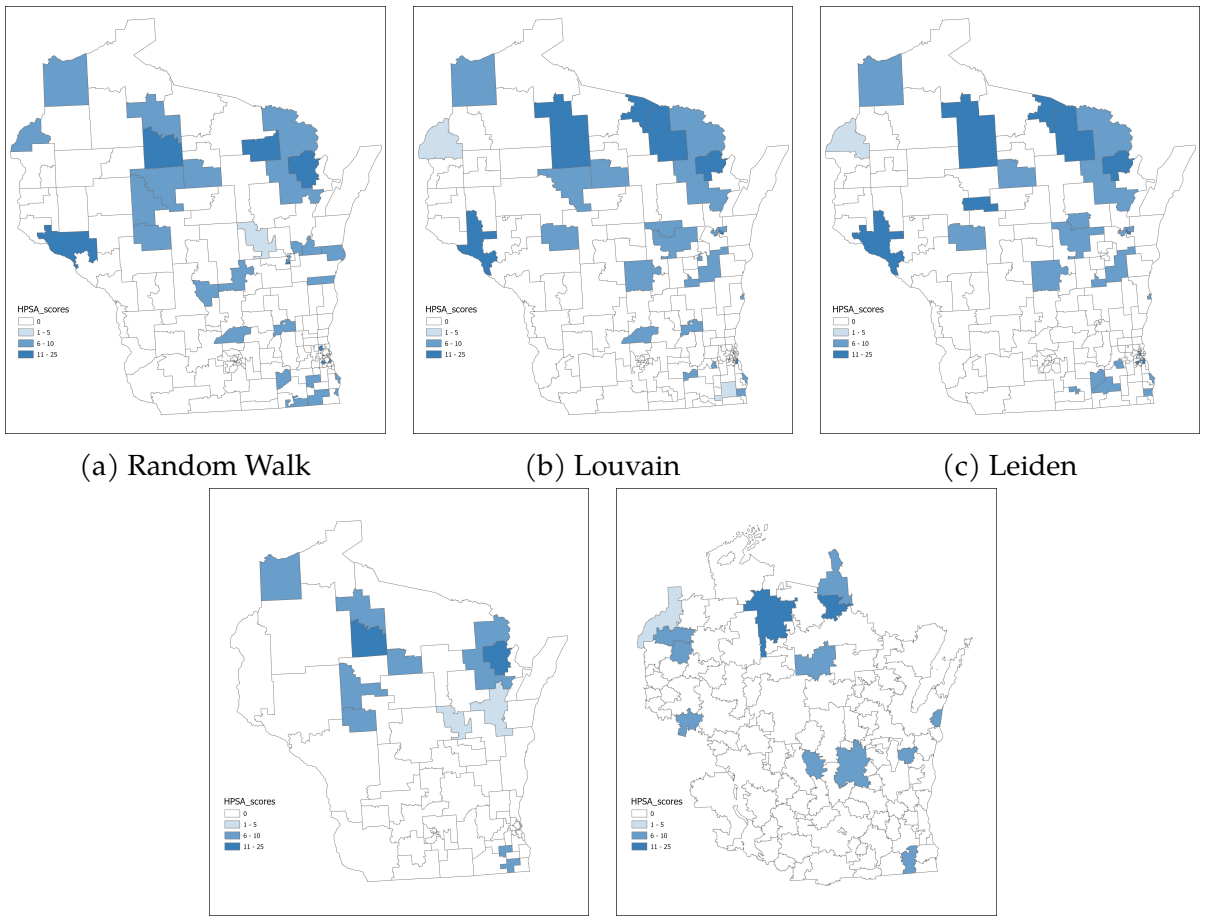

(a) Random Walk (b) Louvain (c) Leiden

(d) Random Walk Baseline (e) Dartmouth HSA

Figure 2.10: The maps of HPSAs for the five scenarios.

Table 2.2: The HPSA statistics for all the scenarios.

Scenario	**1**	**2**	**3**	**4**	**5**
Method	Random Walk	Louvain	Leiden	Random Walk baseline	Dartmouth
Number of RSAs	164	169	165	70	100
Number of HPSAs	36	32	34	12	13
Population	744681	739796	804277	412464	218872
Provider (FTE)	125.5	121.1	114.6	100.9	46.7
Population: FTE	5932.5	6111.5	7018.1	4086.8	4686.8
Average HPSA score	9.4	9.4	10.2	8	8.6

2.3.4 Sensitivity Analysis

Two parts of the proposed method require parameter setting. The first one is the rural population percentage threshold that decides whether an RSA is considered as rural or urban. The second part is the rural/urban constraints including the population and the number of census tracts that affect whether an RSA should be further split or not. The sensitivity analysis is conducted to understand the effect of those parameters on the results using the Auto-RSA-HPSA method with the random walk algorithm.

Rural Population Percentage Threshold In the process of RSA development, whether an RSA should be assigned the rural or the urban parameters depends on the percentage of the rural population. If the rural population percentage is above the pre-defined threshold, rural parameters are applied; otherwise, urban parameters are applied.

This percentage threshold can vary across regions and affect the final RSA development. To understand and quantify the effects of this threshold, a range of rural population percentages are selected to generate the RSAs. As the ultimate goal of RSA development is to identify areas with healthcare shortages for future resource allocation, the performances are measured primarily based on the HPSAs that can be identified from the results. The number of HPSAs, the rural and urban populations covered by HPSAs, and the amount of providers in the HPSAs are calculated as evaluation metrics.

As shown in Table 2.3, the number of RSAs and HPSAs generated from different

thresholds are almost the same, with a slight change for thresholds 0.7 and 0.8. The results for rural and urban populations covered by HPSAs are shown in Figure 2.11a, where from threshold 0.2 to 0.6, the results are relatively stable. The rural population (represented by the orange bar) drops at thresholds 0.7 and 0.8. Compared with previous thresholds, a higher rural population percentage threshold will make more areas be defined as urban and assigned with urban parameters. This can affect the final numbers and shapes of RSAs and HPSAs. At threshold 0.8, both the rural population and the urban population are lower than the result of the remaining thresholds. Figure 2.11b shows the providers covered by the HPSAs. Similar to the population trend shown in Figure 2.11a, the number of FTE of the HPSAs is stable for a threshold from 0.2 to 0.6. The total FTE starts decreasing at threshold 0.7 and reaches its lowest value at threshold 0.8.

In summary, when the rural population percentage threshold changes from 0.2 to 0.8, the numbers of RSAs and HPSAs are very stable. There are some variances for population and providers covered, but the results are generally stable, especially between the range of 0.2 to 0.6. The threshold of 0.5 is used in the proposed method presented above.

Table 2.3: The number of HPSAs and RSAs using different rural population percentage thresholds.

Rural Population Threshold	**0.2**	**0.3**	**0.4**	**0.5**	**0.6**	**0.7**	**0.8**
Number of HPSAs	36	36	36	36	36	34	34
Number of RSAs	165	164	164	164	164	163	163

Rural/Urban Population Constraints As mentioned above, the population constraint is applied to determine whether an RSA should be further split and this constraint is different for rural and urban areas. The selected population and census tract thresholds can affect the desired community scales. According to the National Shortage Designation Process in the U.S. (HRSA, 2020), a whole county is considered rational for an RSA with no further justification. The counties have been frequently used as RSAs by state officials from the Department of Health Services in Wisconsin. Therefore, the population thresholds are

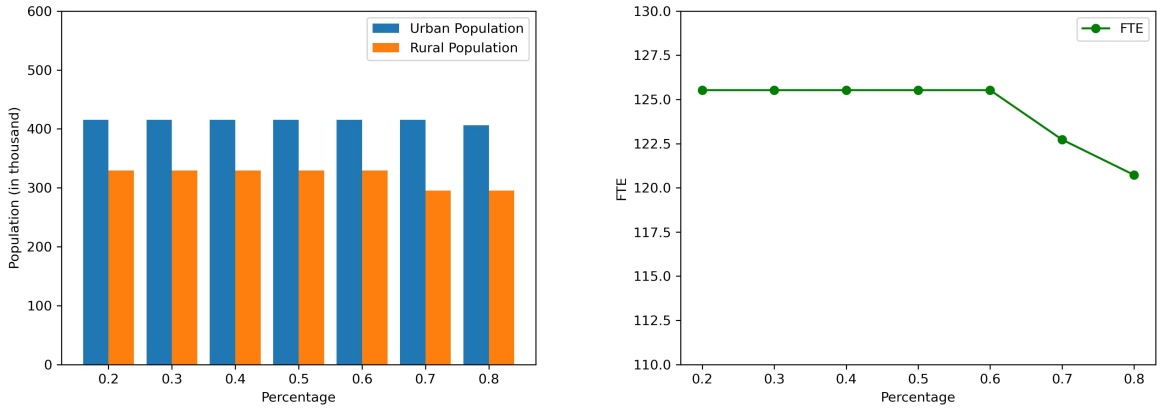

(a) Rural and urban population (b) FTE

Figure 2.11: The total rural and urban population and FTE covered by HPSAs using different rural population percentage thresholds.

selected based on the population statistics of counties in Wisconsin in Table 2.4. The 25% and 75% of the population percentiles are used as the approximate range of our population threshold to ensure that the final RSAs derived from our proposed method have a similar size with counties in Wisconsin. Our method can take different parameter values as the inputs of the Python tools embedded in a GIS environment, which enables users from other States to select their preferred population thresholds.

Table 2.4: The quartile statistics of county population in Wisconsin

Min	25%	50%	75%	Max
4254	18773	39336	84304	929362

Multiple sets of parameters are selected to examine their effects on the final RSAs and HPSAs for the proposed Auto-RSA-HPSA method using the random walk algorithm (Table 2.5). Generally, the rural parameters are smaller than the urban parameters so that rural areas can have finer-resolution RSAs. Take Case 1 as an example, if there is an RSA with 60,000 population and 15 census tracts in urban areas, it would remain the same RSA; but if it is in rural areas, it should be split because it meets the constraint of rural areas. Case 3 has the same parameters for rural and urban areas, and it is used as a comparison with

our proposed Auto-RSA-HPSA method to represent the case where there is no parameter difference for rural and urban areas. The other cases are listed in descending order of population constraints.

Table 2.5: The parameters selected for rural and urban constraints (Pop: population, CT: number of census tracts)

	Urban Pop	**Urban CT**	**Rural Pop**	**Rural CT**
Case 1	80000	20	60000	15
Case 2	60000	15	40000	12
Case 3	40000	10	40000	10
Case 4	40000	10	20000	3
Case 5	30000	8	10000	2

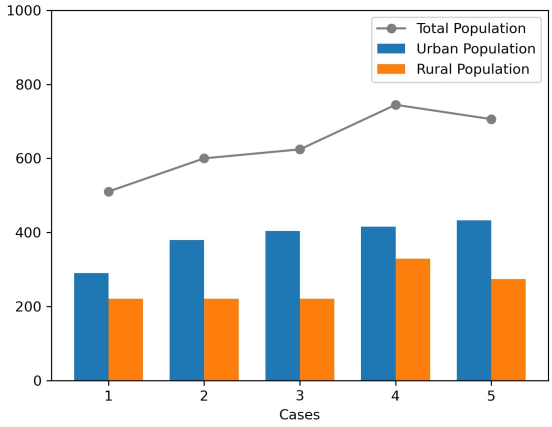

(a) Population (in thousand) covered

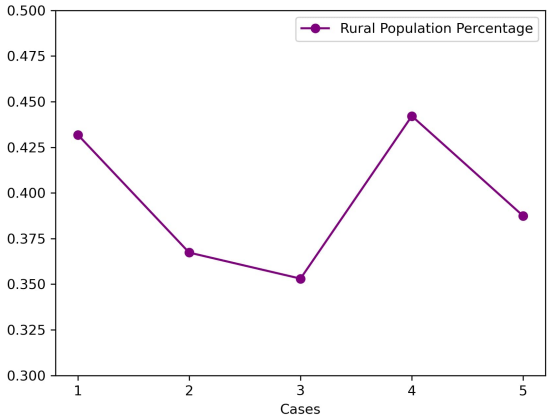

(b) Rural population percentage

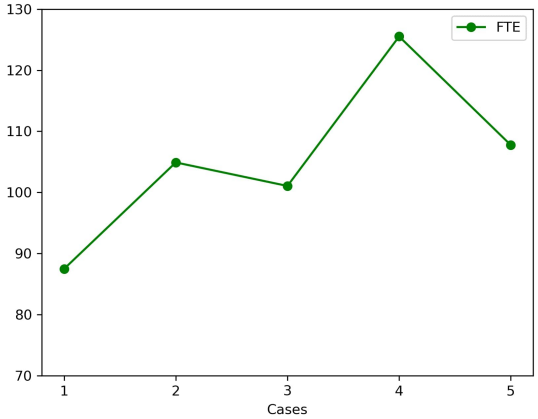

(c) FTE

Figure 2.12: The total population, rural population percentage, and FTE covered by HPSAs using different urban/rural parameters.

The urban population, rural population and total population covered by the HPSAs from the five cases are plotted in Figure 2.12a. The urban population covered (represented by the blue bar) shows an increasing trend for the five cases. For the rural population (represented by the orange bar), it remains stable for Cases 1 to 3, reaches its peak for Case 4 and drops a little for Case 5. Compared with Case 3, Case 4 has the same urban parameters and smaller rural parameters, and Case 4 has significantly more rural population and total population covered. The result of Case 3 is what one would obtain when rural and urban areas are treated in the same way, with fewer rural populations covered in the shortage areas. Based on the comparison between Case 3 and Case 4, applying different rural and urban population constraints helps identify more rural populations in the shortage areas, and the urban population covered is not affected. This demonstrates the advantage of the proposed Auto-RSA-HPSA method as it takes the difference between rural/urban areas into consideration, while other traditional methods do not.

Figure 2.12b shows the rural population percentage covered by the HPSAs for all the cases. Case 3 has the lowest rural population percentage due to its same parameter setting for rural and urban areas, and also indicates the disadvantages of rural areas in the traditional methods. Case 4 has the highest rural population percentage. In Figure 2.12c of total Full-Time Equivalent providers covered, Case 4 also obtains the maximum value. Case 5 has the smallest population constraints, but the performance drops for Case 5, with a lower rural population, slightly higher urban population and lower FTE compared with Case 4. Therefore, Case 4 is used as a representative result of our proposed method using the random walk algorithm.

2.3.5 GIS Tools for Automating the RSA and HPSA Delineations

To further support the utilization of the proposed Auto-RSA-HPSA method in public health decision-making, a set of Python toolboxes in ArcGIS is developed. As presented in Figure 2.13a, this toolbox set has multiple steps including data preparation (tools 1-2),

RSA generation (tool 3), candidate HPSAs evaluation (tool 4), travel time calculation (5) and the HPSA scoring steps for all types of HPSAs (tool 6-10). The whole process follows the Shortage Designation Process (HRSA, 2020) and is developed under iterative discussions with the state officials from the Wisconsin Department of Health Services. The community detection for RSA development is completed in an external Python script that can be executed automatically with different rural/urban parameters. The community/RSA membership result is used as one input for the toolboxes. Figure 2.13b shows the required parameters for creating RSAs in tool 3. The user needs to provide the base census tract layer from the previous toolbox (step 2), and the community membership file. Then, the toolbox can generate the RSA layer and the population centroid, which can be further used for HPSA scoring.

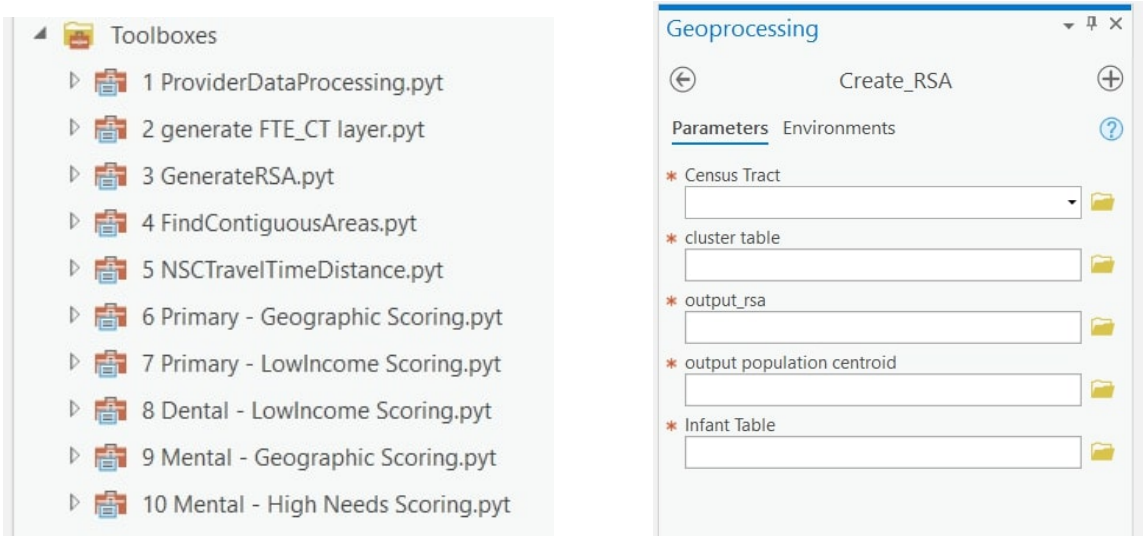

(a) The overview of all toolboxes (b) The toolbox for RSA generation

Figure 2.13: The toolboxes for the Auto-RSA-HPSA method in ArcGIS.

2.4 Conclusion

RSAs are fundamental units for understanding health-care markets and evaluating resource allocation effectiveness. In this chapter, a spatially-constrained community detection method with the consideration of rural/urban differences to identify RSAs is proposed.

The method can better reflect the fact that health resources are unevenly distributed across space. The proposed method generates more regularly shaped RSAs and is more balanced in region sizes than other baselines. The identified RSAs are further used to establish the Health Professional Shortage Areas through multiple spatial and non-spatial scoring criteria. The introduction of rural/urban parameters helps identify more shortage areas, cover more rural populations and receive higher shortage scores. The result demonstrates the importance of such consideration by showing more rural shortage areas can benefit from the new designation plan. The method also provides more possibilities for solving such health inequality problems using GIS tools.

The proposed method is a data-driven approach without any additional manual adjustment if using our default parameter settings. Compared with the manual process that many public health officials are using, this method builds a carefully designed methodological framework that can be automated through the provided toolbox. In addition, the result RSAs can be generated at different geographic scales. One can adjust the population constraints based on different regional characteristics to create desirable area sizes. Due to this ability, the method can support repeatable and efficient analysis to assess the results under different scenarios. This also helps policymakers evaluate the proposed RSA plan in a more consistent and statistically sound way. In addition, a Python toolbox embedded in a GIS environment was developed, and it requires very little programming knowledge to execute. This enables a broader range of users to access the toolbox and conduct analyses on their own.

Compared with existing studies, which mostly used patient-hospital flows, this study uses mobility-based health place visits to extract RSAs. The mobility patterns may provide another dimension to understanding the local healthcare market as they reflect how people travel to receive health services. As shown by the result, valuable information from human mobility can support better RSA and HPSA development in the public health domain.

There are also some directions to improve for future work. First, the spatial network is

directed in reality but taken as undirected in this research. More analyses can be conducted to understand the effects of different graph construction methods on the final RSA/HPSA results. Second, the health visits data used in the method may still contain some bias as it may not include all the health-related places; it is suggested that more analyses can be added with hospitalization data when available. Also, the mobility flow is from people's home locations to different places, while people may also travel from work locations to visit providers/hospitals. Additional data sources, such as commuting flows, can also be explored in the future.

3 GEOAI FOR COMMUNITY DETECTION USING NODE FEATURES AND EDGE CONNECTIONS

3.1 Introduction

Networks or graphs are often used to model many phenomena and relationships in the real world. For example, traffic moves along the transportation networks in geographic space, people connect through social networks, and academic scholars reference each other in the citation network. A network or graph usually consists of nodes and edges. The nodes can represent real-world entities and the edges are the connections between entities. In a spatial network, nodes can be geographic entities such as locations, roads, road intersections or administrative areas (Zhu et al., 2020), and edges can represent the spatial interactions among nodes (Barthélemy, 2011; Gao et al., 2013; Liu et al., 2016; Ye and Andris, 2021). The spatial interaction intensity can be used as the edge weights. Such spatial networks contain rich information, but they are always in a complex structure with many interrelated components.

Community detection algorithms have been widely used to extract information from complex networks and detect densely connected nodes in a network. Through the detected communities, studies can further identify the hidden relationship among network components and reveal the underlying network structures (Su et al., 2021; He et al., 2021; Expert et al., 2011). Traditional community detection algorithms focus on using the edge connections to form communities. However, there is valuable information in the node attributes as well. Traditional community detection algorithms also face the challenge that the computational cost increases dramatically with the expansion of networks (Su et al., 2021). Real-world networks may contain millions of nodes/edges with complex information and high-dimensional attributes. The past few years have witnessed a significant development in adopting DL methods to solve the limitations of traditional community detection methods.

The integration of multiple information sources in DL is especially helpful for spatial networks. While other networks may only have one type of edge connection, nodes in spatial networks can have an additional geographic relationship related to their closeness. In many cases, the geographic places or regions may be spatially next to each other, leading to an adjacent relationship. For example, if a study area is divided into grids, each grid can have multiple neighboring grids surrounding it. Therefore, given a spatial network, two graphs can be constructed: a graph for the spatial interactions among nodes where edges can be quantified using flow connections and a graph for the geographic adjacency where edges can represent the binary relationship of whether two nodes are adjacent. According to the first law of geography, "near things are more related than distant things" (Tobler, 1970), which means that the nodes in spatial networks are naturally affected by their geographic neighbors, and such effects decay as two nodes become further away (Liu et al., 2012). The relationship can also be interpreted as a similarity measure, where nodes that are closer in geographic spaces tend to be more similar.

The convolutional graph-based models are great candidates to model such relationships. Convolutional Neural Networks (CNNs) were first proposed for image analysis and can consider input topology by updating each input based on its surrounding inputs in a filter (LeCun et al., 1995). Graph Convolutional Networks (GCNs) were further proposed for graph-structured data to apply CNN directly on graphs. Instead of using a fixed filter, the surrounding relationship is determined by the edge connections (Kipf and Welling, 2017). In fact, GCN has gained great attention due to its performance on node classification for graph-structured data (He et al., 2021; Kipf and Welling, 2017). GCN leverages the inherent structure of the data, and aggregates neighbor nodes' information when updating the central node's representation (Kipf and Welling, 2017). Later on, Graph Attention Networks (GATs) were proposed to improve the neighborhood aggregation function in GCN, where a self-attention mechanism is used to learn the neighborhood importance for each pair of nodes (Velickovic et al., 2017). Compared with GCN, which usually uses a

fixed rule to aggregate neighborhood information (Kipf and Welling, 2017), GAT uses the implicit attention coefficients to reflect that neighbors can have different importance to the central nodes. The advantages of GCN and GAT in modeling graph-structured data make them very useful for community detection on spatial networks and geographic contexts learning in GeoAI, especially for incorporating spatial concepts such as spatial dependence, geo-semantics, and neighborhoods (Zhu et al., 2020; De Sabbata and Liu, 2023; Janowicz et al., 2020).

Nevertheless, applying GCN and GAT to community detection faces certain challenges. The lack of labels in community detection tasks makes it hard to train GCN or GAT models directly, as they are usually supervised or semi-supervised. How to solve the unsupervised learning problem using supervised models remains a challenge (Xiao et al., 2022). Second, although GCN and GAT are used to understand graph structures and generate latent representations for nodes, their goal is not community detection or regionalization-oriented (Jin et al., 2019; Liang et al., 2022). The learning objective for GCN and GAT needs to be re-designed to meet the requirements of community detection tasks.

With the consideration of those problems, GCN-based and GAT-based unsupervised learning methods for community detection and regionalization are proposed in this research. The proposed method builds a family of GeoAI-enhanced unsupervised learning methods that are guided by a community detection-oriented loss. The GeoAI-enhanced methods consider two types of edge relationships in the spatial network: spatial interactions and geographic adjacency, and combine multi-attribute information using the GCN and GAT models to learn node representations. The communities (i.e., geographic regions) are further identified through an additional clustering step. The proposed GeoAI-enhanced community detection methods are called *region2vec*; the name indicates a general type of method that can extract latent representations (i.e., encodings) based on regions' characteristics. The used GCN and GAT models may be replaced with other models based on different use cases. This study will focus on understanding the efficacy of the proposed

methods in spatial network community detection.

The remainder of the sections are organized as follows: the proposed community detection methods is first introduced in Section 3.2. Then the comparative analyses of the proposed method against other baselines and one public health application are presented in Section 3.3. Finally, the conclusion of the study and some directions for future work are shared in Section 3.4.

3.2 Method

Some definitions for the network-based community detection problem with all the notations used in the following sections are introduced first, and the data sources used in the model are shown. Then, the proposed *region2vec* graph embedding algorithms and the clustering method are presented.

3.2.1 Notations and Problem Definitions

Graph $G = (V, E)$ is defined via a set of nodes $V = (v_1, ..., v_n)$, $|V| = n$ and edges E with $e_{ij} = (v_i, v_j)$. $A = [a_{ij}]_{n \times n}$ is an adjacency matrix representing geographic adjacency, where $a_{ij} = 1$ if $e_{ij} \in E$, otherwise $a_{ij} = 0$. $S = [s_{ij}]_{n \times n}$ is a spatial interaction matrix, where s_{ij} represents the flow intensity between node v_i and v_j. An $n \times m$ attribute matrix X is used to denote the node attributes.

The community detection groups the n nodes into K communities $\{C_1, C_2, ..., C_K\}$ and each node will be assigned with a label c_i indicating its community membership, $c_i \in \{1, 2, ..., K\}$.

3.2.2 Data

The spatial network is constructed using the SafeGraph business venue database (SafeGraph, 2023). The visit patterns to different places are collected from anonymous smartphone users and each visit contains an origin location and a destination visited place. As

a general regionalization task, the visits used in this chapter cover all types of Points of Interest (POIs) to reflect the overall travel patterns of populations. The place visit origins and destinations are then aggregated to the same geographic level (census tract in this study) to build the spatial interaction network (Kang et al., 2020). Note that other geographic scales of regions such as census block groups and counties can also be used to construct spatial interaction networks. The shapefile of U.S. census tracts is used to construct the geographic adjacency matrix (U.S. Census Bureau, 2023). The census tract level demographic attributes (e.g., income, population, race) are gathered from U.S. Census American Community Survey (ACS).

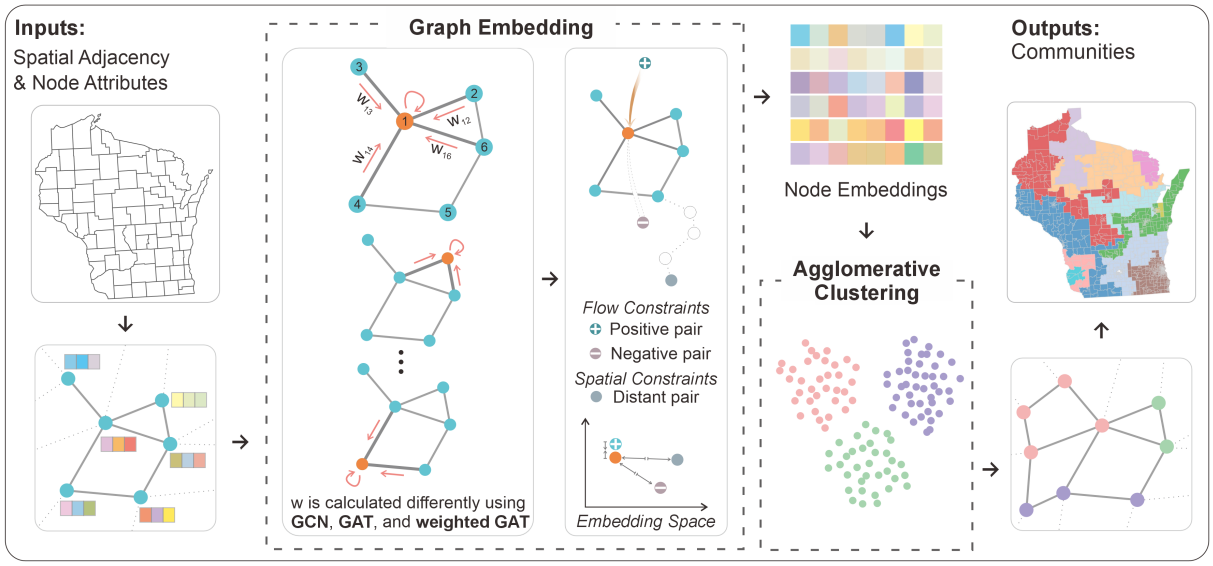

Figure 3.1: The workflow for community detection using the region2vec method.

3.2.3 Algorithms

Based on the proposed method, the identified communities should contain nodes (i.e., geographic regions) that satisfy the following three aspects: 1) share similar attributes, 2) have strong spatial interactions, and 3) are geographically adjacent. A two-stage community detection algorithm is proposed to fulfill the three requirements by considering node attributes and edge connections (spatial interactions and geographic adjacency) together.

As shown in Figure 3.1, stage one focuses on generating node representations encoded with the attribute, adjacency, and flow information, and stage two focuses on clustering nodes into communities based on their similarities in the embedding space.

Stage One: Node Representation Learning Based on the first law of geography, nearby things are more related to distant things (Tobler, 1970). Applying that to any node in a spatial network, its neighborhood nodes should have larger effects than distant nodes. Therefore, graph convolution becomes a natural tool that can aggregate neighbor information when updating the central node representation (Kipf and Welling, 2017). Two models are used respectively in the study to learn node embedding.

The first model used in the study is a GCN model with two convolutional layers. $Z^{(1)}$ and $Z^{(2)}$ are defined as the outputs of the first and second graph convolutional layers, and $W^{(0)} \in \mathbb{R}^{m \times n_{hidden}}$ and $W^{(1)} \in \mathbb{R}^{n_{hidden} \times n_{output}}$ as the weights of two layers, the forward propagation model can be formalized as Equation 4.1:

$$\begin{aligned} Z^{(1)} &= ReLU(\tilde{D}^{-\frac{1}{2}}\tilde{A}\tilde{D}^{-\frac{1}{2}}XW_0), \\ Z^{(2)} &= \tilde{D}^{-\frac{1}{2}}\tilde{A}\tilde{D}^{-\frac{1}{2}}Z^{(1)}W_1, \end{aligned} \tag{3.1}$$

where A and I are the geographic adjacency matrix and the identity matrix, $\tilde{A} = A + I$, and $\tilde{D}$ is the degree matrix of $\tilde{A}$.

The second model is a GAT model, which aggregates the neighborhood nodes with a self-attention mechanism. The proposed method follows the original GAT model by Velickovic et al. (2017). The input is a set of node features, $\mathbf{z} = \{\vec{z_1}, \vec{z_2}, ..., \vec{z_n}\}, \vec{z_i} \in \mathbb{R}^m$, where n is the number of nodes, m is the number of features in each node. The layer generates a new set of node representations, $\mathbf{z'} = \{\vec{z'_1}, \vec{z'_2}, ..., \vec{z'_n}\}$, $\vec{z'_i} \in \mathbb{R}^{m'}$ (the new node representations may have a different cardinality m').

A shared linear transformation weight matrix $W \in \mathbb{R}^{m' \times m}$ is applied to every node.

The self-attention mechanism $a : \mathbb{R}^{m'} \times \mathbb{R}^{m'} \mapsto \mathbb{R}$ then computes attention coefficients:

$$e_{ij} = a(W\vec{z_i}, W\vec{z_j}) \tag{3.2}$$

For each node i, only e_{ij} is computed for nodes $j \in N_i$, where N_i is the neighborhood of node i. The softmax function is used to normalize the attention coefficients:

$$\alpha_{ij} = \text{softmax}_j(e_{ij}) = \frac{\exp(e_{ij})}{\sum_{k \in N_i} \exp(e_{ik})} \tag{3.3}$$

The final output representation for every node is a linear combination of the features weighted by the normalized attention coefficients:

$$\vec{z_i'} = \sigma(\sum_{j \in N_i} \alpha_{ij} W\vec{z_j}) \tag{3.4}$$

However, the attention coefficients are learned from the node features in the original model based on a binary adjacency matrix. But GAT can not consider the case when there is a weighted input matrix that may contain different types of edges (Velickovic et al., 2017). An additional weight s'_{ij} (a normalized flow intensity coefficient, $s'_{ij} \in [0, 1]$) is added to the attention coefficient to adjust the effects of spatial interaction on neighborhood node importance. The additional weight matrix S' is generated with a threshold t' to remove small-value flows, then the spatial flows are re-scaled and normalized to make sure the coefficients are comparable with the attention coefficients. This model is called the weighted GAT model:

$$\vec{z_i'} = \sigma(\sum_{j \in N_i} s'_{ij} \alpha_{ij} W\vec{z_j}) \tag{3.5}$$

Both the traditional GAT following the equation 3.4 and the weighted GAT model using equation 3.5 are adopted in the study. The input for GAT is the geographic adjacency matrix and the spatial positive flow matrix with a threshold t as shown in Equation 3.6.

$$A_{GAT} = A + S_{p_t} \tag{3.6}$$

However, GCN and GAT are not community detection-oriented models. A new loss function was proposed to guide the learning process. The loss function contains two constraints. The spatial interaction flow constraint will draw nodes with spatial interactions (positive pairs) closer and push nodes without spatial interactions (negative pairs) further in the embedding space. The spatial distance constraint uses a hop-distance threshold to discourage distant nodes from having similar embedding. The loss function is shown in Equation 4.2:

$$\begin{aligned} L_{hops} &= \sum \frac{\mathbb{I}(hop_{ij} > \epsilon) d_{ij}}{\log(hop_{ij})}, \\ L &= \frac{\sum_{p=1}^{N_{pos}} \log(s_p) d_{pos_p} / N_{pos}}{\sum_{q=1}^{N_{neg}} d_{neg_q} / N_{neg} + L_{hops}}, \end{aligned} \tag{3.7}$$

where hop_{ij} is the number of hops of the shortest path between v_i and v_j in the graph, and d_{ij} is the euclidean distance between the node embedding. $\mathbb{I}(\cdot)$ is set to 1 if $hop_{ij} > \epsilon$, or 0 otherwise. $pos_p, p \in [0, N_{pos}]$ and $neg_q, q \in [0, N_{neg}]$ represent the positive and negative pairs based on spatial interactions, where N_{pos} and N_{neg} are numbers of positive and negative pairs. The pseudo code of *region2vec* using the GCN model is shown in Algorithm 1 and *region2vec* using the weighted GAT model is shown in Algorithm 2.

Stage two: Agglomerative Clustering The second stage is conducting clustering to obtain the final community memberships based on the node representation from the first stage. An agglomerative clustering method is used to aggregate similar nodes (i.e., regions) into larger groups. As a bottom-up approach, each node is an independent cluster at first and is grouped successively to form the final clusters (Pedregosa et al., 2011). The connectivity constraint is enforced in the clustering algorithm to allow only clusters that are geographically adjacent to be merged together. Many regionalization problems using spatial networks might have an inherent spatial contiguity requirement to support further

Algorithm 1: Region2Vec for GCN

Input: Graph $G = (V, E)$; adjacency matrix A; flow matrix S; input features X; the shortest path $hops_{i,j}, \forall i, j \in V$ and threshold ϵ; number of layers L; weight matrices $W^l, \forall l \in \{0, \cdots, L-1\}$

Output: Node representations z_v for all $v \in V$

$Z^{(0)} \leftarrow X$;

$\tilde{A} \leftarrow A + I$;

$pos_m \leftarrow (i, j)$, for all $s_{ij} > 0$;

$neg_n \leftarrow (i, k)$, for all $s_{ik} = 0$;

for *each iter* **do**

  for $l = 0, \cdots, L-1$ **do**

    $Z^{(l+1)} = ReLU(\tilde{D}^{-\frac{1}{2}}\tilde{A}\tilde{D}^{-\frac{1}{2}}Z^{(l)}W^l)$;

  end

  $d_{ij} = \|z_i - z_j\|$;

  $L_{hops} = \sum \mathbb{I}(hop_{ij} > \epsilon) d_{ij} / \log(hop_{ij})$;

  $L = \frac{1}{N_{pos}} \sum_{p=1}^{N_{pos}} \log(s_p) d_{pos_p} / (\frac{1}{N_{neg}} \sum_{q=1}^{N_{neg}} d_{pos_q} + L_{hops})$;

  Compute $g \leftarrow \nabla L$;

  Conduct Adam update using gradient estimator g

end

$z_v \leftarrow z_v^L, \forall v \in V$

Algorithm 2: Region2Vec for weighted GAT

Input: Graph $G = (V, E)$; adjacency matrix A; flow matrix S; positive flow matrix S_{p_t} with a threshold t; the normalized flow weight matrix S' with a threshold t'; input features X; the shortest path $hops_{i,j}, \forall i, j \in V$ and threshold ϵ; number of layers L; weight matrix W

Output: Node representations z_v for all $v \in V$

$Z^{(0)} \leftarrow X$;

$A_{GAT} \leftarrow A + S_{p_t}$;

$pos_m \leftarrow (i, j)$, for all $s_{ij} > t$;

$neg_n \leftarrow (i, k)$, for all $s_{ik} = 0$;

for *each iter* **do**

  for $l = 0, \cdots, L-1$ **do**

    $\vec{z_i'} = \sigma(\sum_{j \in N_i} s'_{ij} \alpha_{ij} W \vec{z_j})$

  end

  $d_{ij} = \|z_i - z_j\|$;

  $L_{hops} = \sum \mathbb{I}(hop_{ij} > \epsilon) d_{ij} / \log(hop_{ij})$;

  $L = \frac{1}{N_{pos}} \sum_{p=1}^{N_{pos}} \log(s_p) d_{pos_p} / (\frac{1}{N_{neg}} \sum_{q=1}^{N_{neg}} d_{pos_q} + L_{hops})$;

  Compute $g \leftarrow \nabla L$;

  Conduct Adam update using gradient estimator g

end

$z_v \leftarrow z_v^L, \forall v \in V$

interpretation and analysis of the obtained regions. Therefore, it is necessary to have this spatial contiguity setting in the algorithm.

3.2.4 Baseline Algorithms

The following community detection algorithms are included in this study as baselines to compare with our proposed GeoAI-enhanced *region2vec* models.

Louvain community detection The Louvain algorithm (Blondel et al., 2008) first generates small communities through local modularity gain maximization, then the identified communities are treated as nodes and recursively aggregated again. The input of the Louvain method is the spatial interaction network and it is used to detect communities using only human mobility connections in this study.

Random walk based model Two random walk based graph embedding models, Deepwalk (Perozzi et al., 2014) and Node2vec (Grover and Leskovec, 2016) are used as baselines. Deepwalk uses short walks to generate random paths of connected nodes (Perozzi et al., 2014). The Node2vec algorithm further develops a biased random walk procedure to control different node neighborhood exploration strategies (Grover and Leskovec, 2016). The input of the two methods is the geographic adjacency matrix. After obtaining the node embedding, the same agglomerative clustering algorithm is applied to generate the final communities.

LINE Large-scale Information Network Embedding (LINE) proposed by Tang et al. (2015) is a network embedding method. It specifically preserves the local and global network structure through a carefully designed objective function that considers both first-order and second-order proximities. The input of LINE is the geographic adjacency matrix.

K-Means The K-Means clustering algorithm can group nodes with similar attributes and assign each node to the cluster that is the nearest by measuring feature space distance (MacQueen et al., 1967). The K-Means clustering algorithm takes the node attributes as the only input and cannot consider the edge connections.

3.2.5 Evaluation Metrics

Four individual metrics and one synthetic metric are used to compare the method performance from different perspectives.

Intra-Flow Ratio The intra-flow ratio is used to measure the ability to group nodes with strong flow connections. The intra-flow ratio used in this paper is a more robust metric with a fixed range of [0,1] that supports comparison across different scenarios. It divides the sum of edge weights within each community (intra-flow weights) by the sum of intra-flow and inter-flow edge weights in the whole network. The equation for computing this ratio is shown in Equation 3.8, where s_{ij} represents the flow intensity between nodes i and j. This ratio ranges from 0 to 1, with a higher value indicating a better performance to group nodes with strong connections together.

$$\begin{gathered} R_{IntraFlow} = \frac{\sum_{c_i=c_j} s_{ij}}{\sum s_{ij}}; \\ c_i, c_j \in 1, 2, \cdots, K \text{ (K is the number of communities)} \end{gathered} \tag{3.8}$$

Inequality The inequality metric was initially designed to reflect the infrastructure inequality (Pandey et al., 2022). The inequality reflects the heterogeneity of all the samples and how it varies with the average value. It is calculated using Equation 3.9 where σ is the standard deviation and μ is the mean. A value of 1 means maximum inequality and a value of 0 means no inequality. In this study, the inequality is measured using all the node features. For each feature, the inequality in each community is calculated and the median inequality in all communities is selected as a representation for that feature dimension. The

final score is the product of all inequality scores (Equation 3.10) where m is the number of features. The inequality is then converted into a range of 0 to 1 using the min-max normalization (Equation 3.11).

$$I_i = \frac{\sigma_i}{\sqrt{\mu_i(1-\mu_i)}}; 0 < \mu_i < 1 \tag{3.9}$$

$$I = \prod_{i=1}^{m} I_i \tag{3.10}$$

$$I_{norm} = \frac{I - I_{min}}{I_{max} - I_{min}} \tag{3.11}$$

Cosine Similarity The cosine similarity is used to measure the ability of grouping nodes when they share similar attributes. Cosine similarity calculates the L2-normalized dot product of vectors (Pedregosa et al., 2011), which is the cosine of the angle between the two vectors, and therefore, is not dependent on the magnitudes of the vectors (Manning et al., 2010). The cosine similarity for all pairwise nodes in each community and the median values in all communities are calculated.

Synthetic Score The previous three metrics are measured along different dimensions of the community detection result. To summarize all the different aspects, a synthetic score S is calculated as the product of the three metrics. To make it comparable, all metrics should be within the same range. For intra-flow ratio and cosine similarity, they range from 0 to 1 with a monotonic increase to indicate a better performance. For inequality, originally, it ranges from 0 to infinity, after the min-max normalization, it ranges from 0 to 1 with a smaller value indicating better performance. Therefore, it is then converted using a monotonically decreasing function to match with the other two metrics. The synthetic score S is then calculated based on Equation 3.12, where a larger synthetic score represents a better performance.

$$S = R_{IntraFlow} * CosineSimilarity * (1 - I_{norm}) \tag{3.12}$$

Join count ratio The join count ratio is used to measure the spatial dependence (Cliff and Ord, 1973; Kang et al., 2022). It is based on the join count statistics to measure the proportion of neighborhood nodes that belong to the same community across all the neighborhood nodes. For each pair of geographically adjacent nodes that share a boundary, whether their community is the same will be calculated. The join count ratio is shown in Equation 3.13, where J_{same} is the number of neighborhood pairs that belong to the same community and J_{diff} is the number of neighborhood pairs belongs to the different communities. The J_{ratio} ranges from 0 to 1 and represents how well geographic-adjacent nodes are grouped into the same community. A higher value indicates a stronger ability to maintain spatial contiguity.

$$J_{ratio} = \frac{J_{same}}{J_{same} + J_{diff}} \tag{3.13}$$

3.2.6 Case Study

One application of the proposed GeoAI-enhanced community detection methods in spatial networks is to support the Rational Service Area (RSA) development, which is a critical issue in the public health domain. The rational service areas are self-contained geographic units that reflect how people move and seek health services, and they should be defined based on travel patterns, physical barriers or social-economic similarities (Health Resources and Services Administration, 2020; Lopes, 2000). Therefore, the developed RSA designation should reflect how people move across the region and also the social-economic factors among local residents. However, existing rational service areas are mainly developed by manual work with local health knowledge (Hu et al., 2018). There is a lack of systematic approaches to formalize the rational service area development and support adaptive, repeated and flexible designation updates.

The rational service areas serve as the basic geographic unit for identifying Health Professional Shortage Areas (HPSAs). After establishing rational service areas, each of them is evaluated from multiple spatial and non-spatial aspects to generate a health shortage score (more details can be found in section 2.2.3). Areas with a score larger than zero are defined as the Health Professional Shortage Area and will receive additional funding to support local health providers. The ultimate goal of RSA development is to accurately group areas that lack health services so that they can be identified in the HPSAs scoring process.

The communities detected from the proposed *region2vec* method and several baselines are used as the delineated rational service areas, respectively. The generated communities are the input for the HPSA scoring process, and the results are then evaluated based on the following metrics. The number of delineated HPSAs, the area covered, and the population-to-provider ratio will be calculated. The provider locations are downloaded from the Bureau of Health Workforce (HRSA, 2023). The population-to-provider ratio can reflect, on average, how many people are assigned to one provider. The higher this value is, the more severe the health shortage this area is facing.

3.3 Results

There are two major parts of the results section. First, the performance of community detection on spatial networks measured by various metrics will be compared together with visualizations for all the introduced methods. Then, a case study for how the proposed *region2vec* method can be applied to the rational service area development in public health is presented. The number of communities for all methods is set as 14, which is the community number calculated from the Louvain algorithm. The performance of different community numbers is also discussed. For the traditional GAT model, the threshold t in S_{p_t} is set to 5 to include most of the positive flow edges. For the weighted GAT model, the threshold t in S_{p_t} is set to 200 and the threshold t' in S' is set to 100.

Table 3.1: The metrics comparison of all methods. (In **bold**: best; Underline: second best)

Methods	Intra-Flow Ratio	Normalized Inequality	Cosine Similarity	Synthetic Score
Region2vec-weightedGAT	**0.843**	1.879E-07	0.975	**0.821**
Region2vec-GAT	0.702	1.523E-04	0.967	0.679
Region2vec-GCN	0.782	1.130E-05	0.974	0.762
DeepWalk	0.721	6.469E-04	0.960	0.691
LINE	0.214	1.000E+00	0.872	0.000
Node2vec	0.731	1.394E-03	0.951	0.694
K-Means	0.305	**0.000E+00**	**0.983**	0.299
Louvain	0.829	1.711E-04	0.967	0.801

3.3.1 Comparison with Existing Methods

Metric Comparison The results of different metrics used to compare method performances are listed in Table 3.1. Overall, the proposed *region2vec* method with weighted GAT has the best performance for intra-flow ratio and the synthetic score, and the second-best performance for inequality and cosine similarity. While K-Means is the best one for inequality, and cosine similarity, it has the second lowest intra-flow ratio, which indicates that it fails to consider edge interaction during the clustering process compared with other methods. The proposed *region2vec* method with weighted GAT is the best when one takes all aspects into consideration and this is also indicated by the synthetic score.

First, the intra-flow ratio represents the ratio of intra-community flows out of all the flows. Our proposed *region2vec* method with weight GAT has the highest score, meaning that it performs the best in grouping nodes while considering the spatial interactions among them. The Louvain method takes the spatial interaction matrix as its input and obtains the second-highest flow ratio value. The proposed *region2vec* method with GCN has the third-best performance. After them, Node2vec and Deepwalk obtain similar ratios and are listed as fourth and fifth best. The *region2vec* method with traditional GAT does not reach a very high intra-flow ratio. The K-Means method and LINE have the lowest ratios, much smaller than the rest of the methods.

A lower normalized inequality value means that nodes within communities have more

similar attributes and are more equal. The K-Means clustering method obtains the lowest value. As K-Means groups nodes only using their features, it is expected to perform well in this metric. The proposed *region2vec* method with weighted GAT has the second lowest inequality, meaning that the nodes within each community are also very homogeneous in the feature space. The proposed *region2vec* method with GCN has the third lowest inequality, showing that in general, our proposed method has advantages over other baselines in grouping nodes with similar attributes.

The cosine similarity is another metric to measure node attribute similarity in communities. K-Means clustering obtains the highest cosine similarity. The *region2vec* method with weighted GAT is the second best and the *region2vec* method with GCN is the third best. This demonstrates the ability to group nodes with similar attributes from another perspective, and the *region2vec* methods outperform most of the baselines besides K-Means.

For the synthetic score, the *region2vec* method with weighted GAT has the highest value, meaning that after combining all aspects, it is the best one with a comprehensive consideration across different dimensions, including node attributes and spatial interactions. The Louvain method is the second best partly due to its high intro-flow ratio. The *region2vec* method with GCN is the third best and also demonstrates the advantage of the proposed method. In summary, the proposed *region2vec* method with weighted GAT has the best score and is in the top two across all the metrics used, showing that it can maintain a great balance between grouping nodes with strong spatial interaction and grouping nodes with similar attributes.

In addition, to better understand the metrics, 3D plots are generated in Figure 3.2. The three dimensions are intra-flow ratio, cosine similarity and normalized inequality, where the direction of arrows represents a better performance. On the left side, all methods are plotted where LINE is very distant from all other methods due to its large normalized inequality and low intra-flow ratio. On the right side, LINE is excluded to enable a zoomed-in view of other methods. It is clear to see that K-Means is away from others due to its low

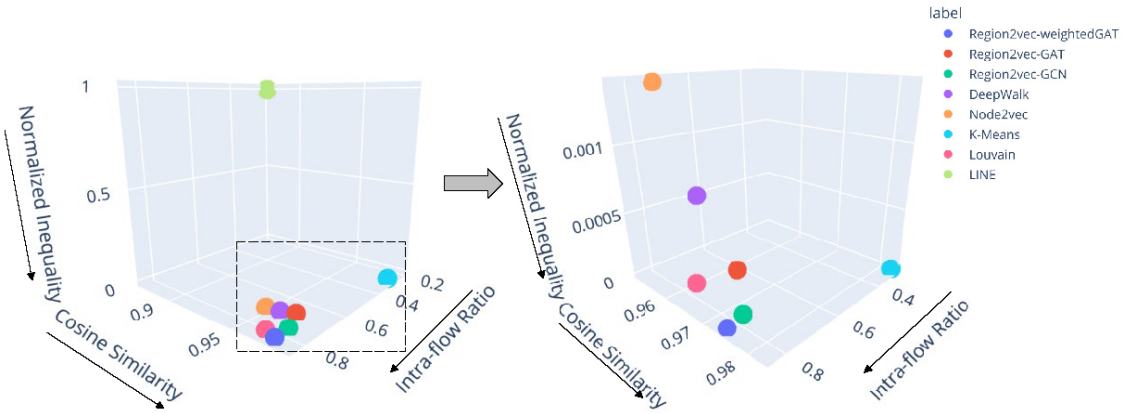

Figure 3.2: The 3D view of three metrics for all the methods. Left: the view of all methods, Right: the zoomed-in view without LINE

intra-flow ratio. DeepWalk and Node2vec have relatively higher normalized inequality scores that separate them from other methods. The rest of the methods are clustered around the area with the best performances across three dimensions as the arrows indicate. Among them, *region2vec* with weighted GAT and *region2vec* with GCN are closer to the best-performance corner, showing the advantages of the proposed method.

3.3.2 Sensitivity Analysis

Since the ground-truth community structure for unsupervised machine learning is unavailable, there is a lack of knowledge of the exact number of communities. In the previous analysis, the number was set according to the Louvain algorithm for easy comparison. Here, to further verify the effectiveness of the proposed *region2vec* methods, a sensitivity analysis is conducted to test the performance under different settings of community numbers. The result is shown in Figure 3.3, which demonstrates the scoring distribution of all methods based on cosine similarity and intra-flow ratio along with their scoring 95% confidence-level standard deviation ellipse. For the same algorithm, dots with lighter colors represent results derived from different community number settings, while darker ones denote the average score. Along the x-axis (cosine similarity), K-Means, the proposed *region2vec* with weighted GAT and *region2vec* with GCN have the highest values and can

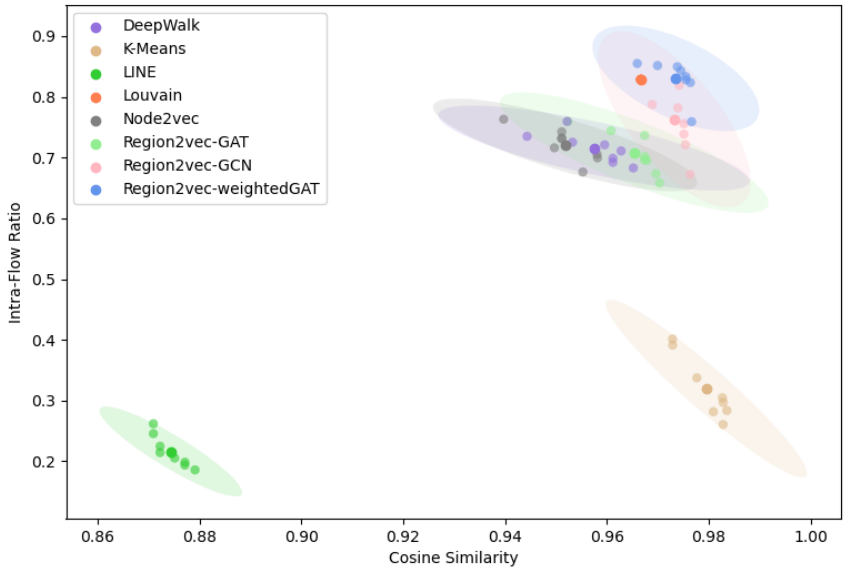

Figure 3.3: The distribution of all methods based on cosine similarity and intra-flow ratio.

always outperform the rest of the methods. DeepWalk, Node2vec and *region2vec* with GAT fall within a similar range of cosine similarities. LINE has the worst performance. Along the intra-flow ratio dimension, the proposed *region2vec* with weighted GAT outperforms all other methods with very stable intra-flow ratios. Louvain is the second best and is followed by *region2vec* with GCN with some fluctuations in the ratio values. DeepWalk, Node2vec and *region2vec* with GAT show similar ranges of intra-flow ratios and LINE is again the worst. In summary, the *region2vec* with weighted GAT has very stable performances across different community numbers. Out of all the methods, it maintains a great balance of grouping nodes with similar attributes (indicated by cosine similarity) and grouping nodes with stronger flow connections (represented by the intra-spatial interaction flow ratio).

3.3.3 Community Visualization

Since the nodes in spatial networks are geographic regions (i.e., census tracts in this study), the resulting communities can be visualized on the map. The map visualization of the detected communities for all the methods is shown in Figure 3.4. The whole study area is

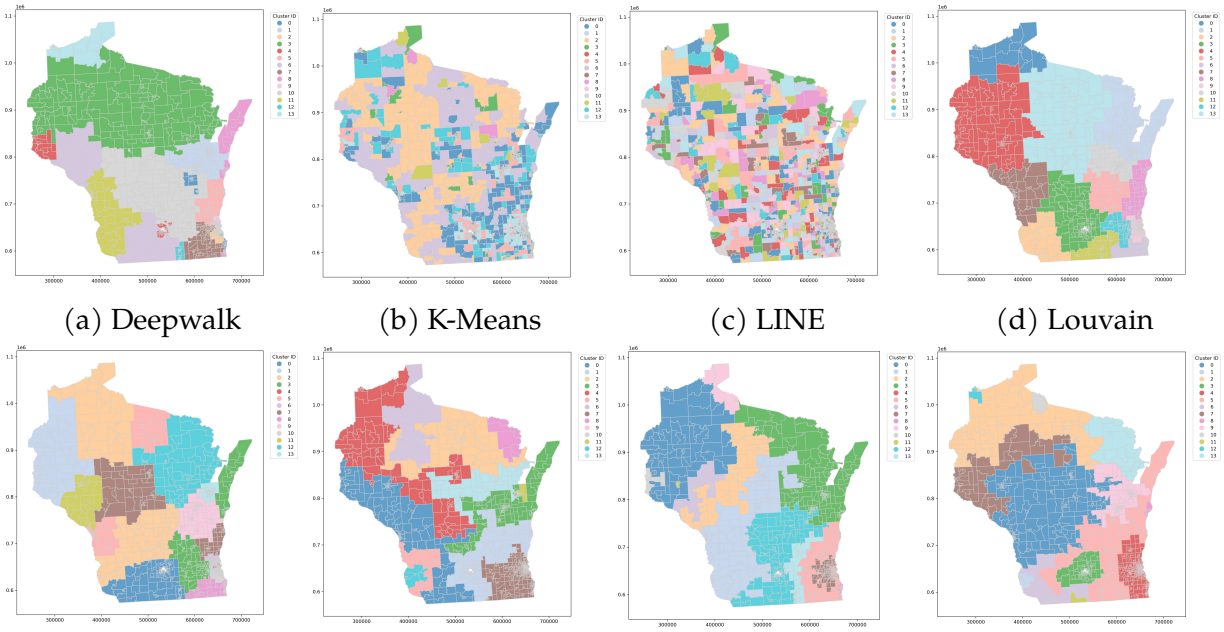

(a) Deepwalk (b) K-Means (c) LINE (d) Louvain

(e) Node2vec (f) Region2vec-GCN (g) Region2vec-GAT (h) Region2vec-WeightedGAT

Figure 3.4: The resulting communities maps of all methods.

divided into 14 communities, represented by different colors. Overall, *region2vec* with GCN, GAT, weighted GAT, Deepwalk, Node2vec and Louvain generate relatively regular shapes of communities that are mostly connected, while K-Means clustering and LINE have very scattered results. As the resulting spatial network communities in most cases should be spatially contiguous for downstream tasks, the results from K-Means clustering and LINE cannot satisfy such requirements and are excluded from the following comparisons. Due to algorithm limitations, Deepwalk and Node2vec generate some communities that are actually spatial discontiguous, such as community 6 (in light purple) in Deepwalk and community 2 (in light orange) in Node2vec, which might affect the downstream tasks as some nodes in the same community are not geographically adjacent to each other. To quantitatively evaluate how well the spatial contiguity of nodes is maintained, the join count ratio is calculated for each method and the result is shown in Table 3.2. Louvain has the greatest ratio, meaning that it has the highest proportion of neighborhood pairs that share the same community labels. The *region2vec* with weighted GAT has the second

highest ratio, indicating that the spatial contiguity is also well maintained. Similar to the visualization maps, LINE and K-Means have the lowest join count ratios and cannot maintain spatial contiguity.

Table 3.2: The join count ratios of all methods (In **bold**: best; Underline: second best).

Methods	Join Count Ratio
DeepWalk	0.902
K-Means	0.315
LINE	0.112
Louvain	**0.929**
Node2vec	0.900
Region2vec-GCN	0.873
Region2vec-GAT	0.838
Region2vec-WeightedGAT	<u>0.904</u>

In terms of the area shape, Louvain and Node2vec have more compact area shapes by visual examination. It is noticeable that the shape of communities in *region2vec* tends to be particularly long or irregular. The geographic distances between census tracts in the same community may be very large due to the long shape of the community. One potential reason behind this is that there exists long-distance mobility flows in the spatial networks: people living in rural areas of Wisconsin need to travel long-distance to visit other areas and such connections may not be reflected in results from Louvain, Deepwalk and Node2vec. This is one advantage of the proposed *region2vec* algorithm: not only the areas that are geographically adjacent should be in the same community, but also areas that are connected by the transportation infrastructure (reflected in the daily human mobility flows). Therefore, the results of *region2vec* may be more helpful for revealing regional human movement patterns and maintaining the socioeconomic similarities of clustered regions. In particular, *region2vec* with weighted GAT identifies two major urban areas in Wisconsin, community 8 (in green) containing Dane County, where the capital is located, and community 7 (in red) containing Milwaukee area - the largest city in Wisconsin.

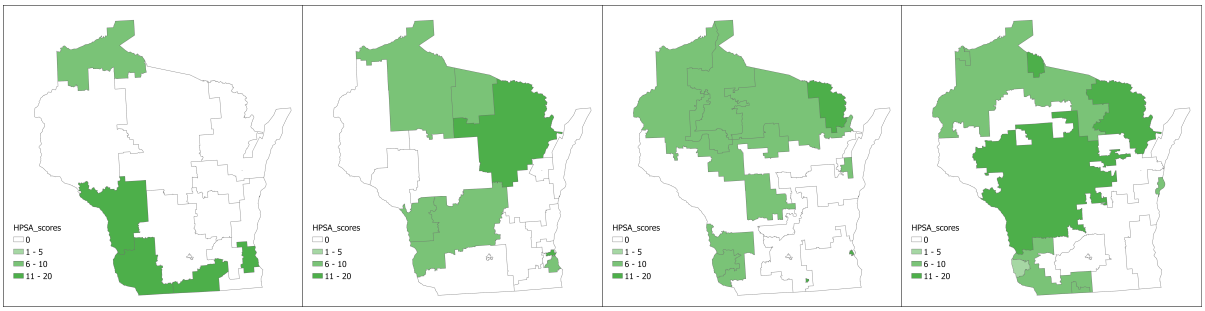

(a) Louvain (b) Node2vec (c) Region2vec-GCN (d) Region2vec-WeightedGAT

Figure 3.5: The final Health Professional Shortage Area with scores for four methods.

Table 3.3: The HPSA delineation performance of four methods (Bold indicates the best).

Methods	HPSA number	Population:Provider	Total Areas (km^2)
Louvain	5	4796.608	33728.846
Node2vec	5	5382.736	70718.458
region2vec-GCN	**9**	**5900.010**	75677.092
region2vec-weightedGAT	**9**	4779.635	**89848.260**

3.3.4 Case Study in Public Health

Based on the community map visualization, the results of *region2vec* with GCN, *region2vec* with weighted GAT, Node2vec and Louvain are selected to be applied in the Rational Service Area development problem in public health. The communities are used as the basic units, and then four scoring criteria are applied to find the shortage area. The final Health Professional Shortage Area (HPSA) scores are shown in Figure 3.5. The areas with green color are identified Shortage Areas and the transparency represents the value of the scores where lighter greenness has lower scores. As shown in Table 3.3, the *region2vec* - weighted GAT method identifies a significantly large area coverage while Louvain shows a much smaller area coverage. The *region2vec* with GCN and Node2vec have similar area coverages. For HPSA numbers, the *region2vec* with GCN and *region2vec* - weighted GAT method generate 9 HPSAs, while Louvain and Node2vec have 5 HPSAs. The number of HPSAs is an important criterion for measuring public health needs. The lower number of HPSAs in Louvain and Node2vec indicates that they may fail to identify some areas with

potential health shortages. The population-to-provider ratio indicates the level of shortages as to how many populations are allocated to one provider. The *region2vec*-GCN achieves the highest population-to-provider ratios, meaning that it identifies the areas with the greatest shortage. However, the *region2vec* with weighted GAT cannot outperform the other two baselines for this ratio. It is possible that the criteria used in the HPSA establishment are not directly considered in the *region2vec* method and lead to uncertainty with the specific task. However, the *region2vec*-GCN still outperforms the two baselines and demonstrates the potential of applying the proposed method to identify health shortage areas.

The proposed *region2vec* methods are specifically designed for spatial networks that consider both the node attributes and spatial interactions, so the derived communities will have similar characteristics and strong spatial flow connections. As the designation of Rational Service Areas requires evidence of travel patterns or similar socio-economic attributes, the proposed method meets the requirement and is very suitable to be applied to this problem. Through the comparisons with other baselines, the *region2vec* methods family has shown its great performance using various metrics in practical applications.

3.4 Conclusion

This chapter proposes a new family of GeoAI-enhanced unsupervised community detection methods on spatial networks called *region2vec*. Based on graph neural network models, including GCN and GAT, the *region2vec* methods use graph embedding to learn node representations with the consideration of multiple edge relationships and node attributes. The learning process is guided with a self-designed community detection-oriented loss so that nodes with strong interactions, similar attributes, and close adjacency are encouraged to have similar representations. The communities (i.e., geographic regions) are further formed through a post-clustering process. By comparing with multiple baselines using different metrics, the GeoAI-enhanced proposed methods have shown the greatest performances in the flow intensity score and the combined synthetic score. In particular, the *region2vec*

method with weighted GAT integrates an additional spatial interaction weight on top of the attention coefficients and performs the best among all the methods. The *region2vec* methods have also been applied to the rational service area development problem in public health and show their promise in regionalization problems.

There are some aspects that need further improvement. The shapes of generated communities using *region2vec* are not compact enough compared with other methods such as Node2vec or Louvain as the current spatial constraints cannot strictly affect the shape of communities. Our future work will aim to develop different approaches of integrating multiple graphs and node attributes to generate more compact communities. For this research, even though the *region2vec* with weighted GAT identified HPSAs with the greatest coverage, its population-to-provider ratio is not the highest. More node attributes may be included in the algorithm to help generate communities with more similar characteristics.

This research shows the ability to use graph embedding on spatial networks to solve regionalization problems. There are interesting relationships in geographic graphs that can be further explored using DL models, such as geographic contiguity requirements and certain area shape requirements (concave or convex).This study contributes to the increasing interest in GeoAI development in GIScience, urban analytics, and beyond (Janowicz et al., 2020; Liu and Biljecki, 2022; De Sabbata et al., 2023).

4 UNDERSTAND GRAPH PREDICTION FOR REGIONALIZATION USING EXPLAINABLE AI

4.1 Introduction

Artificial Intelligence (AI), which refers to technology that allows computers/machines to simulate human intelligence (McCarthy et al., 2007; IBM, 2024), has gained considerable attention in recent decades due to the availability of big data and the fast development of computing power. AI techniques have the advantage of extracting hidden information from large-scale complex data. It automates a variety of manual processes and supports data-driven decision-making with high efficiency. It has been widely used and proven to outperform many traditional methods in areas such as natural language processing, computer vision, pattern recognition, predictive modeling, etc.

The growth of AI techniques also brings more possibilities for understanding geospatial problems and inspires a major topic of new research in geography called Geospatial Artificial Intelligence (GeoAI). Specifically, GeoAI refers to the "integration of geospatial studies and AI machine (deep) learning and knowledge graph technologies" (Gao et al., 2024). Examples of GeoAI applications include real-time disaster response (Huang et al., 2018; Peng et al., 2021), agricultural management (Barbosa et al., 2020; Jiang et al., 2020), satellite image analysis (Yang and Newsam, 2010; Li et al., 2020; Khan et al., 2019), disease spread prediction (D'Orazio et al., 2020; Kavak et al., 2018), social sensing (Mai et al., 2022; Kruse et al., 2021), and network analysis (Chen et al., 2020; Fayyad et al., 2020; Yu et al., 2017).

Compared with many traditional Machine Learning tasks with Euclidean data such as images or tasks, many spatial phenomena can only be modeled using more complex graph structures, for example, transportation networks and mobility flows. The graph structure contains nodes and edges, where nodes can represent roads or geographic regions, and edges can represent the interactions between nodes. The complexity of graph-structured

data has led to many difficulties using traditional methods because the relationship and interdependency between entities are not easy to model. GeoAI methods, especially Graph Neural Networks (GNNs) and their extensions, have been very powerful in solving hard graph problems and generating desirable results in a short time. They have been very useful in extracting meaningful patterns from the graph and identifying latent representations from the high-dimensional inputs.

In particular, many researchers have used Graph Convolutional Neural Networks (GCNs) and Graph Attention Networks (GATs) to solve various geospatial problems. For instance, Yao et al. (2020) proposed a spatial interaction GCN model for origin-destination flow imputation, Zhu et al. (2022) designed a knowledge representation-driven spatial-temporal GCN method for traffic forecasting, Guo et al. (2019) proposed a novel attention-based spatial-temporal GCN model traffic flow forecasting. GNN models can consider the neighbor relationships via the convolutional layers, and GATs consider the impact of pairwise nodes on each other. Both GCN and GAT models are very helpful for modeling the interdependency of geographic objects.

However, most AI methods are considered black-box models that cannot be easily explained. This may hinder the applications of AI techniques because it is hard for users to interpret and provide trustful reasoning behind the predictions (Yuan et al., 2022). In the domain of geography, the interpretability of a model is particularly crucial. It is important for researchers to learn why certain predictions are obtained to better understand geographic phenomena. Being able to explain a model may lead to insights into hidden relationships, important features, or potential theoretical findings. For traditional methods, the parameters and the coefficients from the model can assist the interpretation of each factor, supporting the explanation of certain observations. However, in GeoAI models, there can be a large number of parameters, making it very hard to provide insights directly from the model. Therefore, it is very necessary to develop approaches that can better explain GeoAI methods so that the opportunity to flexibly model, interpret and visualize

complex geographical phenomena and processes can be provided (Li, 2022).

There are multiple research on applying Explainable AI methods to GNN models, such as GNNExplainer, GraphLIME and SHAP (Li, 2022; Huang et al., 2022; Liu et al., 2023). They try to provide an explanation of GNN results from different angles, including important node features or important subgraphs. However, there is a lack of Explainable AI applications for geospatial tasks, especially spatial networks.

To promote a new generation of spatial analytics with high intelligence and interoperability, this study proposed a framework for understanding the explainability of GCN models to support geospatial regionalization studies. A GCN model called *region2vec* is adopted, which is used for solving community detection-based unsupervised tasks by combining node attributes and node connections. The model considers both spatial interaction and geographic adjacency to learn graph embedding effectively. Additional clustering is then conducted using the graph embedding to identify the final communities. To further provide an explanation of the GCN-generated results, GNNExplainer is applied to the GCN model to understand how the embedding is generated and what key features and graph structures contribute the most to the prediction. Individual-based and community-based explanations are both presented to provide a comprehensive understanding of community detection results.

The remainder of the paper is organized as follows: the method is first introduced in Section 4.2, then the results of the GCN model and the GNNExplainer are presented in Section 4.3, and finally, some discussions and conclusions are shared in Section 4.4.

4.2 Method

The designed GCN model and its structure are first introduced, then the GNN Explainer model that is used to explain the GCN model is presented. The purpose of this study is not to develop a GCN model with the best performance but to evaluate how GNNExplainer can be used to interpret the GCN result on a spatial network.

4.2.1 Notations and Problem Definitions

Graph $G = (V, E)$ is defined via a set of nodes $V = (v_1, ..., v_n)$, $|V| = n$ and edges E with $e_{ij} = (v_i, v_j)$. $A = [a_{ij}]_{n\times n}$ is an adjacency matrix, where $a_{ij} = 1$ if $e_{ij} \in E$, otherwise $a_{ij} = 0$. $S = [s_{ij}]_{n\times n}$ is a spatial interaction matrix, where s_{ij} represents the flow intensity between node v_i and v_j. An $n \times m$ attribute matrix X is used to denote the multidimensional attributes of nodes.

The community detection aims to partition the n nodes into K communities $\{C_1, C_2, ..., C_K\}$ and each node will have a label c_i indicating its community membership, $c_i \in \{1, 2, ..., K\}$.

4.2.2 *Region2vec* model

One special characteristic of spatial networks is that the nodes that are spatially adjacent tend to be similar in attributes, according to the first law of geography (spatial dependency effect) (Tobler, 1970). Since the critical operation of graph convolutional neural networks is to aggregate neighbor information, making it a natural tool that fits this characteristic when given spatial adjacency matrix and node attributes as inputs.

$Z^{(1)}$ and $Z^{(2)}$ are defined as the outputs of the first and second graph convolutional layers, and $W^{(0)} \in \mathbb{R}^{m\times n_{hidden}}$ and $W^{(1)} \in \mathbb{R}^{n_{hidden}\times n_{output}}$ as the weights of two layers, the forward propagation model can be formalized as Equation 4.1:

$$\begin{aligned} Z^{(1)} &= ReLU(\tilde{D}^{-\frac{1}{2}}\tilde{A}\tilde{D}^{-\frac{1}{2}}XW_0), \\ Z^{(2)} &= \tilde{D}^{-\frac{1}{2}}\tilde{A}\tilde{D}^{-\frac{1}{2}}Z^{(1)}W_1, \end{aligned} \tag{4.1}$$

where A and I are the spatial adjacency and identity matrices, $\tilde{A} = A + I$, and $\tilde{D}$ is the degree matrix of $\tilde{A}$.

However, GCN is a semi-supervised model and not community-oriented. So the spatial interaction flow strength and geographic distance are utilized as constraints to guide the learning process. Specifically, the nodes without flow interactions are considered as

negative pairs and are pushed away in the embedding space, while those with interactions will be treated as positive pairs and drawn closer; the greater the flow intensity, the closer they will be brought together in the embedding space. Moreover, a threshold is set to push away node pairs that are spatially distant from each other to guarantee spatial contiguity. Thus, the loss function is designed as Equation 4.2:

$$\begin{aligned} L_{hops} &= \sum \frac{\mathbb{I}(hop_{ij} > \epsilon) d_{ij}}{\log(hop_{ij})}, \\ L &= \frac{\sum_{p=1}^{N_{pos}} \log(s_p) d_{pos_p} / N_{pos}}{\sum_{q=1}^{N_{neg}} d_{neg_q} / N_{neg} + L_{hops}}, \end{aligned} \tag{4.2}$$

where hop_{ij} represents the hop numbers of the shortest path between v_i and v_j in the graph, and d_{ij} is the euclidean distance between the corresponding embedding representations. $\mathbb{I}(\cdot)$ is set to 1 if $hop_{ij} > \epsilon$, or 0 otherwise. Positive pairs and negative pairs of nodes are denoted by $pos_p, p \in [0, N_{pos}]$ and $pos_q, q \in [0, N_{neg}]$, respectively. Since the intensity of flow s_p has a large range of values, a log transformation is adopted so that the flow values will not get overwhelmed by the extremely large values.

Since this is an unsupervised community detection task, the output from the model is the embedding of each node instead of the class labels in typical supervised tasks. Therefore, the embeddings are first visualized using T-distributed Stochastic Neighbor Embedding (t-SNE) (Van der Maaten and Hinton, 2008). The key idea of t-SNE is to map nearby points in the high-dimensional space to nearby points in the low-dimensional space while separating dissimilar points.

After obtaining the node representation, the agglomerative clustering is utilized to further obtain the final community assignments. The neighboring relationship between nodes defined via the spatial adjacency matrix can be used in the clustering process to preserve the spatial contiguity and impose local structures.

4.2.3 GNN Explainer

The GNNExplainer proposed by Ying et al. (2019) was the first general, model-agnostic approach for explaining predictions of any GNN-based models. For each instance, GNNExplainer provides an explanation in the form of a small subgraph and a small subset of node features that are most important for the prediction. The general framework of GNNExplainer is presented below.

The output of the GCN model ϕ is usually a conditional distribution $P_\phi(Y|G, X)$, where Y indicates the probability of nodes belonging to each class. The key idea of GNNExplainer is based on the computation graph of node v, which contains all the information needed to predict the label $\hat{y}$ for node v. The computation graph is denoted as $G_c(v)$, the adjacency matrix of the computation graph is $A_c(v) \in \{0,1\}^{n \times n}$, and the associated feature set is $X_c(v) = \{x_j | v_j \in G_c(v)\}$.

For the node v, the prediction $\hat{y} = \Phi(G_c(v), X_c(v))$ is only determined by the model, the computation graph $G_c(v)$ and the node feature $X_c(v)$. Therefore, for each node's prediction, only a part of the graph structure and the associated node features are needed. GNNExplainer generates an explanation for prediction $\hat{y}$ as (G_S, X_S^F), where G_S is a small subgraph of the computation graph. X_S is the associated feature of G_S and X_S^F is a small subset of node features that are most important for explaining $\hat{y}$.

During the implementation, GNNExplainer tried to maximize the mutual information *MI* represented by the following formula:

$$\max_{G_S} MI(Y, (G_S, X_S)) = H(Y) - H(Y|G = G_S, X = X_S) \tag{4.3}$$

For node v, *MI* quantifies the change in the probability of prediction $\hat{y} = \Phi(G_C, X_c)$ when v's computation graph is limited to explanation subgraph G_S and its node features are limited to X_S. Since the entropy term $H(Y)$ is constant, the goal of GNNExplainer can be converted to minimizing conditional entropy $H(Y|G = G_S, X = X_S)$. The output

explanation for prediction $\hat{y}$ is a subgraph G_S that minimizes uncertainty of Φ when GNN computation is limited to G_S.

To evaluate the subgraph generated from GNNExplainer, the following statistics are calculated: the number of nodes, the number of edges, the diameter of the graph and the diameter weighted by the geographic distances between nodes. The diameter of a graph is the maximum distance between the pair of vertices, it is usually calculated with the default setting that each edge has a distance of 1. The great-circle distance among census tracts' centroid is also calculated and used as the distance/cost of the edge and generated distance-weighted diameter.

4.2.4 GNNExplainer Experiment Design

The trained *region2vec* model is used as the input into the GNNExplainer. Since community detection is an unsupervised task, there are no ground truth labels. The output of the *region2vec* model is the embedding of each node. Therefore, in the GNNExplainer algorithm, the model configuration is set to be "regression" and the GNNExplainer returns raw values during the optimization. More specifically, when GNNExplainer looks for the important subgraph and features of a node, it compares the differences in the raw values generated from the original model and the model using the subgraph and the subset of features.

For each instance, the expected output from the GNNExplainer contains two parts. The first output is the important subgraph that contributes to the prediction of this instance (node). Each edge in the subgraph also has an edge weight that represents its importance to the node's prediction. The second output for each node is the feature importance scores. The two types of explanations are provided at the instance level, but they can also be aggregated to the community level to support the examination of potential spatial effects or regional characteristics.

4.2.5 Data and Study Area

The study area is the state of Wisconsin in the United States. The spatial networks are constructed using the mobility flow at the census-tract level from August 2021 to October 2021, collected from anonymous smartphone users. The census tracts are used as the nodes in the spatial network and the edges are represented by human movement flow connections with flow intensity as the weights. The geography adjacency graph is constructed using the shapefile of U.S. census tracts. The node features (e.g., income, population, race) are collected from U.S. Census American Community Survey (ACS) 5-year estimates.

4.3 Results

The *region2vec* model and the GNNExplainer are implemented using the PyTorch Geometric (PyG) library (Fey and Lenssen, 2019) with PyTorch as the back-end.

4.3.1 *Region2vec* Communities and Embedding

Figure 4.1a shows the community map of the *region2vec* method for the whole study area, where each census tract is colored based on its community membership. In total, there are 14 communities. By visual examination, there are some relatively large communities, such as communities 0, 3, 4, 9, and 10. Figure 4.1b shows a zoomed-in map of the Milwaukee area, and the boundary of Milwaukee is shown using the hatched gray color. Communities 2, 5, 8, and 13 are mostly within the Milwaukee boundary with relatively small areal sizes, and they are surrounded by community 1, which also overlaps greatly with the Milwaukee boundary.

Figure 4.2 shows the visualization result of embedding in a 2-dimension space using t-SNE. In general, the embedding of all communities forms a continuous shape, and some communities' embedding overlaps in the 2D space. In the middle part of Figure 4.2, community 0 and community 4 overlap. By checking Figure 4.1a, the two communities are adjacency to each other and cover a majority of the central area of Wisconsin. At the left

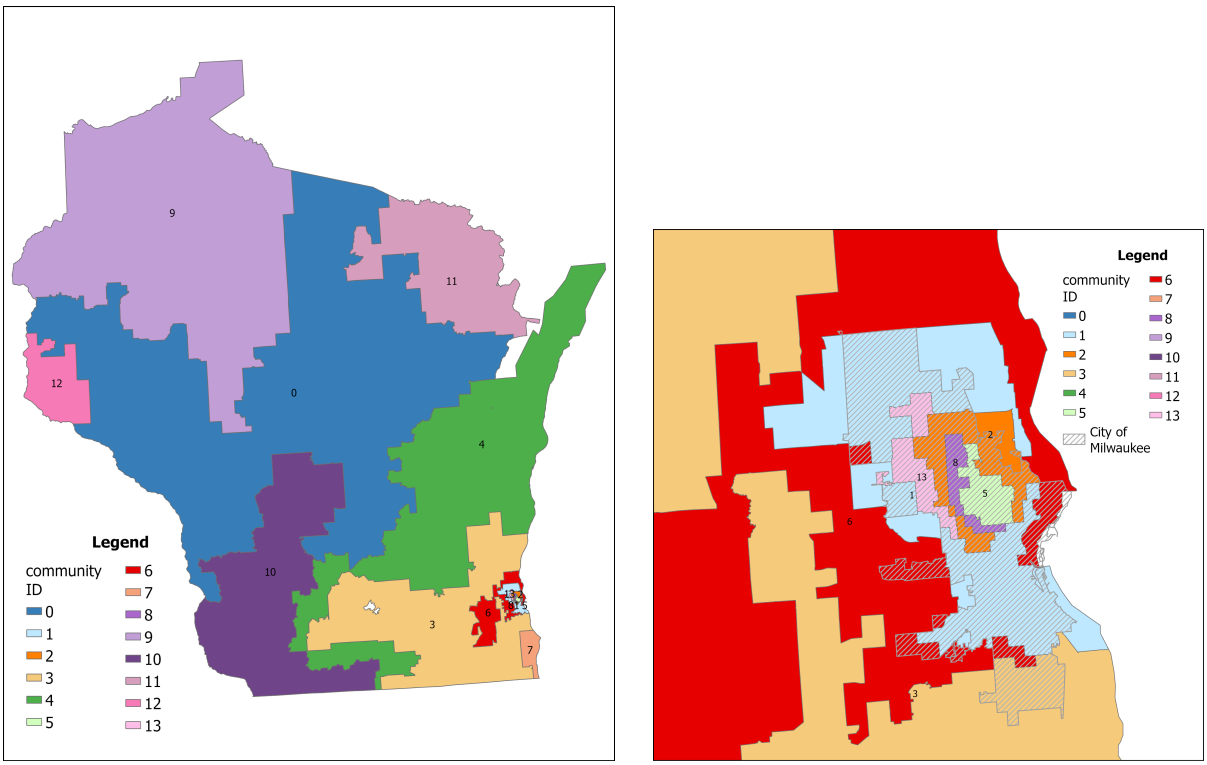

(a) Wisconsin (b) Milwaukee area

Figure 4.1: The resulting communities map of the whole study area (Wisconsin) and a zoomed-in view of the Milwaukee area.

end of the t-SNE plot, communities 9, 10, and 11 also overlap. They are geographically next to communities 0 and 4, and they also have relatively large area sizes. On the right-end part of Figure 4.2, there are some overlapped communities as well, including communities 5, 8, 2, and 13. As shown in Figure 4.1b, those are all the communities in the central Milwaukee area. The adjacency of communities on the t-SNE maps corresponds to their places on the actual geographic maps, meaning that the obtained embedding from *region2vec* is representative and contains important regional characteristics.

4.3.2 Node Importance Analyses

There are in total 9 features used in the model, including the white, black, Asian and Hispanic population percentage, the total household income, the mean household income, the population percentage with income below 50 percent federal poverty level, between 50

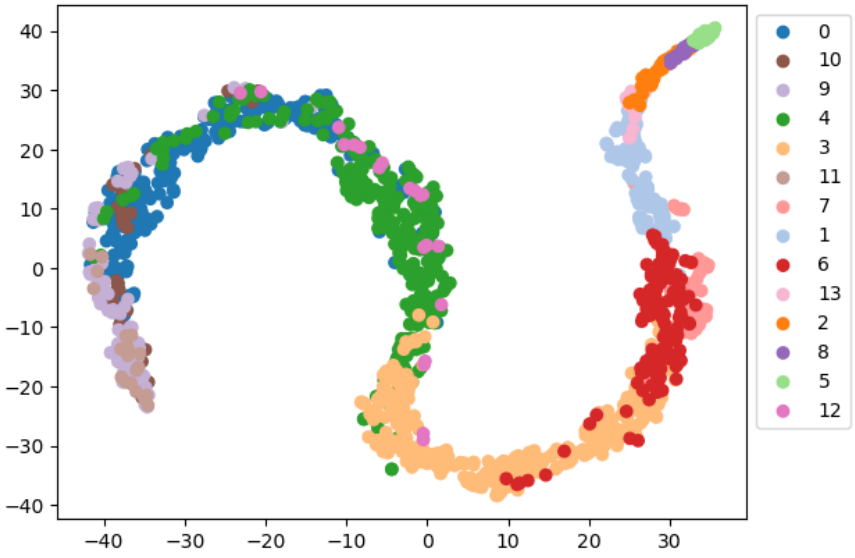

Figure 4.2: The t-SNE plot of the embedding from the *region2vec* method

percent and 300 percent federal poverty level, and above 300 percent federal poverty level.

Take the area of Milwaukee as an example, Figure 4.3a shows the box plot of feature importance scores for the central area of Milwaukee approximately represented by community 2, 5, 8 and 13. For each feature, the box plot shows the distribution of the feature importance values generated using GNNExplainer for all nodes in those communities, and the median value of each feature's importance score is shown on the x-axis label. The top three important features measured by the median values are the percentage of the population with income between 50 to 300 percent of the federal poverty level, the percentage of the population with income below 50 percent of the federal poverty level, and the mean household income. The income related features are the dominant information to predict the embedding of nodes in the central Milwaukee area. The feature 'Asian population percentage' is the least important feature for the four communities.

Figure 4.3b shows the feature importance scores for Community 1, which is the community surrounding the four communities in the central Milwaukee area. The top three important features for nodes in Community 1 are the percentage of the population with income below 50 percent of the federal poverty level, the percentage of the white popu-

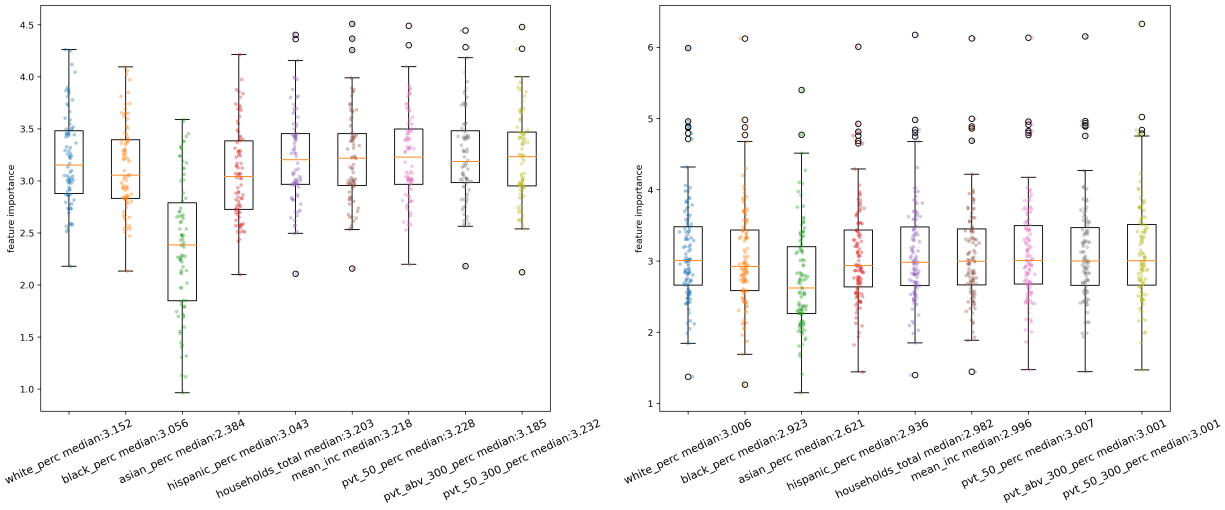

(a) community 2, 5, 8, 13 (b) community 1

Figure 4.3: The distribution of feature importance for all features of different communities.

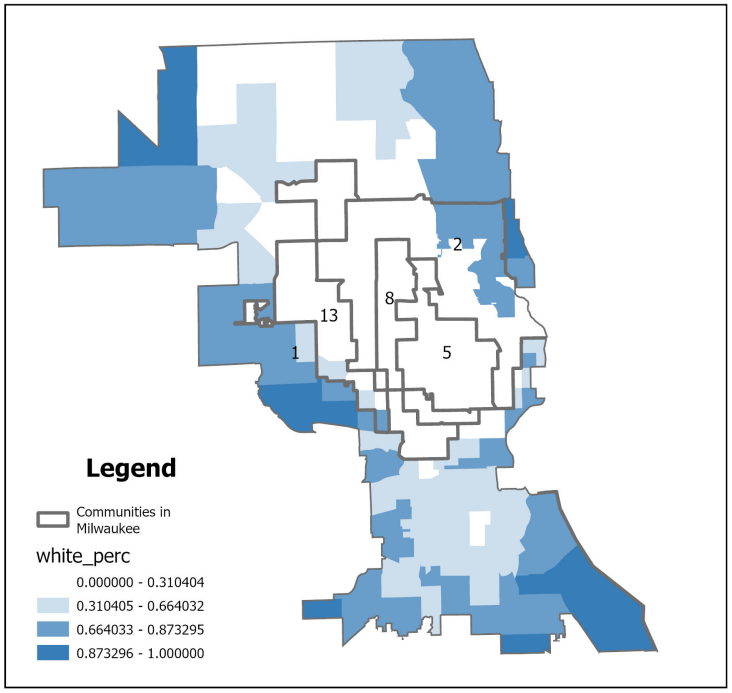

Figure 4.4: The white population percentage in Milwaukee with community boundaries

lation, and the percentage of the population with income between 50 to 300 percent of the federal poverty level. Different from the previous four communities, the percentage of the white population is very important for the nodes' prediction in Community 1. To better understand the reason behind this, the map of the white population percentage at each census tract in the Milwaukee area is presented (Figure 4.4). The color represents the value ranges of the white population percentage, whereas a lighter color means a lower value. Community 5, 8, 13 and 2 have most of their areas white, meaning that the census tracts in those communities have white population percentages lower than 25%. Different from the central Milwaukee area, Community 1 has census tracts in very dark blue colors, representing high values of white population percentage. Milwaukee has been known as one of the most segregated cities in the United States, and different race/ethnicity groups have relatively distinct and less-overlapping living areas compared with other cities (Prestby et al., 2020), so this potentially leads to the form of Community 1 with a majority of white population.

Through the node feature importance scores, the GNNExplainer can detect the importance of the white population percentage for nodes in Community 1. Comparing the important features of Community 1 with the features of nearby Communities 2, 5, 8, and 13 helps the audience to better understand the community detection result and answer questions such as why certain community is formed.

4.3.3 Subgraph Analyses

The first part of the subgraph analysis is for the aggregated level. The top 20 census tracts with the greatest population and the bottom 20 census tracts with the least population are selected as a comparison. The subgraph identified by the GNNExplainer model for each census tract is generated.

In order to evaluate the aggregated graph structures for the two groups of census tracts, four basic metrics of graphs are computed and listed the result in Table 4.1 and Table 4.2.

The minimum, maximum, and three quartiles are calculated for each metric. The number of nodes for the top 20 census tracts has a median of 25, while for the bottom 20 census tracts, the median is 21. For the number of edges, the top 20 census tracts have a median of 40, while the bottom 20 census tracts have a median of 35. In fact, by comparing the minimum, three quartiles, and the maximum of the two metrics, the census tracts with fewer populations tend to have smaller-size subgraphs. The diameter statistics with no edge weights are the same for both groups. However, for the distance-weighted diameter that considers the real-world geographic distribution of the graphs, the top 20 census tracts have much larger diameters for all quartiles except for the maximum value.

Table 4.1: Graph Statistics for top 20 census tracts with largest population

	Number of Nodes	Number of Edges	Diameters	Distance-Weighted Diameter (km)
min	15	26	3	29.51
25%	22	31.25	4	50.66
50%	25	40	4	59.71
75%	38.25	59.75	4	70.35
max	54	83	4	95.13

Table 4.2: Graph Statistics for bottom 20 census tracts with least population

	Number of Nodes	Number of Edges	Diameters	Distance-Weighted Diameter (km)
min	9	12	3	4.06
25%	18.75	29.5	4	4.67
50%	21	35	4	6.44
75%	22.75	39	4	14.50
max	30	47	4	149.57

Figure 4.5 shows the maps of the top three and bottom three census tracts sorted by population using the same map scale, so it is straightforward to compare the geographic size of the subgraphs. By visual examination, the subgraphs for census tracts with the greatest populations tend to cover greater geographic space than the subgraphs for census tracts with the least populations.

Since the subgraph contains important edges that affect the prediction of the targeted node (census tract), a large subgraph in terms of node and edge numbers means that there are more interrelated census tracts with the targeted census tract. The subgraph is generated based on the input graph of the *region2vec* model, which is the geographic adjacency matrix of all census tracts. However, the effects of the spatial interaction matrix representing mobility flows are encoded through the loss function to guide the embedding generation. Therefore, the generated subgraph can be used to understand people's travel patterns.

Different from the aggregated subgraph analyses, instance-level subgraph analyses focus more on understanding individual regional characteristics and revealing certain network structures. Here the subgraph can be considered as an approximation of the activity space, which is defined as "the subset of all urban locations with which the individual has direct contact as the result of day-to-day activities" (Horton and Reynolds, 1971, p. 37). For each census tract, the subgraph reflects the activity space of the population living inside. The activity space is greatly driven by the available services and resources in the area and can be affected by transportation modes that are accessible to the population (e.g., ownership of a private car).

Figure 4.5a and Figure 4.5b show the subgraphs of two census tracts in the Madison area. In Figure 4.5a, the census tract is located in Verona, WI, a city in the suburb of Madison. The city has around 54.4% of all households married couples living together and 39.4% households having children under the age of 18 living with them according to 2010 census data (U.S. Census Bureau, 2010). The suburban environment and the residential component may lead to the generation of large activity spaces, which can be a mixture of work, school, shopping, and entertainment-related activities. In Figure 4.5b, the census tract is located in the University of Wisconsin-Madison campus area. The activity space for the population in this area is much smaller compared with the previous census tract in the suburban area. It may be related to the limited services and resources in the campus area

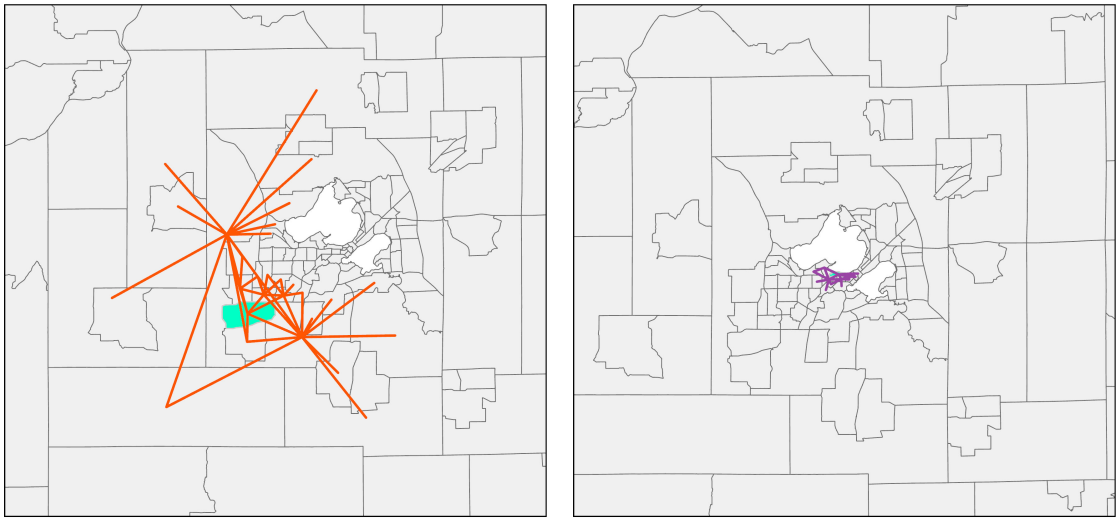

(a) top CT 55025010800 (b) bottom CT 55025001102

Figure 4.5: The subgraph identified by GNNExplainer for one census tract (CT) with top population and one CT with bottom population under the same map scale (1:450,000), the targeted census tract is colored using light green.

and the available transportation mode to the population. For example, households have a higher possibility of owning private cars, whereas people who live in the campus area (e.g., university students) may mostly rely on public transportation or walking.

Besides the Madison area, some subgraphs of census tracts in the Milwaukee area are illustrated in Figure 4.6. All the census tracts selected are census tracts with the bottom 20 population values. Figure 4.6a shows the distribution of the four subgraphs, where subgraph 645 and 648 are located close to each other, subgraph 845 is on the southern part of the map, and subgraph 674 is on the southwestern part of the area. Since Milwaukee is famous for its segregation level, the choropleth map of the area is produced based on population percentages of different race groups. Figure 4.6b shows two subgraphs and the choropleth map of the black population percentage, where a darker color means a higher percentage. The subgraphs of the two census tracts are located in the central area with the highest range of black population percentages as indicated by the color. Their subgraphs' sizes are relatively small, as compared to the other two subgraphs in Figure 4.6a. In Figure 4.6c, the map shows the percentage of the Hispanic population in each census

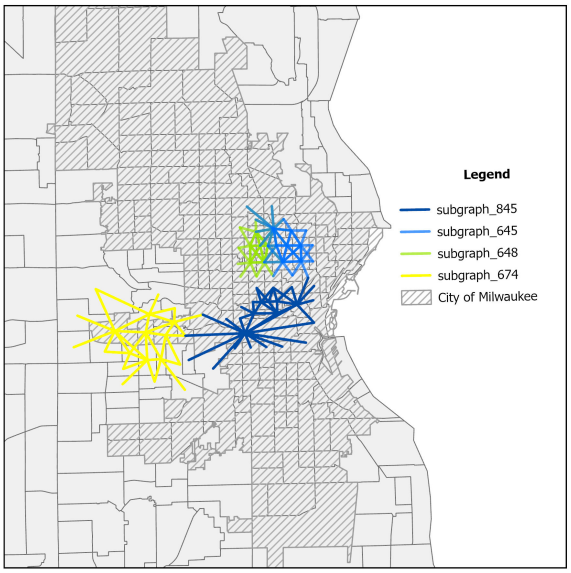

(a) subgraphs examples overview

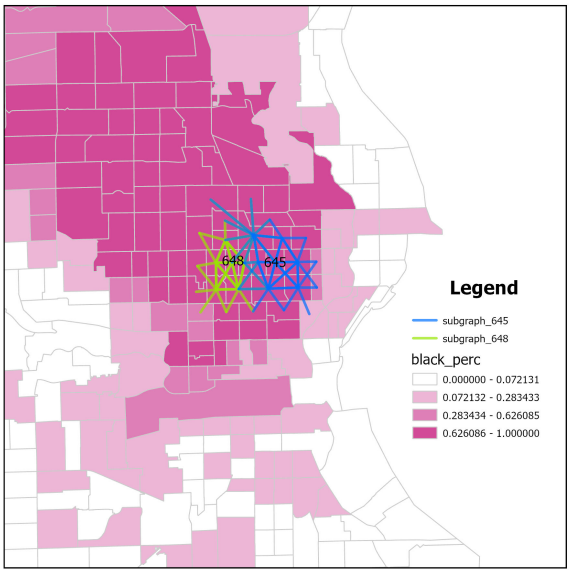

(b) example CTs 55119960500, 55119960300

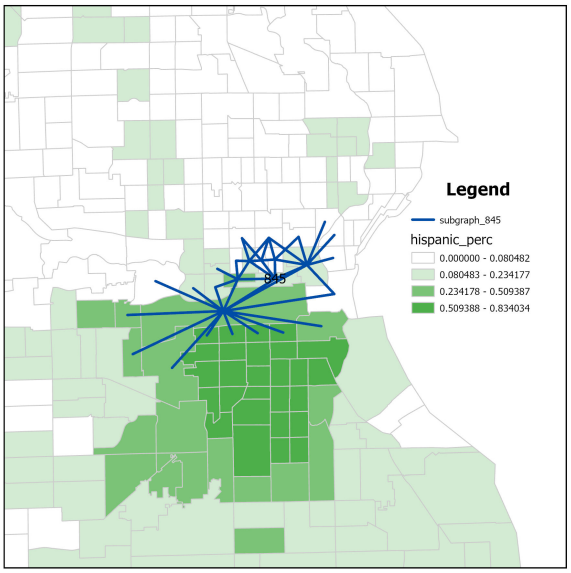

(c) example CT 55059000500

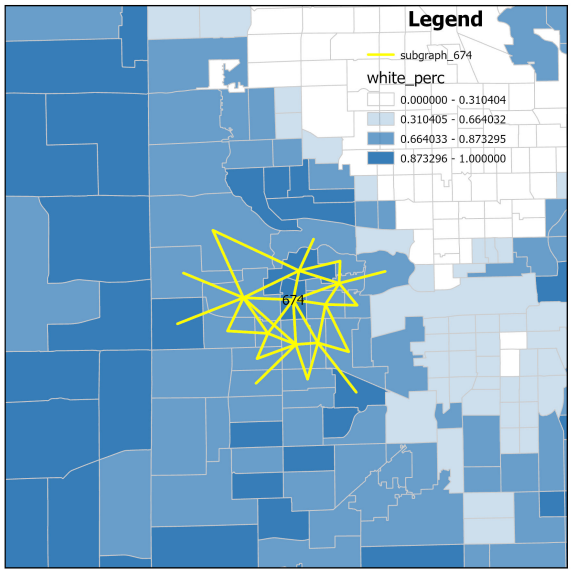

(d) example CT 55027961200

Figure 4.6: The example subgraphs identified by GNNExplainer in Milwaukee, b, c, d having the same map scale (1:120,000), the targeted census tract is shown with its unique ID.

tract. The selected census tract is located near the border of the area with the greatest Hispanic population percentages. Its subgraph has more connections with census tracts that are in the darker green areas and fewer connections with census tracts in the northern part with lower Hispanic population percentages. In Figure 4.6d, The base map shows the population percentage of white people, which are the majority race group in the suburb of Milwaukee. The subgraph has connections with all census tracts having white population percentages in the 3rd or 4th ranges, and the subgraph size is obviously larger than that of the census tract in Figure 4.6b in the central city area of Milwaukee. The results have shown that the subgraphs identified from the GNNExplainer can reflect the activity spaces of people, and different race groups seem to have very particular activity spaces that rarely overlap with other major race groups in the Milwaukee area.

4.4 Conclusion

Even though GeoAI-based methods have been widely used to model and predict geographic phenomena and achieve greater performance than traditional approaches, they are considered black-box methods, and the internal mechanism is hard to explain. The lack of explainability may lead to lower trust and prevent the application of GeoAI approaches to a broader audience.

This chapter explored the explainability of the deep learning method on spatial network regionalization. The GNNExplainer model is applied to the proposed GCN-based *region2vec* model to understand how the node representations are generated in an unsupervised community detection task. For each node, the key subset of features and the important subgraph are identified to provide a closer look into why certain predictions are generated from the GCN model.

The feature importance is aggregated based on community membership, and key features such as white population percentage have been discovered to play a crucial role in delineating some regions in Milwaukee. The subgraph helps to understand people's activity

spaces and significantly different sizes of activity spaces have been identified for census tracts in different functional areas. Additionally, the subgraphs can also reflect the activity spaces of different race/ethnicity groups, where each group tends to travel within specific regions occupied primarily by the same race/ethnicity groups. This chapter provides an example of integrating the XAI method into a deep learning-based regionalization task to support a better understanding of the model results. It demonstrates the potential use of explanation methods in the GeoAI domain.

The current study also has some limitations. First, many GNN explanation methods provide instance-based explanations so that detailed reasoning can be realized. However, the discovery of potential patterns may always require local knowledge or additional information to support. It can be time-consuming when one is not familiar with the study area, or there are a massive amount of individual explanations. How to appropriately aggregate instance-level data to identify regional patterns remains a challenge. In addition, for a graph-structure explanation, it is hard to aggregate multiple subgraphs as the structure of a single subgraph may be lost after the aggregation. How to better extract structural patterns over different subgraphs poses another challenge to GNN Explanations.

For future work, more features, such as different types of points of interest (POIs), can be added to the input graph. The POIs may help understand the major functions of each census tract and to further understand the activity space generated from the explanations. Additionally, the same framework can be applied to other supervised tasks so that the explanation can be combined with the ground truth labels. Potential future applications can be Origin-Destination flow predictions, where regions with different levels of flows can be related to their important features and subgraphs for further understanding of movement patterns.

5 CONCLUSIONS AND FUTURE WORK

5.1 Conclusions

The study of regionalization is crucial for a systematic understanding of geographic phenomena. How regions interact with each other through spatial networks is complicated yet very informative. This dissertation focuses on understanding how can community detection methods be applied to spatial networks to support regionalization tasks. It first explores how human mobility-based spatial networks can be used to delineate Rational Service Areas in the public health domain. Then, given the discovered limitation of the existing regionalization methods, the dissertation proposes a new family of community detection methods based on GeoAI models that can consider both node attributes and edge connections in the spatial network. Lastly, the dissertation combines GeoAI methods with an Explainable AI model to improve the trustworthiness of the GeoAI-based approach and offer reliable interpretability of the regionalization results. The **contributions** of this dissertation can be summarized as below:

(1). Chapter 2 offers new opportunities to understand regionalization in the public health domain using human mobility data. Instead of using data from hospital visits that have limited access, this study uses increasing available mobile phone location-based human mobility data to extract travel patterns for health-related visits. It proposes a new methodological framework that automates the process of Rational Service Area delineation with spatial constraints. The Rational Service Areas identified from the proposed method are more compact than other baselines, and they show the best performance when applied to a downstream task of Health Profession Shortage Area Delineation. The whole area delineation process is automated in a GIS environment to provide automatic, repeated, and adjustable regionalization for a broad range of users. It demonstrates the potential of human mobility data and the use of GIS tools for addressing health inequality problems.

(2). Chapter 3 focuses on methodology innovation of existing community detection

methods. It combines AI methods with geospatial considerations to make contributions to the GeoAI domain. The proposed method can consider two types of networks in the regionalization task: the geographic adjacency graph and the spatial interaction graph. The method manages to integrate the two networks and the node attributes into the regionalization process via the GCN and GAT models. The performance of the proposed model and other baselines are evaluated through various metrics to show that the GeoAI-enhanced community detection has great potential when one wants to maximize both node features and edge connections. It is also applied to the Rational Service Area development problem in public health and shows its promise in real-world regionalization problems.

(3). Chapter 4 explores the direction of applying Explanation AI models to improve the interpretability of GeoAI methods. Very limited research exists on how well humans can understand black-box AI model results in geospatial tasks. This chapter shows how graph-based GeoAI methods can be explained and how the generated explanations can be analyzed to gain further insights into regional characteristics. There are two types of explanations for the prediction of each node: important node features and important subgraphs. By examining individual-level and community-level node features, certain regional characteristics can be discovered. The important subgraphs can reflect the nodes' activity space and be used to understand the travel patterns. This work is among the very first research to analyze how to explain GeoAI-based methods and make them more transparent and trustworthy.

5.2 Future Directions

Based on the contributions and findings of this dissertation, three future directions are proposed.

First, how to fully use spatial networks can be further explored. No matter what data structure is used to represent the geographic phenomena, it will only be an approximation of the real-world event, and some information will be lost. The mobility-based network

adopted in this dissertation is modeled as undirected, even though it is directed in the real world. The Origin-Destination flows are considered pairwise interactions without considering the direction of the movement, which can lead to potential bias and misunderstanding. Most of the studies use undirected flows because they are easier to model and analyze than the directed ones. There are some existing researches on modeling directed graphs (Zhang et al., 2022) and how such methods can be applied to directed spatial networks worthy of further analyses. In addition, what kind of information can be used to construct spatial networks deserves a deep understanding as well. In this dissertation, the collected place visits are only from people's home locations, which are estimated based on people's nighttime dwelling locations. Other types of visit flows, such as commuting flows from people's work locations to different types of places can also be explored to obtain a more comprehensive picture of travel patterns. The mobility patterns are usually not as simple as trips between home and work locations, sometimes people may take a detour to pick up kids in school, stop by certain places for an appointment, etc. How to better model the Origin-Destination flows with considerations of people's real-world trip patterns can be further studied.

Second, an inherent requirement in many regionalization tasks is that the generated regions always need to be spatially contiguous. Sometimes, the shape of regions is also preferred to be convex so that the boundaries are simpler for administrative management, and the delivery of services such as public transportation or healthcare can be more efficient. However, there are some challenges in maintaining spatial contiguity. For example, geographic barriers such as rivers or lakes make the process more complicated, as one needs to consider both natural barriers and other socio-economic perspectives to make sure regions are contiguous. Additionally, it is not very easy to implicitly incorporate such contiguity requirements in the regionalization process. The geographic adjacency relationship among the input units needs to be specifically used to enforce that only neighborhood units can be grouped into the same region, and the process can be tedious in traditional regionalization.

In deep learning methods, this can be even harder because such constraints may not be strictly fulfilled in the training process. Post-training spatial constraint enforcement can lead to sub-optimal results that affect the model performance. Therefore, how to ensure spatial contiguity in regionalization tasks requires careful consideration of different factors including geographic, demographic, economic, etc. There is also a lack of deep learning methods with spatial constraints embedded. Future research can further explore the direction of spatially constrained regionalization.

Third, the dissertation is among the first studies to apply Explainable AI (XAI) models to interpret the behaviors of GeoAI methods. A variety of explainable AI models have been proposed in recent years to understand AI models from different perspectives. However, how different XAI models can be applied to regionalization tasks remains undiscovered. How to compare and evaluate the performance of different XAI models is another direction that is worth further exploration. Currently, there are no uniform standards to evaluate the quality of explanations of various explanation methods. Some research designs synthetic datasets to evaluate the performance of multiple explanation methods (Agarwal et al., 2023). However, most geospatial tasks have their unique real-world datasets, and the dataset may not be structured in a way that allows comparisons of different explanation methods. It is necessary to design synthetic spatial networks to enable the evaluation of different graph-based XAI methods in the future.

REFERENCES

Agarwal, Chirag, Owen Queen, Himabindu Lakkaraju, and Marinka Zitnik. 2023. Evaluating explainability for graph neural networks. *Scientific Data* 10(1):144.

Bai, Lingyao, Zhuolin Tao, Yang Cheng, Ling Feng, and Shaoshuai Wang. 2023. Delineating hierarchical obstetric hospital service areas using the huff model based on medical records. *Applied Geography* 153:102903.

Barbosa, Alexandre, Rodrigo Trevisan, Naira Hovakimyan, and Nicolas F Martin. 2020. Modeling yield response to crop management using convolutional neural networks. *Computers and Electronics in Agriculture* 170:105197.

Barthélemy, Marc. 2011. Spatial networks. *Physics reports* 499(1-3):1–101.

Benítez, José Manuel, Juan Luis Castro, and Ignacio Requena. 1997. Are artificial neural networks black boxes? *IEEE Transactions on neural networks* 8(5):1156–1164.

Blondel, Vincent D, Jean-Loup Guillaume, Renaud Lambiotte, and Etienne Lefebvre. 2008. Fast unfolding of communities in large networks. *Journal of statistical mechanics: theory and experiment* 2008(10):P10008.

Chen, Chen, Jiange Jiang, Ning Lv, and Siyu Li. 2020. An intelligent path planning scheme of autonomous vehicles platoon using deep reinforcement learning on network edge. *ieee access* 8:99059–99069.

Cliff, Andrew David, and J Keith Ord. 1973. *Spatial autocorrelation*. London: Pion.

Cui, Ganqu, Jie Zhou, Cheng Yang, and Zhiyuan Liu. 2020. Adaptive graph encoder for attributed graph embedding. In *Proceedings of the 26th acm sigkdd international conference on knowledge discovery & data mining*, 976–985.

De Sabbata, Stefano, Andrea Ballatore, Harvey J Miller, Renée Sieber, Ivan Tyukin, and Godwin Yeboah. 2023. Geoai in urban analytics.

De Sabbata, Stefano, and Pengyuan Liu. 2023. A graph neural network framework for spatial geodemographic classification. *International Journal of Geographical Information Science* 1–23.

Dikshit, Abhirup, and Biswajeet Pradhan. 2021. Interpretable and explainable ai (xai) model for spatial drought prediction. *Science of the Total Environment* 801:149797.

D'Orazio, Marco, Gabriele Bernardini, and Enrico Quagliarini. 2020. How to restart? an agent-based simulation model towards the definition of strategies for covid-19" second phase" in public buildings. *arXiv preprint arXiv:2004.12927*.

Expert, Paul, Tim S Evans, Vincent D Blondel, and Renaud Lambiotte. 2011. Uncovering space-independent communities in spatial networks. *Proceedings of the National Academy of Sciences* 108(19):7663–7668.

Fayyad, Jamil, Mohammad A Jaradat, Dominique Gruyer, and Homayoun Najjaran. 2020. Deep learning sensor fusion for autonomous vehicle perception and localization: A review. *Sensors* 20(15):4220.

Fey, Matthias, and Jan E. Lenssen. 2019. Fast graph representation learning with PyTorch Geometric. In *Iclr workshop on representation learning on graphs and manifolds*.

Flake, Gary William, Robert E Tarjan, and Kostas Tsioutsiouliklis. 2004. Graph clustering and minimum cut trees. *Internet Mathematics* 1(4):385–408.

Flinn, Edward A, and Eric R Engdahl. 1965. A proposed basis for geographical and seismic regionalization. *Reviews of Geophysics* 3(1):123–149.

Fu, Xinyu, Jiani Zhang, Ziqiao Meng, and Irwin King. 2020. Magnn: Metapath aggregated graph neural network for heterogeneous graph embedding. In *Proceedings of the web conference 2020*, 2331–2341.

Gao, Song, Yingjie Hu, and Wenwen Li. 2024. Introduction to geospatial artificial intelligence (GeoAI). In *Handbook of geospatial artificial intelligence*, 3–16. CRC Press.

Gao, Song, Yu Liu, Yaoli Wang, and Xiujun Ma. 2013. Discovering spatial interaction communities from mobile phone data. *Transactions in GIS* 17(3):463–481.

Geography Education Standards Project. 1994. Geography for life, national geography standards.

Ginzberg, Eli. 1977. The many meanings of regionalization in health. In *Regionalization and health policy*. US Public Health Service Washington, DC.

Goodman, David C, Stephen S Mick, David Bott, Therese Stukel, Chiang-hua Chang, Nancy Marth, Jim Poage, and Henry J Carretta. 2003. Primary care service areas: a new tool for the evaluation of primary care services. *Health services research* 38(1p1):287–309.

Goyal, Palash, and Emilio Ferrara. 2018. Graph embedding techniques, applications, and performance: A survey. *Knowledge-Based Systems* 151:78–94.

Grover, Aditya, and Jure Leskovec. 2016. node2vec: Scalable feature learning for networks. In *Proceedings of the 22nd acm sigkdd international conference on knowledge discovery and data mining*, 855–864.

Guo, Shengnan, Youfang Lin, Ning Feng, Chao Song, and Huaiyu Wan. 2019. Attention based spatial-temporal graph convolutional networks for traffic flow forecasting. In *Proceedings of the AAAI conference on artificial intelligence*, vol. 33, 922–929.

Hamilton, Will, Zhitao Ying, and Jure Leskovec. 2017. Inductive representation learning on large graphs. *Advances in neural information processing systems* 30.

Hart, Gary, Edward Salsberg, Debra M Phillips, and Denise M Lishner. 2002. Rural health care providers in the united states. *The journal of rural health* 18(5):211–231.

He, Dongxiao, Yue Song, Di Jin, Zhiyong Feng, Binbin Zhang, Zhizhi Yu, and Weixiong Zhang. 2021. Community-Centric Graph Convolutional Network for Unsupervised Community Detection 3515–3521.

Health Resources and Services Administration. 2020. Shortage Designation Management System (SDMS): Manual for Policies and Procedures. https://contentmanager.med.uvm.edu/docs/sdms_manual_/ahec-documents/sdms_manual_.pdf.

Hinton, Geoffrey E, and Ruslan R Salakhutdinov. 2006. Reducing the dimensionality of data with neural networks. *science* 313(5786):504–507.

Horton, Frank E, and David R Reynolds. 1971. Effects of urban spatial structure on individual behavior. *Economic geography* 47(1):36–48.

Hou, Xiao, Song Gao, Qin Li, Yuhao Kang, Nan Chen, Kaiping Chen, Jinmeng Rao, Jordan S Ellenberg, and Jonathan A Patz. 2021. Intracounty modeling of covid-19 infection with human mobility: Assessing spatial heterogeneity with business traffic, age, and race. *Proceedings of the National Academy of Sciences* 118(24):e2020524118.

HRSA. 2020. Shortage Designation Management System (SDMS): Manual for Policies and Procedures. https://programportal.hrsa.gov/docs/pco/Manual-for-Policies-and-Procedures.pdf.

HRSA. 2021. Defining rural population. https://www.hrsa.gov/rural-health/about-us/definition/index.html.

HRSA. 2021. What is Shortage Designation? Health Resources Services Administration. https://bhw.hrsa.gov/workforce-shortage-areas/shortage-designation.

HRSA. 2023. The bureau of health workforce portal. https://programportal.hrsa.gov/extranet/landing.seam.

Hu, Yujie, Fahui Wang, and Imam M Xierali. 2018. Automated delineation of hospital service areas and hospital referral regions by modularity optimization. *Health services research* 53(1):236–255.

Huang, Qiang, Makoto Yamada, Yuan Tian, Dinesh Singh, and Yi Chang. 2022. Graphlime: Local interpretable model explanations for graph neural networks. *IEEE Transactions on Knowledge and Data Engineering*.

Huang, Xiao, Cuizhen Wang, and Zhenlong Li. 2018. A near real-time flood-mapping approach by integrating social media and post-event satellite imagery. *Annals of GIS* 24(2): 113–123.

IBM. 2024. What is artificial intelligence (AI)?

Janowicz, Krzysztof, Song Gao, Grant McKenzie, Yingjie Hu, and Budhendra Bhaduri. 2020. Geoai: spatially explicit artificial intelligence techniques for geographic knowledge discovery and beyond. *International Journal of Geographical Information Science* 34(4):625–636.

Jia, Peng, Fahui Wang, and Imam M Xierali. 2017. Delineating hierarchical hospital service areas in florida. *Geographical Review* 107(4):608–623.

Jia, Peng, Imam M Xierali, and Fahui Wang. 2015. Evaluating and re-demarcating the hospital service areas in florida. *Applied Geography* 60:248–253.

Jiang, Hao, Hao Hu, Renhai Zhong, Jinfan Xu, Jialu Xu, Jingfeng Huang, Shaowen Wang, Yibin Ying, and Tao Lin. 2020. A deep learning approach to conflating heterogeneous geospatial data for corn yield estimation: A case study of the us corn belt at the county level. *Global change biology* 26(3):1754–1766.

Jin, Chanwoo, Atsushi Nara, Jiue-An Yang, and Ming-Hsiang Tsou. 2020. Similarity measurement on human mobility data with spatially weighted structural similarity index (spssim). *Transactions in GIS* 24(1):104–122.

Jin, Di, Bingyi Li, Pengfei Jiao, Dongxiao He, and Hongyu Shan. 2019. Community Detection via Joint Graph Convolutional Network Embedding in Attribute Network. *Lecture Notes in Computer Science* (*including subseries Lecture Notes in Artificial Intelligence and Lecture Notes in Bioinformatics*) 11731 LNCS:594–606.

Johnson, Stephen C. 1967. Hierarchical clustering schemes. *Psychometrika* 32(3):241–254.

Kang, Yuhao, Song Gao, Yunlei Liang, Mingxiao Li, Jinmeng Rao, and Jake Kruse. 2020. Multiscale dynamic human mobility flow dataset in the us during the covid-19 epidemic. *Scientific Data* 7(1):1–13.

Kang, Yuhao, Kunlin Wu, Song Gao, Ignavier Ng, Jinmeng Rao, Shan Ye, Fan Zhang, and Teng Fei. 2022. Sticc: a multivariate spatial clustering method for repeated geographic pattern discovery with consideration of spatial contiguity. *International Journal of Geographical Information Science* 36(8):1518–1549.

Kavak, Hamdi, Jose J Padilla, Christopher J Lynch, and Saikou Y Diallo. 2018. Big data, agents, and machine learning: towards a data-driven agent-based modeling approach. In *Proceedings of the annual simulation symposium*, 1–12.

Khan, Nagma, Ushasi Chaudhuri, Biplab Banerjee, and Subhasis Chaudhuri. 2019. Graph convolutional network for multi-label vhr remote sensing scene recognition. *Neurocomputing* 357:36–46.

Kipf, Thomas N., and Max Welling. 2017. Semi-supervised classification with graph convolutional networks. *5th International Conference on Learning Representations, ICLR 2017 - Conference Track Proceedings* 1–14. 1609.02907.

Klapka, Pavel, Stanislav Kraft, and Marián Halás. 2020. Network based definition of functional regions: A graph theory approach for spatial distribution of traffic flows. *Journal of Transport Geography* 88:102855.

Klauss, Gunnar, Lukas Staub, Marcel Widmer, and André Busato. 2005. Hospital service areas–a new tool for health care planning in switzerland. *BMC health services research* 5(1): 1–15.

Kruse, Jacob, Yuhao Kang, Yu-Ning Liu, Fan Zhang, and Song Gao. 2021. Places for play: Understanding human perception of playability in cities using street view images and deep learning. *Computers, Environment and Urban Systems* 90:101693.

LeCun, Yann, Yoshua Bengio, et al. 1995. Convolutional networks for images, speech, and time series. *The handbook of brain theory and neural networks* 3361(10):1995.

Li, Yansheng, Ruixian Chen, Yongjun Zhang, Mi Zhang, and Ling Chen. 2020. Multi-label remote sensing image scene classification by combining a convolutional neural network and a graph neural network. *Remote Sensing* 12(23):4003.

Li, Ziqi. 2022. Extracting spatial effects from machine learning model using local interpretation method: An example of shap and xgboost. *Computers, Environment and Urban Systems* 96:101845.

Liang, Yunlei, Jiawei Zhu, Wen Ye, and Song Gao. 2022. Region2vec: community detection on spatial networks using graph embedding with node attributes and spatial interactions. In *Proceedings of the 30th international conference on advances in geographic information systems*, 1–4.

Liu, Jiexin. 2007. Health professional shortage and health status and health care access. *Journal of health care for the poor and underserved* 18(3):590–598.

Liu, Pengyuan, and Filip Biljecki. 2022. A review of spatially-explicit geoai applications in urban geography. *International Journal of Applied Earth Observation and Geoinformation* 112: 102936.

Liu, Pengyuan, Yan Zhang, and Filip Biljecki. 2023. Explainable spatially explicit geospatial artificial intelligence in urban analytics. *Environment and Planning B: Urban Analytics and City Science* 23998083231204689.

Liu, Xi, Chaogui Kang, Li Gong, and Yu Liu. 2016. Incorporating spatial interaction patterns in classifying and understanding urban land use. *International Journal of Geographical Information Science* 30(2):334–350.

Liu, Yu, Chaogui Kang, Song Gao, Yu Xiao, and Yuan Tian. 2012. Understanding intra-urban trip patterns from taxi trajectory data. *Journal of geographical systems* 14(4):463–483.

Liu, Yu, Zhengwei Sui, Chaogui Kang, and Yong Gao. 2014. Uncovering patterns of inter-urban trip and spatial interaction from social media check-in data. *PloS One* 9(1): e86026.

Lopes, P. M. 2000. State-wide rational service areas for primary care services: Lessons from six states. Tech. Rep.

Lucic, Ana, Maartje A Ter Hoeve, Gabriele Tolomei, Maarten De Rijke, and Fabrizio Silvestri. 2022. Cf-gnnexplainer: Counterfactual explanations for graph neural networks. In *International conference on artificial intelligence and statistics*, 4499–4511. PMLR.

Lundberg, Scott M, and Su-In Lee. 2017. A unified approach to interpreting model predictions. In *Advances in neural information processing systems 30*, ed. I. Guyon, U. V. Luxburg, S. Bengio, H. Wallach, R. Fergus, S. Vishwanathan, and R. Garnett, 4765–4774. Curran Associates, Inc.

Luo, Dongsheng, Wei Cheng, Dongkuan Xu, Wenchao Yu, Bo Zong, Haifeng Chen, and Xiang Zhang. 2020. Parameterized explainer for graph neural network. *Advances in neural information processing systems* 33:19620–19631.

Luo, Wei. 2004. Using a GIS-based floating catchment method to assess areas with shortage of physicians. *Health & place* 10(1):1–11.

Van der Maaten, Laurens, and Geoffrey Hinton. 2008. Visualizing data using t-sne. *Journal of machine learning research* 9(11).

MacEachren, Alan M. 1985. Compactness of geographic shape: Comparison and evaluation of measures. *Geografiska Annaler: Series B, Human Geography* 67(1):53–67.

Machado, Sara R, Sahan Jayawardana, Elias Mossialos, and Muthiah Vaduganathan. 2021. Physician density by specialty type in urban and rural counties in the us, 2010 to 2017. *JAMA network open* 4(1):e2033994–e2033994.

MacQueen, James, et al. 1967. Some methods for classification and analysis of multivariate observations. In *Proceedings of the fifth berkeley symposium on mathematical statistics and probability*, vol. 1, 281–297. Oakland, CA, USA.

Mai, Gengchen, Yingjie Hu, Song Gao, Ling Cai, Bruno Martins, Johannes Scholz, Jing Gao, and Krzysztof Janowicz. 2022. Symbolic and subsymbolic geoai: Geospatial knowledge graphs and spatially explicit machine learning. *Trans. GIS* 26(8):3118–3124.

Manning, Christopher, Prabhakar Raghavan, and Hinrich Schütze. 2010. Introduction to information retrieval. *Natural Language Engineering* 16(1):100–103.

Martin, Lawrence. 1965. *The physical geography of wisconsin*, vol. 36. Univ of Wisconsin Press.

McCarthy, John, et al. 2007. What is artificial intelligence.

Molokwu, Bonaventure, Shaon Bhatta Shuvo, Narayan C Kar, and Ziad Kobti. 2020. Node classification and link prediction in social graphs using rlvecn. In *32nd international conference on scientific and statistical database management*, 1–10.

Nelson, Garrett Dash, and Alasdair Rae. 2016. An economic geography of the united states: From commutes to megaregions. *PloS One* 11(11):e0166083.

Newman, Mark EJ. 2006. Modularity and community structure in networks. *Proceedings of the national academy of sciences* 103(23):8577–8582.

Openshaw, Stan. 1984. The modifiable areal unit problem. *Concepts and techniques in modern geography*.

Pandey, Bhartendu, Christa Brelsford, and Karen C Seto. 2022. Infrastructure inequality is a characteristic of urbanization. *Proceedings of the National Academy of Sciences* 119(15): e2119890119.

Park, Jiwoong, Minsik Lee, Hyung Jin Chang, Kyuewang Lee, and Jin Young Choi. 2019. Symmetric graph convolutional autoencoder for unsupervised graph representation learning. In *Proceedings of the ieee/cvf international conference on computer vision*, 6519–6528.

Pedregosa, F., G. Varoquaux, A. Gramfort, V. Michel, B. Thirion, O. Grisel, M. Blondel, P. Prettenhofer, R. Weiss, V. Dubourg, J. Vanderplas, A. Passos, D. Cournapeau, M. Brucher, M. Perrot, and E. Duchesnay. 2011. Scikit-learn: Machine learning in Python. *Journal of Machine Learning Research* 12:2825–2830.

Peng, Bo, Qunying Huang, Jamp Vongkusolkit, Song Gao, Daniel B. Wright, Zheng N. Fang, and Yi Qiang. 2021. Urban flood mapping with bitemporal multispectral imagery via a self-supervised learning framework. *IEEE Journal of Selected Topics in Applied Earth Observations and Remote Sensing* 14:2001–2016.

Perozzi, Bryan, Rami Al-Rfou, and Steven Skiena. 2014. Deepwalk: Online learning of social representations. In *Proceedings of the 20th acm sigkdd international conference on knowledge discovery and data mining*, 701–710.

Pfeifer, Bastian, Anna Saranti, and Andreas Holzinger. 2022. Gnn-subnet: disease subnetwork detection with explainable graph neural networks. *Bioinformatics* 38(Supplement_2): ii120–ii126.

Pinheiro, Diego, Ryan Hartman, Erick Romero, Ronaldo Menezes, and Martin Cadeiras. 2020. Network-based delineation of health service areas: A comparative analysis of community detection algorithms. In *Complex networks xi*, 359–370. Springer.

Pons, Pascal, and Matthieu Latapy. 2005. Computing communities in large networks using random walks. In *International symposium on computer and information sciences*, 284–293. Springer.

Prestby, Timothy, Joseph App, Yuhao Kang, and Song Gao. 2020. Understanding neighborhood isolation through spatial interaction network analysis using location big data. *Environment and Planning A: Economy and Space* 52(6):1027–1031.

Ratti, Carlo, Stanislav Sobolevsky, Francesco Calabrese, Clio Andris, Jonathan Reades, Mauro Martino, Rob Claxton, and Steven H Strogatz. 2010. Redrawing the map of great britain from a network of human interactions. *PloS one* 5(12):e14248.

Ribeiro, Marco Tulio, Sameer Singh, and Carlos Guestrin. 2016. " why should i trust you?" explaining the predictions of any classifier. In *Proceedings of the 22nd acm sigkdd international conference on knowledge discovery and data mining*, 1135–1144.

SafeGraph. 2023. Fresh, accurate places data built to power modern applications. `https://www.safegraph.com/products/places`.

Samek, Wojciech, Grégoire Montavon, Andrea Vedaldi, Lars Kai Hansen, and Klaus-Robert Müller. 2019. *Explainable ai: interpreting, explaining and visualizing deep learning*, vol. 11700. Springer Nature.

Schlichtkrull, Michael Sejr, Nicola De Cao, and Ivan Titov. 2022. Interpreting graph neural networks for nlp with differentiable edge masking. `2010.00577`.

Shi, Wenzhong, Michael Goodchild, Michael Batty, Qingquan Li, Xintao Liu, and Anshu Zhang. 2022. Prospective for urban informatics. *Urban Informatics* 1(1):2.

Stoer, Mechthild, and Frank Wagner. 1997. A simple min-cut algorithm. *Journal of the ACM (JACM)* 44(4):585–591.

Su, Xing, Shan Xue, Fanzhen Liu, Jia Wu, Senior Member, Jian Yang, Chuan Zhou, and Wenbin Hu. 2021. A Comprehensive Survey on Community Detection with Deep Learning (Xx). `arXiv:2105.12584v2`.

Tang, Jiabin, Lianghao Xia, and Chao Huang. 2023. Explainable spatio-temporal graph neural networks. In *Proceedings of the 32nd acm international conference on information and knowledge management*, 2432–2441.

Tang, Jian, Meng Qu, Mingzhe Wang, Ming Zhang, Jun Yan, and Qiaozhu Mei. 2015. Line: Large-scale information network embedding. In *Proceedings of the 24th international conference on world wide web*, 1067–1077.

Tobler, Waldo R. 1970. A computer movie simulating urban growth in the detroit region. *Economic geography* 46(sup1):234–240.

Traag, Vincent A, Ludo Waltman, and Nees Jan Van Eck. 2019. From louvain to leiden: guaranteeing well-connected communities. *Scientific reports* 9(1):5233.

U.S. Census Bureau. 2010. United States Census Bureau. `"https://www.census.gov/"`.

———. 2023. Tiger/line shapefiles. `"https://www.census.gov/geographies/mapping-files/time-series/geo/tiger-line-file.html"`.

Velickovic, Petar, Guillem Cucurull, Arantxa Casanova, Adriana Romero, Pietro Lio, Yoshua Bengio, et al. 2017. Graph attention networks. *stat* 1050(20):10–48550.

Wang, Changzhen, and Fahui Wang. 2022a. GIS-automated delineation of hospital service areas in florida: from dartmouth method to network community detection methods. *Annals of GIS* 1–17.

———. 2022b. GIS-automated delineation of hospital service areas in Florida: from Dartmouth method to network community detection methods. *Annals of GIS* 00.

Wang, Changzhen, Fahui Wang, and Tracy Onega. 2021a. Network optimization approach to delineating health care service areas: Spatially constrained louvain and leiden algorithms. *Transactions in GIS* 25(2):1065–1081.

———. 2021b. Network optimization approach to delineating health care service areas: Spatially constrained Louvain and Leiden algorithms. *Transactions in GIS* 25(2):1065–1081.

Wang, Daixin, Peng Cui, and Wenwu Zhu. 2016. Structural deep network embedding. In *Proceedings of the 22nd acm sigkdd international conference on knowledge discovery and data mining*, 1225–1234.

Wang, Fahui, and Wei Luo. 2005. Assessing spatial and nonspatial factors for healthcare access: towards an integrated approach to defining health professional shortage areas. *Health & place* 11(2):131–146.

Wennberg, J. E., and M. M. Cooper. 1998. *The dartmouth atlas of health care in the united states*. Chicago, IL: American Hospital Publishing.

Xiao, Shunxin, Shiping Wang, Yuanfei Dai, and Wenzhong Guo. 2022. Graph neural networks in node classification: survey and evaluation. *Machine Vision and Applications* 33: 1–19.

Xie, Yaochen, Sumeet Katariya, Xianfeng Tang, Edward Huang, Nikhil Rao, Karthik Subbian, and Shuiwang Ji. 2022. Task-agnostic graph explanations. *Advances in Neural Information Processing Systems* 35:12027–12039.

Yang, Yi, and Shawn Newsam. 2010. Bag-of-visual-words and spatial extensions for land-use classification. In *Proceedings of the 18th SIGSPATIAL international conference on advances in geographic information systems*, 270–279.

Yao, Xin, Yong Gao, Di Zhu, Ed Manley, Jiaoe Wang, and Yu Liu. 2020. Spatial origin-destination flow imputation using graph convolutional networks. *IEEE Transactions on Intelligent Transportation Systems* 22(12):7474–7484.

Ye, Xinyue, and Clio Andris. 2021. Spatial social networks in geographic information science.

Ying, Zhitao, Dylan Bourgeois, Jiaxuan You, Marinka Zitnik, and Jure Leskovec. 2019. Gnnexplainer: Generating explanations for graph neural networks. *Advances in neural information processing systems* 32.

Yu, Bing, Haoteng Yin, and Zhanxing Zhu. 2017. Spatio-temporal graph convolutional networks: A deep learning framework for traffic forecasting. *arXiv preprint arXiv:1709.04875*.

Yuan, Hao, Haiyang Yu, Shurui Gui, and Shuiwang Ji. 2022. Explainability in graph neural networks: A taxonomic survey. *IEEE transactions on pattern analysis and machine intelligence* 45(5):5782–5799.

Zeng, Hanqing, Hongkuan Zhou, Ajitesh Srivastava, Rajgopal Kannan, and Viktor Prasanna. 2019. Accurate, efficient and scalable graph embedding. In *2019 ieee international parallel and distributed processing symposium*, 462–471. IEEE.

Zhang, Jingnan, Xin He, and Junhui Wang. 2022. Directed community detection with network embedding. *Journal of the American Statistical Association* 117(540):1809–1819.

Zhang, Tianqi, Yun Xiong, Jiawei Zhang, Yao Zhang, Yizhu Jiao, and Yangyong Zhu. 2020. Commdgi: community detection oriented deep graph infomax. In *Proceedings of the 29th acm international conference on information & knowledge management*, 1843–1852.

Zhu, Di, Fan Zhang, Shengyin Wang, Yaoli Wang, Ximeng Cheng, Zhou Huang, and Yu Liu. 2020. Understanding place characteristics in geographic contexts through graph convolutional neural networks. *Annals of the American Association of Geographers* 110(2): 408–420.

Zhu, Jiawei, Xing Han, Hanhan Deng, Chao Tao, Ling Zhao, Pu Wang, Tao Lin, and Haifeng Li. 2022. KST-GCN: A knowledge-driven spatial-temporal graph convolutional network for traffic forecasting. *IEEE Transactions on Intelligent Transportation Systems* 23(9): 15055–15065.